UNIVERSITY OF CALIFORNIA, SAN DIEGO

DESIGN AND TESTING OF SAFE AND VERSATILE BIOMATERIAL THERAPIES FOR CARDIAC REPAIR POST-MYOCARDIAL INFARCTION

A dissertation submitted in partial satisfaction of the requirements for the degree Doctor of Philosophy

in

Bioengineering

by

Sophia Lynn Suarez

Committee in charge:

Professor Adah Almutairi, Co-Chair
Professor Karen L. Christman, Co-Chair
Professor Kirk Knowlton
Professor Andrew McCulloch
Professor Jeffrey Omens

2015

The dissertation of Sophia Lynn Suarez is approved, and it is acceptable in quality and form for publication on microfilm and electronically:

Co-Chair

Co-Chair

University of California, San Diego

2015

DEDICATION

To my family for their abundant love, support and inspiration, especially:

Brandon and Ethan

Mom and dad (Karen and Steve Harrison)

Matt and Raina Harrison

Manny, Kathryn and Austin Suarez

Captain Bob (Robert Harrison)

EPIGRAPH

The heavens declare the glory of God,

and the sky above proclaims his handiwork.

Psalms 19:1

TABLE OF CONTENTS

LIST OF FIGURES

LIST OF TABLES AND SCHEMES

ACKNOWLEDGEMENTS

I would like to thank the people who have made this work possible through their support and intellectual contribution.

Thank you Karen and Adah for giving me the opportunity to come to UCSD and work in your labs. Thank you for your guidance as well as the space to learn on my own. Thank you for the resources to complete fascinating work. Thanks to the rest of my thesis committee: Dr. Andrew McCulloch, Dr. Jeff Omens and Dr. Kirk Knowlton. Your advice and constructive criticism of my experimental design helped to improve the quality of my dissertation.

Thank you to the NSF GRFP for providing funding for three years of my graduate research. Thank you to the HHMI Med-into-Grad program for funding and the opportunity to explore the world of clinical cardiology. Special thanks to Dr. Mark Kamps, Dr. Kirk Knowlton and Dr. Sam Tsimikas for their efforts in organizing the clinical rotations. Thank you also to the rest of the physicians and hospital staff who helped me along the way.

Thank you to Tom and Stacey Siebel for their generous contributions in creating the Siebel Foundation. Thank you to Dr. Shu Chien and the rest of the Siebel scholarship review committee for giving me the honor of being named a 2015 Siebel Scholar.

Thank you to the Christman and Almutairi lab members, past and present. My work would not have been possible without your direct and advisory roles in all my projects. I also value the many great friendships I have gained. Just to highlight a few of you, thank you to Dr. Greg Grover for the help in designing my

studies and troubleshooting experiments. Thank you to Dr. Sonya Sonnenberg for help designing studies and interpreting results. Thank you to Dr. Aboli Rane for the inspiration and tools to complete the optical mapping study. Thank you to Rebecca Braden for all your help with animal surgeries and lab logistics throughout the years. Thank you to Dr. Enas Mahmoud for teaching me how to make and characterize particles. Thank you to Dr. Cathryn McFearin for help navigating the world of graduate school. Thank you to Dr. Amy Moore for helping me to obtain the necessary supplies to complete my studies. A special thank to Adam Muñoz. I was honored to work with you and see you grow and develop as a student, a researcher and as a person. I can't wait to see what your graduate career holds.

Thank you to my study group, Todd Johnson, Hermes Taylor, Mark Chapman, Nate Vacanti and Kevin Vincent. I wouldn't have made it through first year without your friendship and support.

Thank you to the bioengineering department faculty and staff for your continued support of my research endeavors. Special thanks to Jen Lengington for helping me solve numerous administrative problems in the last five years.

Thank you to BEGS and the IAB for allowing me the privilege of serving as the Professional Development Chair for two years and the resources to plan numerous Chutes and Ladders panels.

Thank you to Dr. Jennifer Cochran and Aaron Mitchell for the significant contribution of the HGF-f to the work presented in Chapter 4. Thank you to Dr. Adam Wright for helping me design and complete the optical mapping studies.

The following chapters are, in part, reprints of the following publications:

Chapter 1, in part, is a reprint of the material as it appears in Biomaterial Science 2015. Suarez S, Almutairi A, Christman KL. Micro- and nanoparticles for treating cardiovascular disease. 2015.

Chapters 1 and 2, in part, are a reprint of the material as it appears in the submission to Acta Biomaterialia 2015. Sophia L. Suarez, Aboli A. Rane, Adam Muñoz, Adam T. Wright, Shirley X. Zhang, Rebecca L. Braden, Adah Almutairi, Andrew D. McCulloch, Karen L. Christman. Intramyocardial injection of hydrogel with high interstitial spread does not impact action potential propagation. 2015.

Chapters 1 and 3, in part, are a reprint of the material as it appears in Biomacromolecules 2014. Suarez S**,** Grover GN, Braden RL, Christman KL, Almutairi A. Tunable Protein Release from Acetalated Dextran Microparticles: A Platform for Delivery of Protein Therapeutics to the Heart Post-MI. Biomacromolecules. 2014.

Chapters 1 and 4, in part, is in preparation for submission as: Sophia L. Suarez, Adam Muñoz, Aaron Mitchell, Rebecca L. Braden, Colin Luo, Jennifer R. Cochran, Adah Almutairi, Karen L. Christman. HGF cardioprotective efficacy post-MI is maximized when released from quickly degrading acetalated dextran microparticles.

The dissertation author was the one of the primary investigators and author each of these papers.

VITA

EDUCATION

2015	Ph.D., Bioengineering Department of Bioengineering University of California, San Diego
2013	M.S., Bioengineering Department of Bioengineering University of California, San Diego
2008	B.S., Materials Science and Engineering Department of Materials Science and Engineering Massachusetts Institute of Technology

AWARDS AND HONORS

Siebel Scholar, Class of 2015
National Science Foundation Graduate Research Fellowship, 2011-2014
Howard Hughes Medical Institute Med-into-Grad Fellowship, 2013

PUBLICATIONS

Suarez S, Almutairi A, Christman KL. *Micro- and Nanoparticles for Treating Cardiovascular Disease.* Biomaterials Science. 2015

Suarez S, Grover GN, Braden RL, Christman KL, Almutairi A. *Tunable Protein Release from Acetalated Dextran Microparticles: A Platform for Delivery of Protein Therapeutics to the Heart Post-MI.* Biomacromolecules. 2014

ABSTRACT OF THE DISSERTATION

DESIGN AND TESTING OF SAFE AND VERSATILE BIOMATERIAL THERAPIES FOR CARDIAC REPAIR POST-MYOCARDIAL INFARCTION

by

Sophia Lynn Suarez

Doctor of Philosophy in Bioengineering

University of California, San Diego, 2015

Professor Adah Almutairi, Co-Chair
Professor Karen L. Christman, Co-Chair

Heart failure (HF) post-myocardial infarction (MI) is a leading cause of death in the United States. Injectable biomaterials have been evaluated as potential new therapies for MI and HF. These materials have improved left

ventricular (LV) geometry and function in animal models, but there remains a need for improved design of biomaterial therapies to ensure patient safety and facilitate therapeutic versatility. The goals of this dissertation were to investigate the effect of biomaterial injection on electrophysiology to inform the design of safe therapies and to improve biomaterial versatility by designing microparticles with tunable release profiles.

There remain concerns that biomaterial injection may create a substrate for arrhythmia. We utilized optical mapping to assess the effects of biomaterial injection and interstitial spread on cardiac electrophysiology. Healthy and infarcted rat hearts were injected with a hydrogel with varying degrees of interstitial spread. The degree of the electrophysiological changes depended on the spreading characteristics of the hydrogel, such that hearts injected with highly spread hydrogels showed no conduction abnormalities. Conversely, injection of a hydrogel exhibiting minimal interstitial spread may create a substrate for arrhythmia by causing LV activation delays and reducing gap junction density at the site of injection. Thus, this work establishes site of delivery and interstitial spread characteristics as important factors in the future design of biomaterial therapies for MI treatment.

Biomaterials can protect and sustain release of therapeutic payloads, but most biomaterials have defined degradation kinetics, limiting the payload release to one time frame. We harnessed the tunable degradation and acid-sensitivity of acetalated dextran (AcDex) to design microparticles for injection post-MI. Protein release ranging from days to weeks was shown in low pH

environments similar to what is found in an infarcted heart. Furthermore, we utilized the tunable degradation of AcDex to determine how delivery rate impacts the efficacy of hepatocyte growth factor (HGF), a known cardioprotective growth factor. HGF-f delivery was optimal over three days post intramyocardial injection, yielding the largest arterioles, fewest apoptotic cardiomyocytes bordering the infarct and the smallest infarcts. This work will help inform the design of future HGF-based therapies and provides a platform for tunable delivery of therapeutics to the heart post-MI.

CHAPTER ONE:

Introduction

1.1 Heart failure post-myocardial infarction

Over 80 million adults in the United States have at least one cardiovascular disease (CVD) and one in three deaths in 2010 were attributed to CVD [1]. Heart-failure (HF) post myocardial infarction (MI) causes the majority of deaths resultant from cardiovascular-related disease [2]. Following a MI, reparative mechanisms lead to collagenous scar formation in place of the damaged myocardium. The non-contractile nature of the scar leads to hypertrophy of the viable myocardium, infarct wall thinning and ventricular dilation [3]. If left untreated these processes progress until the heart no longer pumps adequately to supply sufficient blood to the body, defined as HF. The current gold standard treatment for end-stage HF is heart transplantation, a highly invasive surgery for which only a fraction of patients are eligible due to the limited availability of donor hearts. In addition, left ventricular assist devices (LVADs) prolong and improve quality of life for some patients with end-stage HF, however, LVAD implantation increases risk of stroke and infection. Furthermore, no current therapy prevents the negative remodeling process that leads to HF. Given the drawbacks of current state-of-the-art treatments, development of new therapies to mitigate negative left ventricular (LV) remodeling post-MI is crucial to patient quality of life and survival. Intramyocardial injection of biomaterials is becoming increasingly popular in the development of new treatments.

1.2 Biomaterial therapies

The field of biomaterials for treating MI has rapidly expanded over the past decade and in particular, injectable biomaterials, have been evaluated as potential minimally invasive therapies for MI and HF [4-7]. Biomaterials are desirable because they potentially provide biochemical cues for myocardial protection and/or regeneration, a scaffold for cellular delivery or endogenous cell infiltration, and/or a vehicle for delivery of therapeutic agents including growth factors, enzymes, and/or small molecule drugs over time. Injectable biomaterials can be classified in two main categories: hydrogels and particles.

Injection of hydrogels composed of a number of naturally derived materials including collagen [8, 9], alginate [10, 11], fibrin [12], chitosan [13], small intestinal submucosa [14], myocardial matrix [15, 16] and degradable synthetic materials [17-19] have shown therapeutic benefit post-MI. Hydrogels can protect and sustain release of growth factors [20-23] and help improve transplant survival of cells [4, 5, 24, 25]. Yet hydrogels also show promise for healing post-MI as material-alone therapies [10, 12, 16]. Most excitingly hydrogel injection post-MI has repeatedly influenced global cardiac parameters including improved or maintained LV geometry and ejection fraction (EF) [4-6]. These improvements in structure and function are accompanied by other positive changes including reduced fibrosis, increased angiogenesis and/or arteriogenesis and decreased apoptosis. The majority of these studies have been completed in small animal models, but as these therapies show positive results with potential for catheter delivery in some cases [11, 15], injectable hydrogels

are beginning to advance to large animal pre-clinical models [11, 16] and recently clinical trials [26, 27].

Another form of injectable biomaterial with promise for treating the heart post-MI is micro- and nanoparticles. While numerous materials have been used to create particle therapies for other applications, those used in the heart only include gelatin [28-32], PLGA [33-36] and polyketal-based polymers [37-41]. The most common use for directly injected microparticles to date is delivery of proteins including growth factors and enzymes, as well as small molecule drugs. While proteins can stimulate many important cellular processes needed for healing, their stability and longevity *in vivo* is short-lived due to enzymatic degradation and/or physical clearance [42]. Encapsulation within microparticles protects them against these external factors and provides a means of sustained release. While small molecules tend to be more stable than proteins, particle delivery still enhances their benefit through sustained release. Similar exciting results to those observed following hydrogel injections have been observed following particle injections post-MI. For example, vascular endothelial growth factor (VEGF) released from microparticles caused significantly greater growth of capillaries and arterioles in the borderzone and infarct areas and reduced wall thinning compared to free VEGF or empty particles [33]. Superoxide dismutase (SOD)-containing particles reduced superoxide levels in the borderzone and the number of apoptotic cells in the LV to the same level as in sham-treated rats three days after treatment [37]. Furthermore, SOD-containing particles reduced the impact of ischemia on fractional shortening, whereas free SOD and empty

particle had no impact on the decline of fractional shortening post-MI. Injection of microparticles containing a p38 inhibitor significantly inhibited p38 phosphorylation, superoxide production, and tumor necrosis factor alpha (TNF-α) production compared to free p38i or empty particles [38]. Finally, injection of nanoparticles containing insulin growth factor (IGF-1) was more effective in reducing LV dilation, thickening infarct wall, reducing infarct area, and enhancing fractional shortening and ejection fraction 21 days post-injection compared to unencapsulated IGF-1 and empty particles [36]. So far particle-based therapies post-MI have only been tested in small animal models.

Thus, with the promise of injectable biomaterials, it is exceedingly important to understand the mechanisms by which biomaterials affect the underlying tissue and the impact on not only treatment of the pathological condition, but also patient safety. Furthermore there is room for improved design of biomaterials therapies to increase therapeutic versatility.

1.3 Biomaterial safety

Many patients eligible for a cell and/or biomaterial therapy may already be at increased risk of ventricular arrhythmia [43], so it is essential that the therapy does not increase the ventricular vulnerability above the baseline level. However, previous studies have shown that injection of certain cell types disturbs normal electrical propagation through the tissue and increases vulnerability to dangerous ventricular arrhythmias [44-46]. Along similar lines, injection of a biomaterial in the myocardium could cause conduction abnormalities and alter

action potential propagation. If such changes occurred, the biomaterial could create a substrate for arrhythmia and ultimately a pose hazard to patient safety. However to date, studies aimed at understanding the effect of biomaterial injection on cardiac electrophysiology and arrhythmogenesis are lacking. Preliminary research from our group showed that injection of a bulk hydrogel into healthy myocardium caused an increase in LV activation time, while injection of microparticles did not [47]. The varying impact of the two forms of biomaterials on electrophysiology may be due to their varying degrees of interstitial spread.

Different hydrogels demonstrate varying degrees of interstitial spread [48-50]. Hydrogels with low spread stay confined in a localized region resulting in myocardium being pushed to the perimeter of the hydrogel structure. In contrast, highly spread hydrogels occupy the interstitial space between neighbouring cardiomyocytes resulting in the presence of myocardial fibers throughout the hydrogel structure. Particles are typically highly spread interstitially following injection. The amount of integration with the native myocardium may therefore influence how the biomaterial impacts the electrophysiological properties of the underlying tissue.

Furthermore, there is also heterogeneity in the site of delivery of biomaterials. Injection of a hydrogel in the infarcted region of the myocardium has been advantageous through augmentation of LV wall mechanics [8] and promoting cellular migration into the region [51]. In contrast, injection into the viable border zone has shown improved myocardial salvage and prevention of infarct expansion [52]. The latter is also a common injection site when delivering

cells. One concern is that the presence of the biomaterial in viable tissue may make that region vulnerable to alterations in electrical propagation.

1.4 Biomaterial versatility

In healthy tissues, regulation of processes such as angiogenesis, fibrosis and apoptosis are controlled by precisely tuned spacio-temporal presentation of certain molecules. Alterations in this tight regulation occur following MI resulting in scar formation instead of tissue repair. Thus mimicking a normal healing pathway by delivering exogenous or inducing expression of endogenous molecules at the proper time could facilitate positive tissue remodelling following ischemic damage. While biomaterials have the ability to protect and sustain release of bioactive payloads, most biomaterials have a defined degradation profile, thus limiting payload release to one time frame. Expanding on this limitation slightly, a couple studies showed that two payloads could be released over different time frames from the same material; alginate hydrogels were used to sequentially release two growth factors in the heart post-MI [22, 23]. However, since the sequential release was due to different binding strengths of the two growth factors to the hydrogel the growth factors could not be released in the opposite order nor released at more than one rate to study the optimal delivery rate of each. Furthermore the release rate was determined by the structure of the payload thus limiting its versatility.

In studies not designed for delivery to the heart post-MI, a few strategies have been developed to deliver multiple payloads at different rates from

biomaterials. Several promising approaches for tunable delivery of growth factors have been developed, but each is limited to a specific category of payloads or is difficult to manipulate to provide more than two rates of release. The first approach takes advantage of growth factors' variable heparin-binding strength with sulfated materials to create an affinity scaffold to sequentially release VEGF, PDGF-BB, and TGF-β1 [53] Here only molecules with heparin-affinity or a positive charge can be delivered. Using a similar strategy, polyelectrolyte multilayers were used to control the release of charged growth factors, in this case bFGF (+), layered with heparin (-) and a polymer (+), was released at a rate dependent on the number of layers assembled [54], limiting deliverable cargo to charged molecules. Polyelectrolyte multilayers have also been employed to create microcapsules using the Layer-by-Layer (LbL) encapsulation method. These microcapsules provide sustained release of several payloads including bFGF, however, to date the system has not been specifically designed for delivery to the heart post-MI. For instance, payload release often occurs around neutral pH [55, 56] and in some cases is actually prohibited in mildly acidic conditions [56]. Some studies have shown permeability of the microcapsules at low pH (<6) and impermeability at high pH (>8) [57] but no studies to date have shown impermeability at neutral pH (7.4) with permeability in mildy acidic pH (6-7) [58], as desired for this application. Furthermore, in the majority of studies shown ~80% release of the payload occurs in 3-4 days [55, 56, 59] and no studies show sustained release over several weeks, a time frame that will likely be needed for healing post-MI. In one study changing layer thickness showed a

difference in release rate, but only of 5% at the time points shown [59]. A greater difference in release rate may be achieved by varying the loading method between pre- or post-loading, since these showed a larger difference in total protein released at 72 hours, but the long-term release trends were not explored [59]. The third approach embedded PDGF-loaded PLGA microspheres in an alginate hydrogel containing VEGF [60] to release VEGF followed by PDGF. Creating more than two rates of release with this system would require changing hydrogel density, particle size and/or particle concentration, and no hydrophobic payload could be released from the alginate hydrogel. The growth factors delivered in these studies are likely to be important in some healing pathways post-MI, but other payloads including hydrophobic small molecules, enzymes, and plasmid DNA have also shown promise in aiding healing post-MI [7]. Finally, these approaches are not designed for the mildy acidic environment of an infarct (pH 6.0-7.0) [61, 62].

Tighter control over payload delivery rates would allow a more thorough investigation into when and for how long each therapeutic should be delivered after injury, thus informing the design of biomaterial-based therapies with optimal release kinetics. Furthermore, precisely tuned degradation would allow delivery of combinations of therapeutics to activate complementary healing pathways. Thorough biological mimicry of natural tissue repair processes would require numerous molecules delivered at different time points, and these combinations are not yet fully understood. However progress has been made towards understanding the influence of timing and order of therapeutic delivery in some

relevant processes. For instance, bFGF and VEGF are well known to stimulate blood vessel formation. Yet their efficacy is improved when a second factor, platelet derived growth factor (PDGF) or sphingosine-1-phosphate (S1P), respectively, is delivered subsequently. The combination of bFGF followed by PDGF or VEGF followed by S1P generates more mature vessels than either pair of factors delivered at the same time or in the opposite order [63, 64]. This type of investigation into the optimal time frame for delivering therapies to modulate other processes post-MI has not been studied.

A few candidate therapeutics that may be optimized by finely tuned temporal delivery include acidic fibroblast growth factor (aFGF) and neuregulin (NRG-1), two proteins important for cardiomyocyte survival, which were delivered in microparticles at the same time but did not produce the predicted synergistic effect, potentially due to an overlap in signalling pathways [35]. Perhaps if they were delivered sequentially this outcome would be different. Another potential target for finely tuned delivery post-MI is matrix-metalloproteinases (MMPs). MMP-1 plasmid DNA delivered in microparticles reduced scarring post-MI [31]. However, MMPs have another important role in contributing to post-MI damage, namely breakdown of native extracellular matrix (ECM) proteins immediately following ischemic injury and cardiomyocyte death [65]. Thus, early downregulation and late upregulation of MMPs may be an effective strategy to minimize damage, by preserving healthy ECM and preventing scar formation, respectively.

1.5 Dissertation scope

The goals of this dissertation were to investigate the effect of biomaterial interstitial spread on electrical conduction to inform the design of safe injectable biomaterial therapies and to improve biomaterial versatility by designing microparticles with tunable release profiles to study the optimal time frame for delivery of a promising cardioprotective growth factor.

Chapter one provided an introduction to the need for new therapies to treat patients with heart failure post-MI, the promise of injectable biomaterials to fill this need, and areas for improvement regarding patient safety and biomaterial versatility.

Chapter two investigates the effect of injecting a hydrogel with varying degrees of interstitial spread into healthy and infarcted hearts on cardiac electrophysiology in terms of LV activation time, action potential duration, and repolarization. Furthermore changes in cellular connectivity following hydrogel injection are studied through quantification of gap junctions.

Chapter three describes the design of microparticles with tunable degradation rate and protein release profiles. Microparticles are shown to release a model protein and formulation-sensitive growth factor at rates varying from days to months, while maintaining growth factor activity. Finally biocompatibility of the microparticles is shown in healthy hearts setting the stage for use of the particles as a delivery vehicle for therapeutics to the heart post-MI.

Chapter four is a first of its kind study of the optimal time frame for delivering a known cardioprotective growth factor to the heart post-MI using

tunable microparticles. The study shows that microparticle degradation can be tuned even within the infarcted heart. Furthermore the study determines the optimal time frame for delivering a promising cardioprotective growth factor to the heart post-MI.

Chapter five provides a summary, conclusions and future work.

Chapter 1, in part, is a reprint of the material as it appears in Biomaterial Science 2015. Suarez S, Almutairi A, Christman KL. Micro- and nanoparticles for treating cardiovascular disease. 2015.

Chapter 1, in part, is a reprint of the material as it appears in Biomacromolecules 2014. Suarez S**,** Grover GN, Braden RL, Christman KL, Almutairi A. Tunable Protein Release from Acetalated Dextran Microparticles: A Platform for Delivery of Protein Therapeutics to the Heart Post-MI. Biomacromolecules. 2014.

Chapter 1, in part, is a reprint of the material as it appears in the submission to Acta Biomaterialia 2015. Sophia L. Suarez, Aboli A. Rane, Adam Muñoz, Adam T. Wright, Shirley X. Zhang, Rebecca L. Braden, Adah Almutairi, Andrew D. McCulloch, Karen L. Christman. Intramyocardial injection of hydrogel with high interstitial spread does not impact action potential propagation. 2015.

Chapter 1, in part, is in preparation for submission as: Sophia L. Suarez, Adam Muñoz, Aaron Mitchell, Rebecca L. Braden, Colin Luo, Jennifer R. Cochran, Adah Almutairi, Karen L. Christman. HGF cardioprotective efficacy

post-MI is maximized when released from quickly degrading acetalated dextran microparticles.

The dissertation author was the one of the primary investigators and author each of these papers.

CHAPTER TWO:

Intramyocardial Injection of Hydrogel with High Interstitial Spread Does Not Impact Action Potential Propagation

2.1 Introduction

With myocardial infarction (MI) affecting over one million Americans each year [66], there has been a push for the development of novel therapies for the treatment of MI, subsequent left ventricular (LV) remodeling and eventual heart failure (HF). The field of biomaterials for treating MI has rapidly expanded over the past decade and in particular, injectable biomaterials, including hydrogels, have been evaluated as potential minimally invasive therapies for MI and HF. With the promise of injectable hydrogels, it is exceedingly important to understand the mechanisms by which this type of biomaterial affects the underlying tissue and the impact on not only treatment of the pathological condition, but also patient safety.

Many patients eligible for a cell and/or biomaterial therapy may already be at increased risk of ventricular arrhythmia [43], so it is essential that the therapy does not increase the ventricular vulnerability above the baseline level. Injection of a hydrogel in the myocardium could cause conduction abnormalities and alter action potential propagation. If such changes occurred, the hydrogel could create a substrate for arrhythmia and ultimately a pose hazard to patient safety. However to date, studies aimed at understanding the effect of hydrogel injection on cardiac electrophysiology and arrhythmogenesis are lacking.

A variety of both biologically derived and synthetic hydrogels have been injected into infarcted tissue as a potential therapy for MI. There is heterogeneity in both the site of delivery and interstitial spread of these biomaterials. One

concern is that the presence of the hydrogel in viable tissue may make that region vulnerable to alterations in electrical propagation. Another important concern is that different hydrogels demonstrate varying degrees of interstitial spread [48-50]. The amount of integration with the native myocardium may therefore influence how the hydrogel impacts the electrophysiological properties of the underlying tissue.

Optical mapping is widely established as a robust technique for the detection, visualization and quantification of electrophysiological changes in cardiac tissue [67]. This technology has been recently utilized for the assessment of changes in electrophysiology and potential arrhythmogenesis after infarction [68, 69] and cellular transplantation at the site of infarction [70, 71]. Herein, we utilize optical mapping as a tool to assess the effects of injection of a hydrogel with varying interstitial spread on LV activation and repolarization in healthy and cryoinfarcted hearts. This work assesses the potential of this type of biomaterial to become a substrate for arrhythmias.

2.2 Methods

All experiments in this study were conducted in accordance with the guidelines established by the Institutional Animal Care and Use Committee and the American Association for Accreditation of Laboratory Animal Care and were approved by the Institutional Animal Care and Use Committee at the University of California, San Diego.

2.2.1 Preparation of injectable materials

Hydrogels were prepared by mixing solutions of 4-arm polyethylene glycol-succinimidyl glutaramide (PEG-SGA, JenKem Technology USA, Plano, TX; 50 mg/mL in phosphate buffer pH 4.0) and 4-arm polyethylene glycol-amine (PEG-NH_2, JenKem Technology USA, Plano, TX; 50 mg/mL in borate buffer pH 8.0) to create PEG hydrogels by chemical crosslinking. PEG-ASG and PEG-NH_2 were combined in a 1:1 ratio and gelation occurred 40 seconds after mixing *in vitro*.

2.2.2 Experimental Design

Sixty-six Sprague-Dawley rats were divided into healthy (n = 31) and cryoinfarct (n = 35) groups. Healthy animals received either hydrogel injection (n = 15), saline injection (n = 8) or no injection (n = 8) into the LV free wall. Animals undergoing the cryoinfarct surgery were allowed to recover for one-week prior to injection surgeries. At the time of injection surgery animals were divided into treatment groups: hydrogel injection into the borderzone (n = 17) or no injection (n = 18). Twenty-minutes after injection, the hearts were excised and hung on a Langendorff apparatus to complete optical mapping experiments. After completing the mapping, hearts were prepared for histological analysis. Specific methods are detailed below.

2.2.3 Cryoinfarction surgery

Female Sprague Dawley rats (n = 35) were anesthetized using 5% isoflurane, intubated and maintained at 2.5% isoflurane for the surgery

procedure. A left thoracotomy was used to access the heart. A custom cryoprobe filled with liquid nitrogen was held at the apical end of the LV free wall for thirty seconds to create the cryoinfarct. The animals were sutured closed and allowed to recover. One week after cryoinfarction, hemodynamic measurements and an injection surgery were performed as described below for hydrogel-injected and non-injected groups. Hydrogel injections were made at the border zone of the basal side of the infarct. Cryoinfarct location was selected so that the entire injury would be visible in the imaging frame and so that hydrogel injections could be made in a similar location to healthy hearts. If the probe location was inconsistent leading to a cryoinfarct that was too close to the apex (out of the viewing frame) or too close to the base (interfering with hydrogel injection) the hearts were excluded from analysis (n = 4 excluded from each group). No mortality occurred during these procedures.

2.2.4 In vivo hemodynamic measurements and injection surgery

Female Sprague Dawley rats (n = 31 healthy; n = 35 cryoinfarcted) were anesthetized using 5% isoflurane, intubated and maintained at 2.5% isoflurane for the surgery procedure. The animals were ventilated using a respirator at 75 breaths/minute. The right carotid artery was carefully isolated and a pressure transducer (Millar; SPR-407) was inserted in through the carotid artery and advanced into the left ventricle. The isoflurane was reduced to 1% and the ECG and LV pressures were monitored and recorded. End diastolic pressure (EDP) was defined as the LV pressure at the peak of the QRS complex while peak systolic

pressure (PSP) was established as the maximum LV pressure. All pressure measurements were averaged over 10 beats in the cardiac cycle. After acquiring pressure measurements, the heart was exposed using a left anterior thoracotomy and injected once with either 75 μl of the hydrogel or saline using a 27 G needle into LV free wall or not injected, as a sham group. To create a range of resulting interstitial spread of the hydrogel, the mixed solution was injected into the LV myocardium between 25 and 35 seconds after mixing. In general, the earlier the mixture was injected, the more interstitial spread occurred before gelation and vice versa. There was some variability in spread within one injection time point, but this method enabled a broader range of interstitial spread from approximately 20 to 50 % (see results). Isoflurane was maintained at 2.5% during the injection procedure. Presence of the injection was verified by temporary discoloration of the tissue. If the hydrogel was partially or fully extruded from the tissue immediately following injection the hearts were excluded from final analysis (n = 3 healthy and n = 3 cryoinfarcted excluded). Post-injection hemodynamic parameters were measured 20 minutes after injection, or an equivalent time point after the heart was exposed for non-injected controls, as described at baseline. No mortality occurred during these procedures.

2.2.5 Optical mapping of the polymer injection in Langendorff-perfused rat heart

Final group numbers that were included in the optical mapping analysis were as follows: healthy (hydrogel: n = 12, saline: n = 8, no injection: n = 8) and cryoinjured (hydrogel: n = 10, no injection: n = 14. Immediately after post-

injection hemodynamic measurements (20 minutes post-injection), the hearts were excised and arrested using a solution containing 25 mM $NaHCO_3$, 2 mM $CaCl_2$, 5 mM Dextrose, 2.7 mM $MgSO_4$, 22.8 mM KCl, 121.7 mM NaCl, 20 mM 2,3 butanedione monoxime. The aorta of the heart was cannulated and attached to a Langendorff apparatus. The hearts were then retrograde perfused with a Tyrode's solution (25 mM $NaHCO_3$, 2 mM $CaCl_2$, 5 mM Dextrose, 2.7 mM $MgSO_4$, 4.8 mM KCl, 121.7 mM NaCl, 10 mM Blebbistatin) at 37° C in a custom designed optical mapping chamber. A constant pressure of 70 mmHg was maintained and the flow rate was monitored. Blebbistatin (EMD Millipore, Darmstadt, Germany) was used as an electromechanical decoupler as previously shown to minimize motion artifact [72].

The heart was perfused with the voltage sensitive fluorescent dye di-4-ANEPPS (Biotium, Hayward, CA) that was dissolved in dimethysulfoxide (DMSO) and diluted to 5.2 mM with Tyrode's solution. A 10 mL bolus of this solution was injected into the perfusion line. The LV free wall was imaged with a high-speed CMOS camera (MiCAM Ultima L, Brainvision) using a custom-built tandem lens imaging system, with an objective lens of 0.5X and imaging lens of 1X (Leica planapo objective). Images were collected with a spatial and temporal resolution of 100 x 100 pixels at 0.2 mm x 0.2 mm per pixel, and a frame rate of 1000 frames per second. The dye-stained LV epicardial surface was excited by an LED lamp (LEDtronics) at 470 nm (excitation of the LED lamps) and the emitted fluorescence was collected and filtered with a long-pass filter >610 nm (Figure 2.1). The images were collected at intrinsic cardiac rhythm.

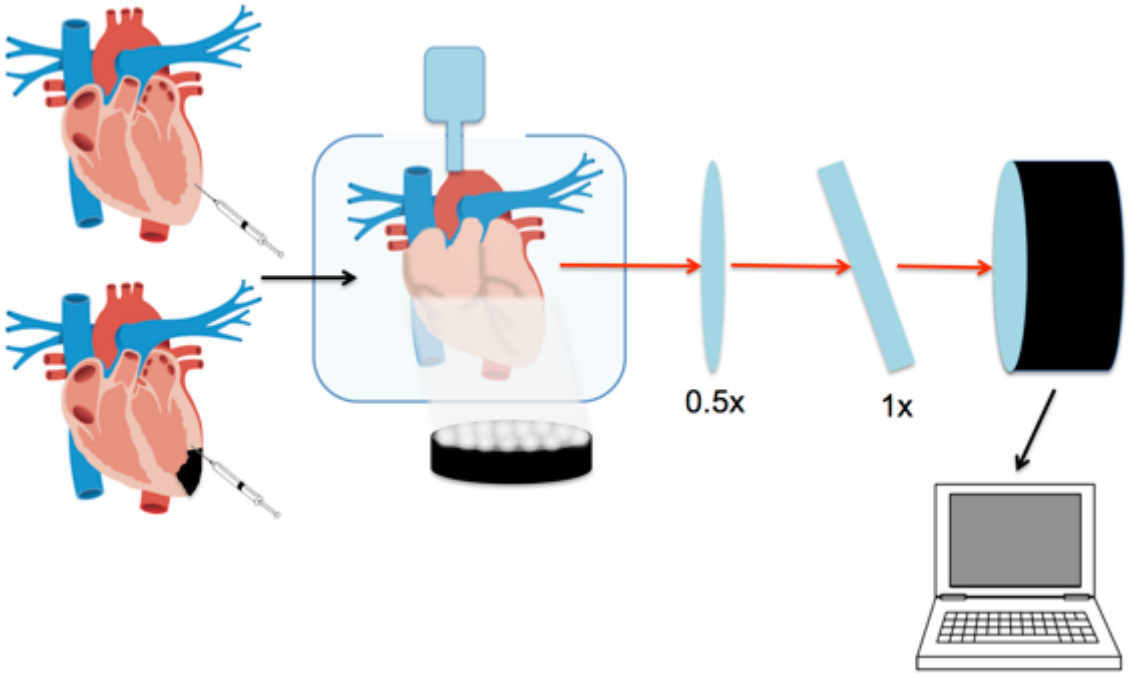

Figure 2.1. Schematic of experimental procedure. The healthy and cryoinfarcted hearts injected with the hydrogel or saline are depicted, followed by the optical mapping setup. The heart is excised and the aorta is cannulated for perfusion of the tissue with Tyrodes solution, allowing the heart to remain viable *ex vivo*. A voltage sensitive dye (di-4-ANNEPS) is perfused through the coronaries. A LED light excites the dye at 470 nm (black arrow) and the emitted fluorescence is collected at a wavelength greater than 610 nm using a 0.5X objective lens and a 1X imaging lens (red arrows). The incident fluorescent signal is captured by a high-speed camera (1000 frames/second) and then computational techniques are used to analyze the data.

2.2.6 Data analysis

Optical signals were imported into Matlab and analyzed using custom software as previously described [73]. Briefly, activation time was identified at each pixel as the time of maximum rate of change of fluorescence for the action potential upstroke for each beat $(dF/dt)_{max}$. To calculate the time of repolarization, the time at which the action potential recovered to 20%, 50%,

and 80% of the peak value were determined. The action potential duration (APD) at 20%, 50%, and 80% were calculated as the difference between repolarization time at the respective level and activation time of the action potential. The dispersion in APD and repolarization times was calculated as the difference between the maximum and minimum APD or repolarization time over the LV epicardium in the field of view respectively. Heterogeneities in dye perfusion created increasing variability in dispersion values at longer repolarization times. Therefore dispersion in APD and repolarization in healthy hearts were only determined at 20% repolarization. Furthermore due to the resultant dye perfusion differences in the cryoinfarcted hearts (ie. non-perfused infarcts), dispersion values were not determined in these hearts.

2.2.7 Histology

After the completion of the optical mapping experiments, the heart was removed from the cannula, embedded and fresh frozen in Tissue-Tek O.C.T. freezing compound. Short axis cross sections (10 μm thick) were taken every 350 μm from apex to base and stained with hematoxylin and eosin (H&E). Cryoinjury size, measured as percent of LV circumferences, was quantified as previously described [74]. Slides were imaged with a Carl Zeiss Observer D.1 and hydrogel spread was quantified using Photoshop software (Adobe Photoshop CS3). Specifically, the injection region was selected to include the hydrogel with any respective penetrating muscle. The hydrogel within the injection region was identified by the lightly pink stained material, and histological artifacts were

carefully avoided in all measurements. The pixel count was recorded for both the 'injection' and 'hydrogel' regions for each heart slice. Known spacing between slices enabled calculation of 'injection volume' and 'hydrogel volume' and the percent muscle within the hydrogel was determined as:

$$Percent\ muscle\ within\ hydrogel = \left[\frac{Volume_{Injection} - Volume_{hydrogel}}{Volume_{Injection}}\right] x\ 100$$

Cryoinjury size, measured as percent of LV circumferences, was quantified as previously described [74].

2.2.8 Gap junction staining and quantification

To assess gap junction density, immunohistochemistry was performed on two representative slides from each heart. Slides containing the largest area of hydrogel were used in the hydrogel group, and equivalent anatomical locations were used in non-injected and saline-injected hearts. Cryosections were fixed with acetone, incubated with anti-connexin 43 antibody (EMD Millipore, Billerica, MA; 1:200 dilution) and anti-cardiac troponin antibody (Abcam, Cambridge, United Kingdom; 1:100 dilution), and then stained with Alexa Fluor 568 anti-mouse antibody (Invitrogen, Carlsbad, CA; 1:500 dilution) and Alexa Fluor 488 anti-rabbit antibody (Invitrogen, Carlsbad, CA; 1:500 dilution). Nuclei were visualized with fluorescent Hoechst 33342. Slides were imaged using a Leica DM6000B (Leica Microsystems Inc, Buffalo Grove, IL) immune-fluorescent microscope at 20x magnification and analyzed using a proprietary Leica software suite. Gap junction densities in the hydrogel groups were measured in the injection regions

as well as in a region on the LV free wall adjacent to the injection. A representative area within the LV free wall was selected for analysis in all other groups. Gap junction density was calculated as:

$$Gap\ junction\ density = \left[\frac{Area\ of\ connexin43\ positive\ staining}{\#\ of\ nuclei}\right]$$

2.2.9 Statistical analysis

A one-way analysis of variance (ANOVA) test with a Dunnet post-hoc test analysis was used to detect differences among groups for the pressure measurements. ANOVA with Newman-Keuls post-hoc analysis was used to detect differences in LV activation time in healthy hearts, in dispersion of APD and repolarization at 20%, as well as in gap junction densities between groups. A t-test was used to compare LV activation times of cryoinfarcted heart treatment groups. Correlation analysis was performed to determine whether LV activation time, dispersion of 20% repolarization and gap junction density depended on the percent muscle within the hydrogel injection. All measurements were reported mean ± SEM, unless otherwise specified. Significance was accepted at $p < 0.05$.

2.3. Results

2.3.1 Hemodynamic measurements

Hemodynamic measurements were performed at baseline to ensure normal cardiac behavior prior to the injection surgery and also as a comparison between injected and non-injected hearts prior to optical mapping. The

average baseline LV EDP and PSP in the rat hearts included in the study was 8.31 ± 1.02 mmHg and 96.02 ± 11.8 mmHg respectively, signifying normal cardiac function. Measurement of the hemodynamic properties acutely after injection demonstrated no statistical differences in LV EDP and PSP between injected hearts and respective non-injected controls, indicating no acute changes in hemodynamic parameters upon injection of the biomaterials (Table 2.1).

Table 2.1. Hemodynamic data.

	Baseline		Post-injection	
	EDP (mmHg)	PSP (mmHg)	EDP (mmHg)	PSP (mmHg)
None - Healthy	9.03 ± 0.47	99.87 ± 3.40	8.37 ± 0.45	81.27 ± 4.45
Saline - Healthy	7.96 ± 0.34	95.35 ± 2.16	8.06 ± 0.45	74.50 ± 5.39
Hydrogel - Healthy	8.05 ± 0.41	91.10 ± 9.15	8.57 ± 0.45	73.88 ± 8.23
None - Cryoinfarct	8.16 ± 0.31	95.94 ± 3.16	7.94 ± 0.37	95.82 ± 3.09
Hydrogel – Cryoinfarct	8.34 ± 0.29	97.82 ± 2.44	8.38 ± 0.35	82.06 ± 5.04

2.3.2 Optical mapping and histological analysis

Immediately after post-injection hemodynamic measurements the hearts were excised and arrested. Electrical propagation in the isolated rat heart was studied using a Langendorff, aorta-perfused setup. Fluorescent images of the epicardial surface of the hearts were obtained to verify the perfusion of the dye over the entire healthy epicardium; the dye did not perfuse the cryoinfarct region (Figure 2.2A & 2.2E, respectively). Histological analysis was performed upon completion of the optical mapping study to verify the presence and distribution of material in the injection region. In Figure 2.2B & 2.2F the hydrogel injection region is clearly visible as denoted by the black arrows. Non-injected

and saline-injected healthy heart slices are shown for comparison (Figure 2.2C & 2.2D, respectively). In Figure 2.2F and 2.2G the cryoinfarct is visible and denoted by red arrows for hydrogel-injected and non-injected hearts, respectively.

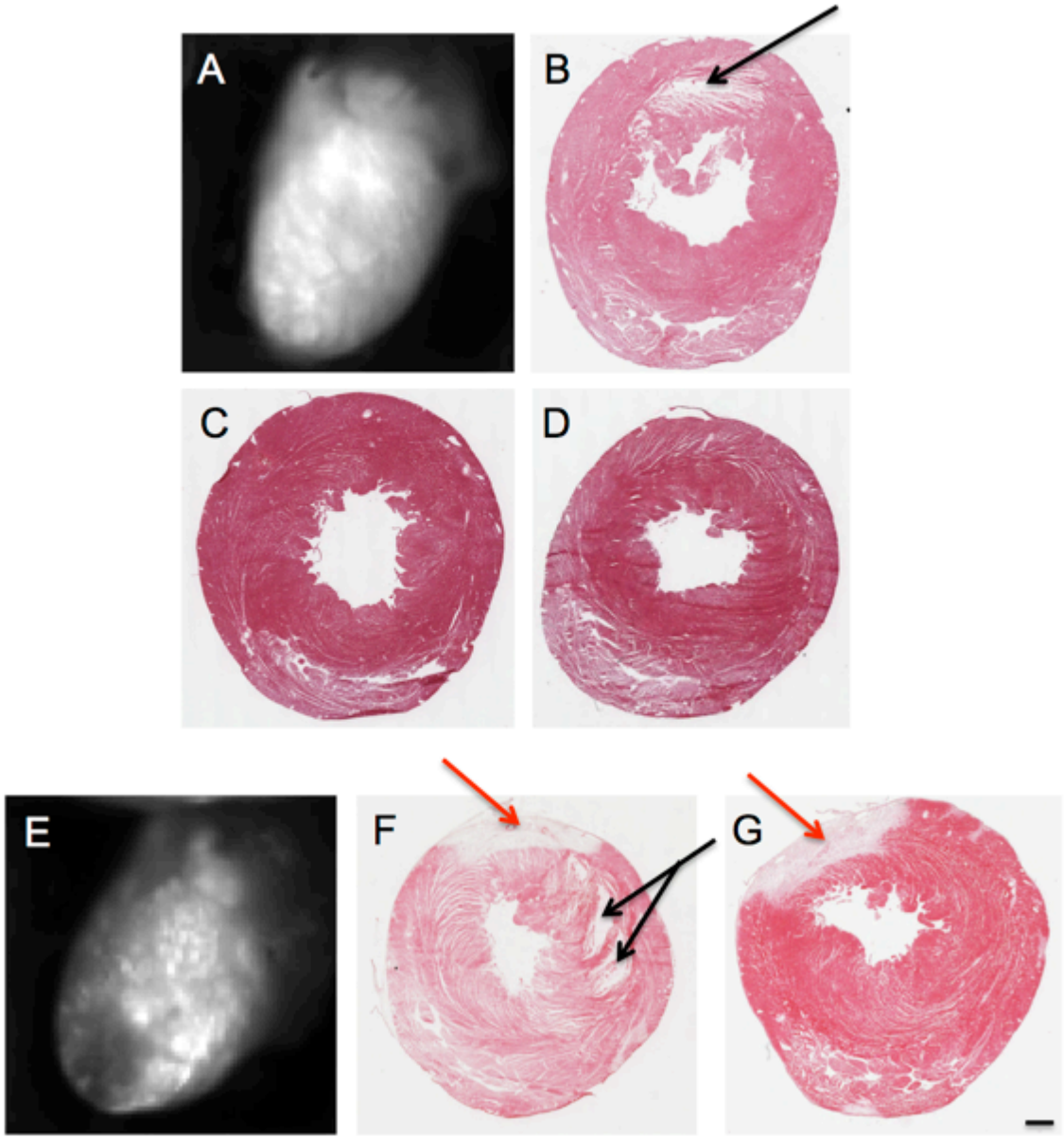

Figure 2.2. Histological analysis. (A) Representative fluorescent image of the di-4-ANNEPS-perfused healthy heart. Note: dye perfusion over the entire epicardial surface. Representative slides stained with H&E for histological assessment of (B) hydrogel-injection (C) no-injection (D) and saline-injection after optical mapping. A black arrow denotes the hydrogel in the myocardium. All photomicrographs are taken at 1X and scale bar is 1mm. (E) Representative fluorescent image of the di-4-ANNEPS perfused cryoinfarcted heart. Note: dye perfusion over the entire epicardial surface except the cryoinfarct. Representative slides stained with H&E for histological assessment of (F) hydrogel-injection (G) and no-injection after optical mapping. Red arrows denote the cryoinfarction.

2.3.3 Action potential propagation

The timing of hydrogel injection was varied to generate a wide range of interstitial spread. For initial analysis all hydrogel-injected hearts were combined into one group. To detect any alterations in action potential propagation due to the presence of the hydrogel, LV activation maps were constructed to depict action potential propagation. Representative color maps indicate that LV activation times were higher in the healthy hydrogel-injected hearts compared to non-injected and saline-injected, particularly towards the base (Figure 2.3A). When including all degrees of hydrogel spread, on average injection of the hydrogel led to a significant increase in total LV activation time, 5.2 ± 0.4 ms compared to saline 3.5 ± 0.4 ms ($p < 0.01$) and no-injection 4.1 ± 0.2 ms ($p < 0.05$), indicating slowed action potential propagation across the LV (Figure 2.3B). To determine whether similar increases in LV activation time would occur following hydrogel injection in infarcted hearts, the hydrogel was injected into the borderzone one week following cryoinfarction surgery. There was no difference in cryoinfarct size between hydrogel-injected (22 ± 3%) and non-injected controls (18 ± 2%). Again significantly higher LV activation times were observed following hydrogel injection, 6.1 ± 0.4, compared to no-injection, 4.6 ± 0.3 ($p < 0.02$; Figure 2.3C & 2.3D), revealing slowed action potential propagation through hydrogel-injected tissue bordering an infarct.

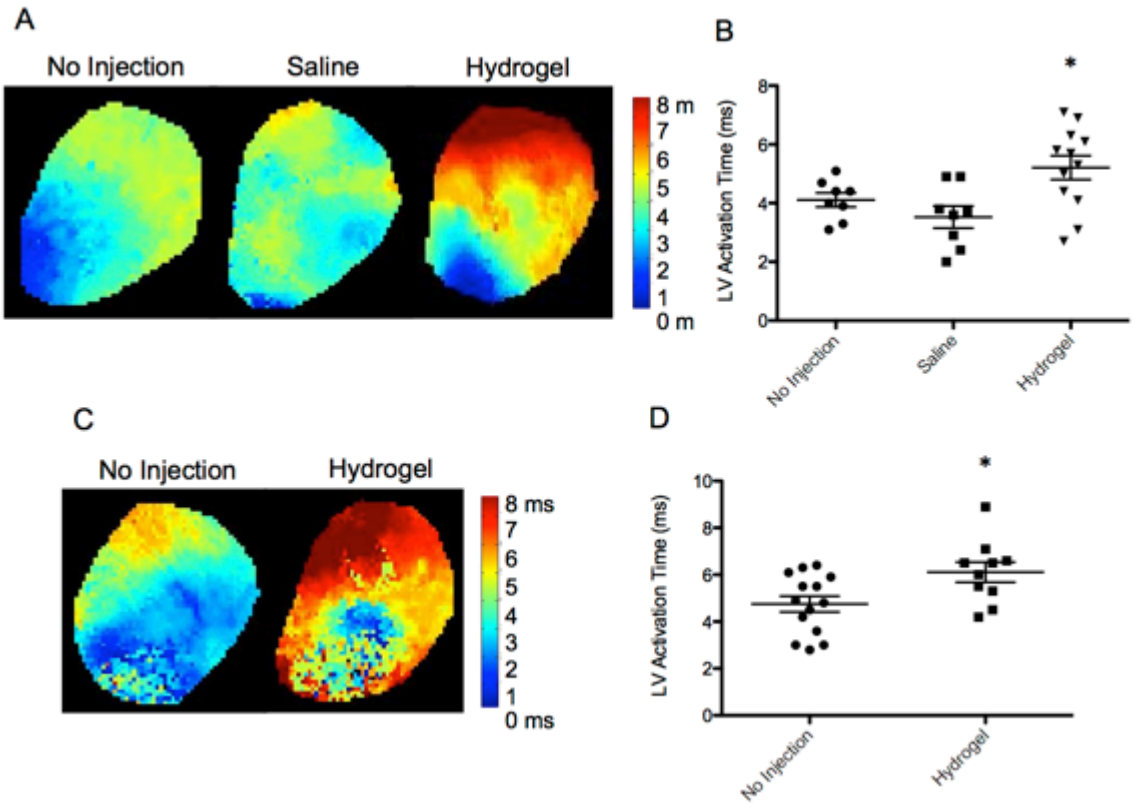

Figure 2.3. LV activation time. (A) Representative activation maps of the LV free wall of healthy hearts demonstrate high LV activation time at the base in the hydrogel injected group indicating slowed action potential propagation when compared with saline and no-injection. (B) Total LV activation time was significantly greater in the hydrogel injected group compared to all other groups (*$p < 0.01$). (C) Greater LV activation time was also found in cryoinfarcted hearts injected with a hydrogel compared to no-injection. (D) Moreover, total LV activation time was significantly greater in cryoinfarcted hearts in the hydrogel group compared to no-injection (*$p < 0.02$).

To investigate the effect of hydrogel spread on action potential propagation, the amount of myocardium penetrating the hydrogel in each heart was determined histologically. High and low percent muscle within the hydrogel was the metric used to define high and low interstitial spread, respectively. Representative images of hydrogels exhibiting low and high interstitial spread are shown in Figure 2.4A-D. The percent muscle within the

hydrogel was then compared to the LV activation time for each heart. There was a significant correlation between the percent of muscle within the hydrogel injection and the LV activation time for healthy ($r = -0.78$; $p < 0.01$; Figure 2.4E) and cryoinfarcted ($r = -0.93$; $p < 0.0001$; Figure 2.4F) hearts. Specifically, lower LV activation times, comparable to non-injected hearts, occurred in hearts with high percent muscle within the hydrogel (>35%), whereas when the percent muscle in the hydrogel was low (<35%), the LV activation times were higher, indicative of slowed conduction. The combined distribution for all hydrogel injected hearts is shown in Figure 2.4G ($r = -0.85$; $p < 0.0001$). We compared the hydrogel volume in each heart to the activation time and found no correlation ($R^2 = 0.03$). Thus, injection of highly spread hydrogels caused no change in action potential propagation across the LV, but propagation was slowed following injection of minimally spread hydrogels.

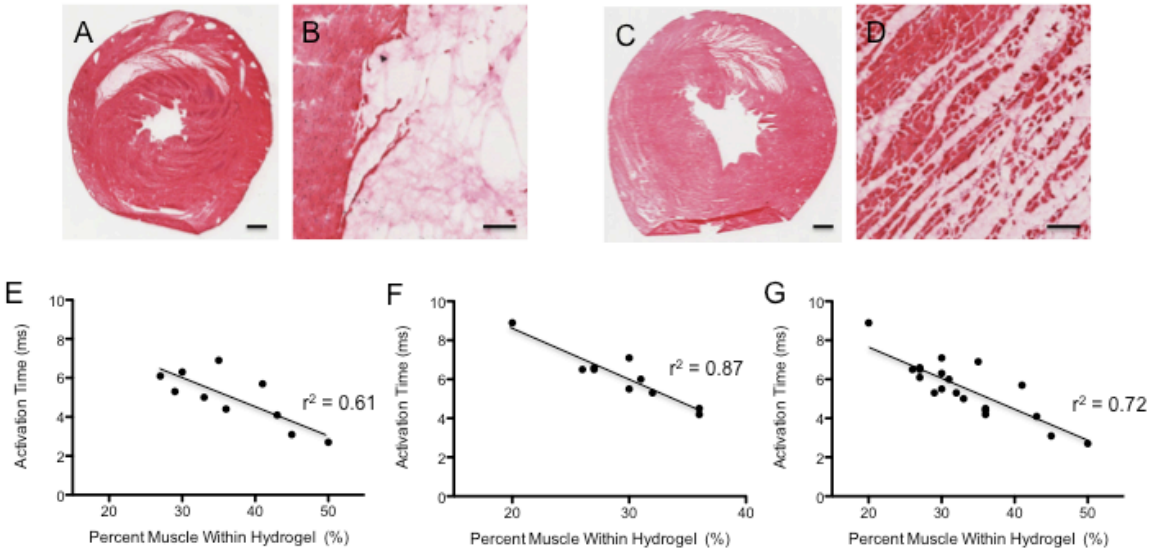

Figure 2.4. Hydrogel interstitial spread. Representative images of myocardium injected with hydrogels exhibiting (A-B) low and (C-D) high interstitial spread. Hearts with an average of 27% and 50% percent muscle within the hydrogel are shown in A and C, respectively. Increased percent muscle within the hydrogel resulted in lower activation time in both (E) healthy ($r = -0.78$; $p < 0.008$) and (F) cryoinfarcted ($r = -0.93$; $p < 0.0001$) hearts. (G) The percent muscle within the hydrogel ranged from 20-50% across all hearts ($r = -0.85$; $p < 0.0001$). Scale bar: 1 mm (A & C); 100 μm (B & D).

2.3.4 Changes in other electrophysiological parameters

Dispersion in action potential duration (APD) and repolarization can increase the likelihood for reentrant arrhythmias by creating local disturbances in the tissue [75]. Measurements of action potential characteristics such as APD at 20%, 50% and 80% repolarization levels demonstrate no significant changes in APD_{20}, APD_{50} and APD_{80} by the injection of the hydrogel in healthy or cryoinfarcted hearts (Table 2.2). There were similarly no differences in dispersion of APD_{20} between groups in healthy hearts (Figure 2.5A). However, there was a trend for increased dispersion at 20% repolarization in the hydrogel-injected healthy hearts compared to the saline and no injection groups ($p = 0.06$; Figure

2.5B). Color maps were created to visualize the time of 20% repolarization at each pixel on the epicardium, which revealed increase 20% repolarization times at the base of some hydrogel-injected healthy hearts (Figure 2.5C). Furthermore, a higher percent of muscle within the hydrogel injection significantly correlated with a lower dispersion of 20% repolarization ($r = -.0.67$; $p < 0.03$). This indicates that the degree of interstitial spread of the hydrogel also impacted the dispersion of repolarization in healthy hearts. As described in the methods section, the absence of dye perfusion in the cryoinfarct resulted in increased variability in repolarization times and thus these values were not reported. Specifically, a highly spread hydrogel did not create heterogeneities in action potential characteristics, while such variability was observed following injection of a hydrogel with low spread.

Table 2.2. Action potential duration data.

	APD20	APD50	APD80
None - Healthy	11.9 ± 0.3	22.1 ± 0.8	47.9 ± 1.5
Saline - Healthy	11.2 ± 0.3	20.5 ± 0.6	45.1 ± 1.6
Hydrogel - Healthy	11.9 ± 0.2	22.2 ± 0.5	48.0 ± 1.2
None - Cryoinfarct	13.7 ± 0.4	26.8 ± 1.0	54.3 ± 1.8
Hydrogel - Cryoinfarct	15.1 ± 0.4	30.2 ± 1.0	57.6 ± 1.4

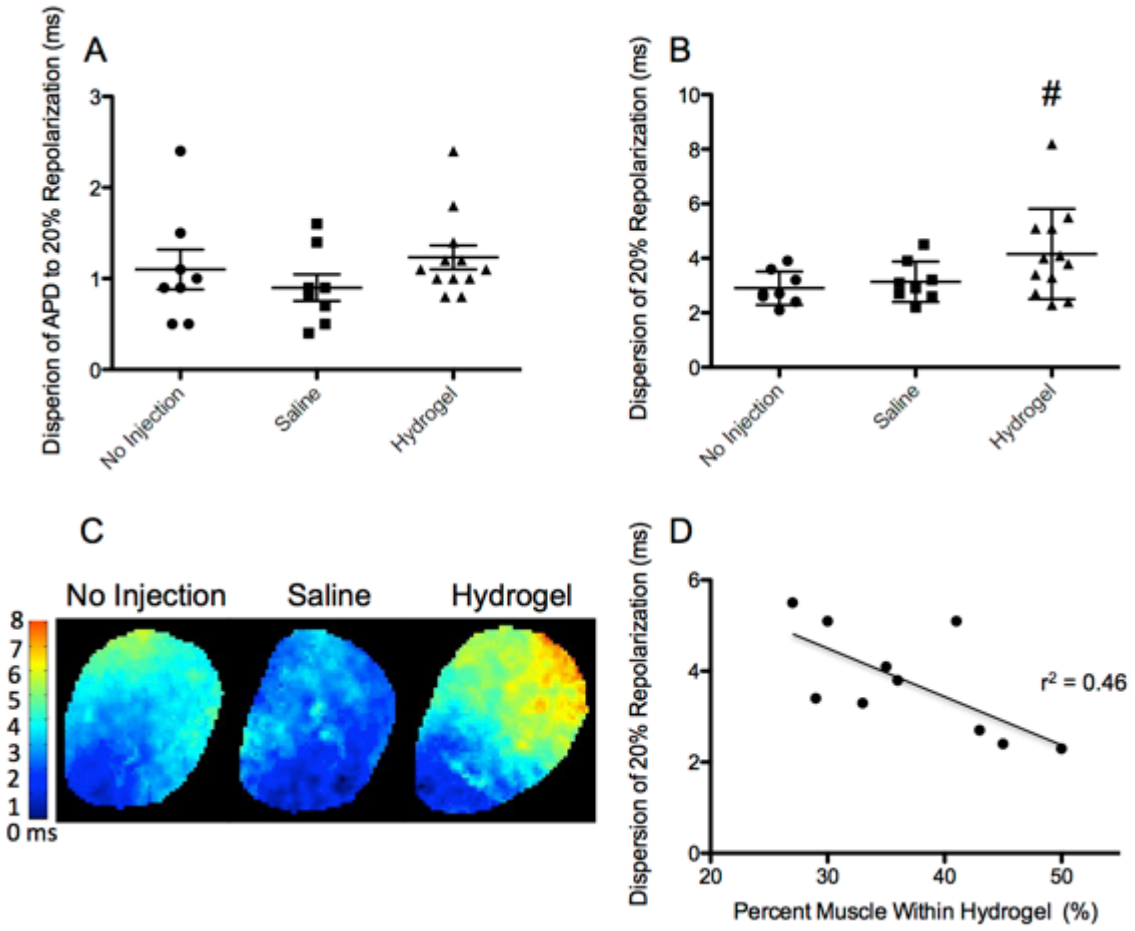

Figure 2.5. Dispersion of APD and repolarization. (A) Dispersion of APD at 20% repolarization revealed no significant differences between groups in healthy hearts. (B) While more variability was visible in 20% repolarization values in hydrogel-injected hearts compared to no-injection and saline-injection, differences were not significant (#p = 0.06) (C) Color maps depicting the time of 20% repolarization at each pixel of the LV free wall show slightly greater dispersion in hydrogel-injected hearts. (D) The increased dispersion in 20% repolarization times correlated significantly with the percent muscle in the hydrogel ($r = -0.67$; $p < 0.03$).

2.3.5 Impact of polymer interstitial spread on gap junction density

To better understand the mechanism behind the effect of hydrogel interstitial spread on action potential propagation, the gap junction densities (Cx43+ area per nuclei) within the hydrogel injection and a region adjacent to

the hydrogel were quantified. For comparison, gap junction density within a representative area of the LV free wall was quantified for non-injected and saline-injected groups. Again including all degrees of hydrogel spread, when compared to all other groups, gap junction densities within the hydrogel injection site were significantly lower on average for both healthy (Figure 2.6A; $p < 0.0005$) and cryoinfarcted (Figure 2.6B; $p < 0.0001$) hearts. Comparison of hydrogel spread and gap junction density revealed that an increase in the percent muscle within the hydrogel injection in healthy and cryoinfarcted hearts correlated with an increase in gap junction density ($r = 0.66$; $p < 0.005$; Figure 2.6C). Gap junction densities within the highly spread hydrogels were close to the densities observed in non-injected hearts, yet were lower within the less spread hydrogels. A representative image of the 'normal' gap junction density of non-injected/saline-injected hearts is shown in Figure 2.6D along with the densities in the injection site of a hydrogel with high and low interstitial spread (Figures 2.6E and 2.6F, respectively).

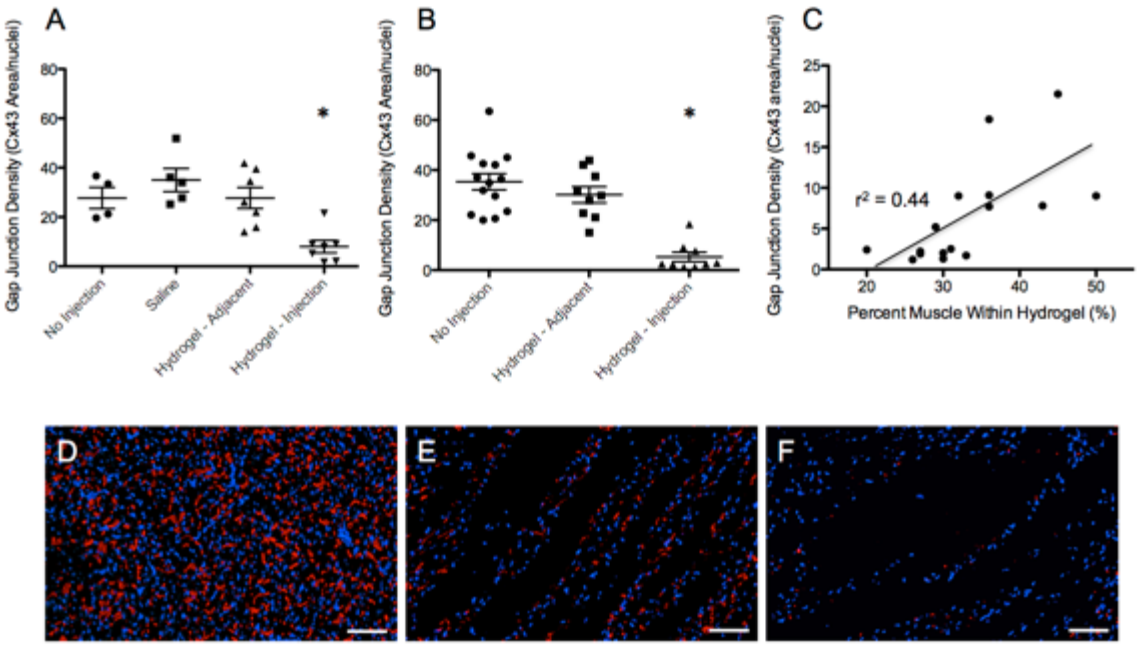

Figure 2.6. Gap junction density. (A) Gap junction densities (Cx43+ area (μm^2)/number of nuclei) within the hydrogel injection site of (A) healthy (*$p < 0.0005$) and (B) cryoinfarcted (*$p < 0.0001$) were significantly lower than all other groups. Density of gap junctions was normalized to cell number to take into account blank regions containing the hydrogel. (C) Increased percent muscle within the hydrogel in healthy and cryoinfarcted hearts resulted in increased gap junction density ($r = 0.66$; $p < 0.005$). Representative images of (D) non-injected, (E) highly spread hydrogel-injected and (F) minimally spread hydrogel-injected hearts display the variability in gap junction (red) density. Scale bar: 100 μm.

2.4 Discussion

With the rapid increase in potential injectable biomaterial therapies for myocardial repair after infarction, the question of safety of biomaterial injection is an important issue and pre-requisite to clinical translation. In this study the important, but often overlooked issue of electrophysiological impact of hydrogel injection during these procedures was studied. Utilizing optical mapping, we were able to assess the acute effect of intramyocardial injection of a hydrogel on the global electrophysiological parameters – activation time, APD, and

repolarization. Most importantly, we found that injection of a hydrogel with high interstitial spread did not affect LV activation time, while injection of a hydrogel with low interstitial spread significantly increased this parameter. Using the metric of 'percent muscle within the hydrogel' to quantify hydrogel spread, we found that a hydrogel injection containing >35% muscle did not increase the LV activation time compared to non-injected hearts (Figure 2.4). Similarly, these highly spread hydrogels did not increase dispersion of repolarization (Figure 2.5D). Thus the electrophysiological impact of the minimally spread hydrogel injection was through delaying action potential propagation across the LV, rather than altering the action potential morphology.

A potential mechanism by which the injection of the hydrogels with low interstitial spread caused slowed action potential propagation may be the disruption of gap junctions between the conductive cardiomyocytes. Disturbance in gap junctions has been associated with induction of harmful ventricular arrhythmias in small animal studies [76]. Here we show that cardiac muscle within the hydrogels with low spread had a reduced gap junction density compared to muscle penetrating highly spread hydrogels. There was likely a combination of factors that lead to the rapid reduction of gap junction density following hydrogel injection. First, connexin43 is rapidly turned over in healthy rat hearts, with a half-life of just over one hour [77]. Furthermore, one response of cardiomyocytes under lethal and sub-lethal stress is a reduction in gap junction density [77]. Thus under the stress of muscle fibers being physically separated by the hydrogel, the cardiomyocytes in the injection region may have initiated a

survival response that included reducing gap junction density. In combination with the already rapid connexin43 turnover rate this could result in low gap junction densities just twenty minutes after hydrogel injection. Gap junction density in the myocardium adjacent to the injection region was unaffected.

The clinically relevant question is whether or not slowing of action potential propagation and reduced gap junction density caused by injection of a hydrogel with low interstitial spread would lead to ventricular arrhythmias. Van Rijen et al. showed that through conditional deletion of connexin43 (Cx43) in adult mice, >70% reduction in Cx43 protein expression was required to significantly slow conduction velocity (CV) and enhance arrhythmogenesis [78]. Even with a 50% reduction in Cx43 expression, CV was maintained at normal levels. In our study, when the hydrogel spread was low enough to cause high LV activation time (<35% muscle in the injection, Figure 2.4), gap junction densities inside the hydrogel were on average >70% reduced compared to healthy myocardium (Figure 2.6). This suggests that the disruption may be enough to enhance arrhythmogenesis. In contrast, in hearts injected with highly spread hydrogels that did not increase global activation time (>35% muscle in the injection, Figure 2.4), gap junction densities within the injection tended to be <70% reduced (Figure 2.6), reducing the risk for arrhythmogenesis based solely on gap junction density.

The gap junction density and distribution seen in the less spread hydrogels (Figure 2.6E) also looked remarkably similar to that observed by Van Veen et al. in mice with severe interstitial fibrosis caused by aging and a 50% knockdown of

the Scn5a sodium channel [79]. Fibrosis has been indicated as a substrate for reentrant arrhythmia in patients with dilated cardiomyopathy [80]. This and other studies [81] have indicated the architecture of the fibrosis as a factor in whether or not conduction block was observed. Small amounts of interstitial fibrosis did not appear to disrupt lateral cell-cell connections, mitigating the generation of anisotropic conduction [80, 81]. Thus, based on comparable disruption of cell-cell coupling, the hydrogel with low spread may act as a substrate for arrhythmia in a similar manner to severe fibrosis. Furthermore, it is also possible that the degree of interstitial spread impacted the stiffness of the hydrogel, which may have contributed in part to the observed differences in conduction. Finally, it is now widely accepted that cardiac electrical conduction is a function of not only the cellular conductivity but also the conductivity of the extracellular space [82, 83]. The presence of a hydrogel with different electrical properties than the native extracellular matrix could affect the local extracellular conductivity, though this warrants further study. All these studies suggest that distribution in the tissue is an important factor to consider when designing injectable biomaterial therapies for MI. Using this information, the direct influence of hydrogel injection on arrhythmia induction should be studied in future work.

Controlling how much hydrogels spread in the tissue is complex due to contribution of several factors. For example, gelation mechanism, injection time and material concentration could all be modified to achieve varying interstitial spread. In this study, we varied injection time of a model PEG hydrogel to allow for a wide range in the degree of hydrogel spread in the tissue. We chose a PEG

hydrogel with a polymer content of 50 mg/mL to create a gel with mechanical properties within the range of other commonly injected material for biomaterial MI therapy [84, 85]. Selecting a concentration in the middle of the range allowed access to both high and low amounts of interstitial spread. Other material properties could however be modulated to achieve differences in interstitial spread. For example, materials such as alginate can be crosslinked *in situ* following intracoronary infusion, which leads to greater interstitial spread of the material in the tissue. In fact both large animal studies [11] and initial clinical trials [26, 27] show no evidence of arrhythmias with this material. Moreover, other materials with higher interstitial spread such as a myocardial matrix hydrogel have not been shown to elicit arrhythmias in large animal models [16]. In contrast, other studies using materials, which appear to have lower interstitial spread, have had potential indicators of arrhythmias. Injection of a different alginate formulation into a chronic canine heart failure model (microembolization) was non-arrhythmogenic in the long-term; however, one hydrogel-injected dog died from ventricular fibrillation shortly after the injection [86]. The histological images of the injected dog hearts reveal fairly low interstitial spread [86], which may have contributed to the rhythm disturbance in the animal that died post-injection. Another fast gelling hydrogel system, a fibrin-alginate composite, was injected into infarcted porcine myocardium [87]; the authors noted that mortality was higher in hydrogel-injected animals, which they believed warrants further study into the impact of the hydrogel on electrical activation patterns. While the exact cause in both studies cannot be definitively

determined given even needle penetration into the myocardium can cause ventricular arrhythmias, these studies along with the results of the current study, suggest that the link between material properties and arrhythmia vulnerability should be continued to be carefully studied prior to clinical translation. This study only investigated the impact of hydrogels, but micro- and nano-particles are another commonly used form of biomaterial for treating cardiovascular disease [7]. These particles typically spread well through the interstitial space and consequently should, based on the results of the current study, provide minimal disruption to cardiac conduction.

Previous studies have shown that the infarct already has slowed or disturbed conduction [68], so injection of a hydrogel into the infarct may not cause conduction abnormalities superseding the effects of infarction injury. In a study by Singelyn et al., arrhythmogenesis was assessed in rat MI model one week after injection of a myocardial matrix hydrogel in the infarct region and there were no increases in incidences of arrhythmia [15]. Similar results were seen after both intracoronary and intramyocardial injection of different hydrogels in a porcine infarct [11, 25]. On the other hand, the borderzone contains electrically viable and vulnerable tissue, so injection or spread of material into this region could be a concern. Herein, we injected a hydrogel first in viable myocardium to specifically understand the effect of material injection and interstitial spread on myocardial tissue containing viable myocytes. Subsequently we injected the hydrogel into the borderzone of an infarct to determine if viable myocardium bordering the injury was susceptible to the same

alterations in action potential propagation. One limitation of this study is the use of a rodent model instead of a large animal model; this was chosen given the high number of animals needed to complete a thorough investigation of hydrogel spread on conduction. In addition, it is acknowledged that the cryoinjury model is not as physiologically relevant as an occlusion model, but it was selected because it allowed dye perfusion of the viable myocardium. Since the dye is introduced to the tissue through retrograde perfusion total occlusion and ischemia-reperfusion models of MI create permanent damage to the vessels preventing sufficient dye perfusion for imaging. The cryoinjury model also enabled control over the location of the infarct and was initiated on the epicardial surface, facilitating consistency across the hearts and clear visualization with the *ex vivo* imaging. Despite having some limitations the cryoinjury model has been employed in large animal models to eliminate the influence of innate coronary collateral branching, to create reproducible infarct sizes and to generate a defined epicardial border [88-90]. In both healthy and cryoinfarcted rat hearts, injection of a highly spread hydrogel into viable myocardium resulted in no change to the LV activation time compared to non-injected controls, while hydrogel injections with low spread increased LV activation time shortly after injection.

In this acute study, PEG was selected due to its bio-inert characteristics in order to isolate and model the impact of the physical presence of a hydrogel on heart electrophysiology. The hydrogel-injected hearts were excised within one hour of injection because a major concern with arrhythmias is in the acute phase

following injection. Our study suggests that it is ultimately important how the injected material resides within the myocardium. Thus, negative initial impacts on electrophysiology can be potentially avoided by designing the material to spread well within the myocardium, and/or injecting into solely the infarct instead of the borderzone. Given the difference in the size and heart rate of the human heart compared to a rodent heart, it will, however, be important to study these parameters in large animal models. Moreover, at later time points, degradation of the biomaterial and resulting cell infiltration will both contribute to its level of risk of becoming a substrate for arrhythmia, and therefore, it is also important to continue to study the risk of arrhythmias for each individual biomaterial overtime prior to use in patients.

Chapter 2, in part, is a reprint of the material as it appears in the submission to Acta Biomaterialia 2015. Sophia L. Suarez, Aboli A. Rane, Adam Muñoz, Adam T. Wright, Shirley X. Zhang, Rebecca L. Braden, Adah Almutairi, Andrew D. McCulloch, Karen L. Christman. Intramyocardial injection of hydrogel with high interstitial spread does not impact action potential propagation. 2015. The dissertation author was the primary investigator and author of this paper.

CHAPTER THREE:

Tunable Protein Release from Acetalated Dextran Microparticles: A Platform for Delivery of Protein Therapeutics to the Heart Post-MI

3.1 Introduction

Cardiovascular disease is the leading cause of death in the United States with the majority of deaths resulting from heart failure post-myocardial infarction (MI) [2]. Current therapies for MI patients ameliorate symptoms and prolong life, but do not treat the injury at the source. Recently, injectable biomaterials (hydrogels and microparticles) have been used in the development of experimental therapies [5, 6, 91, 92]. In contrast to current gold-standard treatment methods, biomaterial-based therapies have the potential to initiate healing at the site of injury. One way of initiating healing is through sustained release of therapeutic agents that promote angiogenesis and positive remodeling. Biomaterials can protect biological cargo from rapid degradation and facilitate delivery over longer time frames than bolus injections.

Several materials have been employed to deliver therapeutic agents to the heart via intramyocardial injection of microparticles [93] [28-30, 32, 38, 94, 95]. These studies demonstrated encouraging results that support the potential for microparticle-based therapies: however, no single therapeutic achieved restoration of function in the heart post-MI. This is most likely due to the complexity of the healing process in the heart, which will require reducing fibrosis, restoring blood flow, and promoting cellular infiltration. Previous studies using therapeutics to restore blood flow highlight the importance of the time and order of therapeutic agent presentation [53, 63]. While not yet thoroughly investigated, it is likely that other healing processes needed for full restoration of

heart function post-MI will also require therapeutics delivered over specific time frames.

Several promising approaches for tunable delivery of growth factors have been developed, but each is limited to a specific category of payloads or is difficult to manipulate to provide more than two rates of release and the systems are not designed for the mildy acidic environment of an infarct (pH 6.0-7.0) [61, 62]. Acetalated dextran (AcDex) microparticles allow tunable release, have the potential to deliver charged, uncharged, hydrophilic, and hydrophobic molecules and release the encapsulated therapeutics in response to acidic pH [54, 60, 96-103]. Tuning release rates from AcDex is straightforward, requiring only variation in the reaction time when acetalating to vary the ratio of cyclic to acyclic acetals; cyclic acetals degrade slower than acyclic acetals. This property is unique compared to the materials previously tested in the heart, which have defined release rates in the ischemic environment. Furthermore, payload release from AcDex particles is minimal in neutral pH conditions but is facilitated in acidic conditions. While PLGA degradation rate can also be catalyzed in acidic environments, the time frame of degradation is long (many weeks) at the pH found in ischemic tissue [104]. The pH must be low (~2) to see appreciable acceleration [105].

AcDex is synthesized by acetalation of the alcohols on the dextran backbone with vinyl ethers in the presence of an acid catalyst. Acetal functionalization of dextran changes the solubility of the polymer from hydrophilic to hydrophobic, allowing AcDex to encapsulate hydrophobic or

hydrophilic payloads via a single oil-in-water (o/w) or double water-in-oil-in-water (w/o/w) emulsion, respectively. In contrast, protein-based microparticles such as gelatin can only be used to deliver hydrophilic payloads. Previous work with AcDex has shown tunable release of a number of payloads including ovalbumin, imiquimod, horseradish peroxidase, rapamycin, plasmid DNA, siRNA and campthomecin [54, 60, 96-103]. These payloads were encapsulated in particles ranging from 100 nm to 10 μm and released at pH 5.0 and 7.4. The size of the particles and target pH in these studies were designed for cellular uptake and lysosomal degradation for immunotherapy, gene delivery and pulmonary drug delivery. To use AcDex for intramuscular delivery in ischemic conditions, particles need to be designed with a diameter of 20-100 μm to avoid cellular uptake and maximize interstitial retention time,[106] a payload release longer than 1-2 days to initiate relevant tissue regeneration processes, and a desired degradation rate in more mildly acidic conditions as seen in ischemic tissue (pH 6.0-7.0). Although not yet tested *in vivo* AcDex is predicted to have mild degradation products, including dextran, which is used in several FDA approved products, and trace amounts of acetone and methanol.[102]

In this study we hypothesize that AcDex microparticles can be designed as a delivery vehicle for therapeutics to the heart post-MI. In mildly acidic conditions (pH 6.0-7.0), tunable release between days and weeks is shown with a model protein and a sensitive growth factor, bFGF. Furthermore, bFGF maintained activity after encapsulation and release. The particles are shown to

be injectable into the heart where they are retained in the extracellular space and elicit an acute inflammatory response that resolved within one month.

3.2 Methods

3.2.1 Materials

Sunsoft surfactant (818SK) was purchased from Taiyo Int. Inc. (Minneapolis, MN). Dextran (from Leuconostoc mesenteroides; average MW 9,000-11,000), myoglobin (from equine skeletal muscle), poly(vinyl alcohol) (PVA; average MW 30,000-70,000), bovine serum albumin (BSA; Fraction V), and heparin sodium salt (from porcine intestinal mucosa) were purchased from Sigma-Aldrich. Alexa Fluor 594-NHS and basic fibroblast growth factor (bFGF) were purchased from Life Technologies. All other reagents and materials were purchased from Sigma, Fisher or Acros and used as received.

3.2.2 Methods

^{1}H NMR spectra were acquired on a Bruker npa600 and processed using MestreNova software. NMR was used to determine the cyclic:acylic acetal ratio of all synthesized AcDex as previously described[107]. Briefly, AcDex was dissolved in a stock solution of D_2O and DCl and then analyzed. The methanol (3.34 ppm) and acetone (2.08 ppm) peaks were integrated and compared under the assumption that degradation of only acyclic acetals would yield a 1:2 ratio of methanol:acetone, and additional acetone peak area results from cyclic acetal degradation[102]. GPC was conducted by the UCSB Material

Research Laboratory using a Waters Alliance HPLC System with a Waters 2414 Differential Refractometer, Viscotek I-MBHMW and I-Series Mixed Bed High Molecular Weight columns. DMF containing 0.01% of LiBr was used as the eluent (flow rate 1 mL/min). Polystyrene standards were used for calibration. The primary emulsion for all microparticles was created using a QSonica Q700 with Cup Horn sonicator. Microparticles were prepared with a membrane emulsifier from Micropore Technologies. Microparticle size was determined using the Beckman Coulter Multisizer 4. Scanning electron microscopy (SEM) was used to visualize intact particles and particle degradation at various time points throughout the protein release studies. Particles suspended in water were dried on a silicon wafer and imaged using an Agilent 8500 FE-SEM. All fluorescence measurements were performed using a fluorometer (FL-1065; Horiba Jobin Yvon).

3.2.3 Synthesis of Acetalated Dextran with High and Low Catalyst

Acetalated dextran was prepared as described previously.[107, 108] Briefly, a flame-dried round-bottom flask (50 mL) was purged with N_2. Dextran (M_w = 10,000 g/mol, 1.00 g, 0.095 mmol) and anhydrous DMSO (10 ml) were added and stirred until dextran was completely dissolved. 2-Methoxypropene (3.4 mL, 37 mmol) was added via syringe, followed by pyridinium *p*-toluenesulfonate (15.6 mg, 0.062 mmol). The system was maintained under positive N_2 pressure and then sealed. At designated time points (2, 5, 10, 15, 30, 60, 120, 180 1200 and 1500 minutes) an aliquot (1 mL) was removed and quenched with triethylamine (100 μL TEA/1ml reaction solution, 7 mmol). The

solution containing the modified dextran was precipitated in Millipore H_2O (pH 8; 1:10 reaction solution:water). The product was isolated by centrifugation (5 000 x g; 10 min). The resulting white pellet was washed with Millipore H_2O (pH 8) by vortexing, centrifugation and removal of supernatant. The hydrated pellet was frozen and lyophilized overnight to remove residual water. The following day the pellet was resuspended in acetone and centrifuged (5 000 x g; 5 min) to separate out any impurities. The acetone solution was precipitated in Millipore H_2O (pH 8), washed, frozen and lyophilized as described above. The resulting product was a white fluffy powder. To access a wider range of cyclic:acyclic ratios, an identical experiment as described above was completed with one-third the catalyst pyridinium *p*-toluenesulfonate (5.2 mg, 0.021 mmol).

3.2.4 Large Scale Synthesis of Acetalated Dextran of Different Cyclic to Acylic Ratios

AcDex was prepared on a 10 g scale using the same mole ratios and concentrations as described in the low catalyst procedure above. The 10 g, scaled up reaction, was performed three times, but quenched at different time-points. A low amount of cyclic acetals on dextran (FAST degrading) was obtained by quenching at 30 minutes. A medium amount of cyclic acetals on dextran (MED degrading) was obtained by quenching at 60 minutes. A high amount of cyclic acetals on dextran (SLOW degrading) was obtained by quenching at 1200 minutes. The cyclic to acyclic ratios on the dextran were determined by ^{1}H NMR as described above.

3.2.5 Myoglobin Labeling and Encapsulation in Microparticles for Release Studies

Myoglobin (6 mg, 339 μM) was dissolved in carbonate-bicarbonate buffer (1mL, pH 8.98). Fluorosceneisocyanate (FITC; 3 mM) in dimethyl sulfoxide (DMSO; 35 uL) was added to the myoglobin solution while stirring. The FITC/myoglobin mixture was stirred for two hours protected from light at 25°C. Free dye was removed by repetitive washing with PBS pH 7.4 through a 3K MWCO Amicon spin filter until no measurable fluorescence was detected in the flow through.

Microparticles were prepared using a w/o/w double emulsion. For the organic phase FAST, MED or SLOW AcDex (630 mg; 10 wt%) was dissolved in dichloromethane (DCM; 6.3 mL) containing Sunsoft surfactant (126 mg; 2 wt%). The primary aqueous phase was composed of Tris buffer (10mM pH 8; 700 μL) with FITC-labeled Myoglobin (1.4 mg; 0.2 wt%) and bovine serum albumin (BSA; 14 mg; 2 wt%).

The organic and primary aqueous phases (9:1 volume ratio) were sonicated (30 seconds; 30% power) and then stirred (2000 rpm, 1 min) three times to generate the primary emulsion. The primary emulsion was injected (rate: 0.5 mL/min) through a 10 μm hydrophobic membrane into a secondary aqueous phase of Tris buffer (10 mM, 150 mL; pH 8) containing 1% poly(vinyl alcohol) (PVA) and stirred (1000 rpm). After the entire primary emulsion was injected, the newly formed particles were stirred in Tris buffer (10 mM, pH 8; 500 mL) with 1% PVA to evaporate the DCM. Following evaporation, the particles were washed three times with Tris Buffer (10 mM, pH 8; 50 mL) and once with Millipore H_2O (pH 8; 50 mL) by centrifuging the particles (5 x g, 5 min) and removing the supernatant.

Washed particles were frozen and lyophilized before release studies and characterization.

3.2.6 Myoglobin Release from Microparticles

Lyophilized myoglobin-loaded particles were suspended (20 mg/mL) in phosphate buffer saline (PBS; 1 mL) pH 6.0, 6.5 or 7.4 and placed on a rotating tube rack at 37°C. At designated time points, particles were centrifuged (12.1k g, 5 minutes) and supernatant (500 μL) was removed and replaced with fresh PBS of the same pH. The supernatant (400 μL) was mixed with DMSO (800 μL) to dissolve the Sunsoft surfactant and pipetted into a quartz fluorimeter cuvette. The solution was excited at 485 nm and emission at 524 nm was recorded and compared to a previously prepared standard curve for FITC-labeled myoglobin at the given pH. Protein release graphs were created to show percent released over time up to 100%. Complete (100%) release was defined as the amount of protein in solution once particles were fully degraded (ie. there was no pellet upon centrifugation and no particles were visible with SEM).

3.2.7 bFGF Labeling and Encapsulation in Microparticles for Release Studies

Basic fibroblast growth factor (bFGF; 0.1 μM) was dissolved in carbonate buffer (pH 9.0; 500 μL). While stirring on ice, Alexa594-NHS (1 μg) was slowly added to the bFGF solution (100 μL), and then stirred for one hour protected from light. After the conjugation procedure, the labeled bFGF was buffer exchanged into Tris buffer (10 mM) containing 5% trehalose and washed using a

10k Amicon spin filter until no measurable fluorescence was detected in the flow through.

Microparticles were prepared using a w/o/w double emulsion. For the organic phase FAST or SLOW AcDex (475 mg; 10 wt%) was dissolved in DCM (4.75 mL). The primary aqueous phase was composed of Tris buffer (10 mM pH 8; 250 μL) with Alexa594-labeled bFGF (1 μg) and heparin (1 μg). The remainder of the microparticle preparation was identical to that described in the model protein studies above.

3.2.8 bFGF Release from Microparticles

Lyophilized Alexa594-labeled bFGF-loaded particles were suspended (20 mg/mL) in PBS (1 mL) pH 6.0 or 7.4 and placed on a rotating tube rack at 37°C. At designated time points, particles were centrifuged (12.1k g, 5 minutes) and supernatant (800 μL) was removed and pipetted into a quartz fluorimeter cuvette. The solution was excited at 590 nm and emission at 617 nm was recorded and compared to a previously prepared standard curve for Alexa594-labeled bFGF. The supernatant was returned to the particle solution after measurement.

3.2.9 bFGF Encapsulation in Microparticles for the Activity Assay

Microparticles were prepared using a w/o/w double emulsion. Two batches of particles were created, one with Alexa594-labeled bFGF to determine the amount of growth factor to add to cells in the control group of

the activity assay, and one with unlabeled bFGF to provide supernatant for the activity assay.

For the organic phase FAST AcDex (285 mg; 10 wt%) was dissolved in DCM (2.85 mL). The primary aqueous phase was composed of Tris buffer (10 mM pH 7.6; 150 μL) with Alexa594-labeled bFGF (600 ng), plus Heparin (1.2 μg) and BSA (12 μg). The remainder of the microparticle preparation was identical to that described in the model protein studies above.

For the organic phase FAST AcDex (475 mg; 10 wt%) was dissolved in DCM (4.75 mL). The primary aqueous phase was composed of Tris buffer (10 mM pH 7.6; 250 μL) with or without bFGF (1 μg), plus Heparin (2 μg) and BSA (20 μg). The remainder of the microparticle preparation was identical to that described in the model protein studies above except that Tris buffer with and without PVA and Millipore H_2O were sterile filtered (0.22 μm) before use. All parts of the membrane emulsifier were sprayed with 70% ethanol immediately before use. In addition, the particles were stirred for only four hours to evaporate the DCM.

3.2.10 bFGF Release from Microparticles for the Activity Assay

For the study to determine the amount of growth factor to add to cells in the growth factor activity assay, the same procedure as the growth factor release study was performed at pH 6.0 over five days.

Particles with and without bFGF were suspended (60 mg/mL) in PBS (pH 6.0) and placed at 37°C on a shaker plate. After 24 hours, tubes were centrifuged to pellet particles and supernatant was removed and filtered

through a 0.22 μm filter. Removed supernatant was replaced with fresh PBS pH 6.0 and returned to 37°C. After an additional 24 hours, supernatant was removed and filtered.

3.2.11 bFGF Activity Assay

3T3 fibroblasts were seeded at 5,000 cells/well in a 24-well plate in growth media (DMEM, 10% FBS, 0.5% Pen-Strep; 1 mL). After 24 hours at 37°C under 5% CO_2, experimental conditions were applied. Growth media (GM; 1 mL; n=4) and low serum (DMEM, 2% FBS, 0.5% Pen-Strep; 1 mL) with fresh bFGF (LS + Fresh; 5 ng bFGF; n=5) were used as positive controls. Low serum (LS; n=5; 1 mL) and low serum with empty particle supernatant (LS + Empty; 250 μL supernatant; n=5) were used as negative controls. Low serum with bFGF supernatant was used as the experimental group (LS + Released; 5 ng bFGF in 250 μL supernatant; n=5). After 24 hours at 37°C under 5% CO_2, all media was removed and replaced with the same experimental conditions listed above including the bFGF (10 ng bFGF in 250 μL supernatant) and empty supernatant (250 μL supernatant) from the second day's release and an equivalent amount of fresh bFGF (10 ng bFGF). After 24 hours at 37°C under 5% CO_2, cells were trypsinized and counted with a hemocytometer.

3.2.12 Statistical Analysis

Statistical analysis was performed using PRISM. Results are presented as mean ± standard deviation. One-way analysis of variance (ANOVA) was used to

evaluate differences in cell number among all groups in the growth factor activity study. Bonferroni's correction was used to detect differences between groups. Significance was defined at $p<0.05$.

3.2.13 Empty Microparticles for *in vivo* Biocompatibility

For the organic phase FAST or SLOW AcDex (475 mg; 10 wt%) was dissolved in DCM (4.75 mL). The primary aqueous phase was composed of only Tris buffer (10 mM pH 7.6; 250 μL). The remainder of the microparticle preparation was identical to that described in the model protein studies above except that Tris buffer with and without PVA and Millipore H_2O were sterile filtered (0.22 μm) before use. All parts of the membrane emulsifier were sprayed with 70% ethanol immediately before use. In addition, the particles were stirred for only four hours to evaporate the DCM.

3.2.14 Intramyocardial Injections for *in vivo* Biocompatibility

All experiments were completed in accordance with the Institutional Animal Care and Use Committee (IACUC) at the University of California, San Diego and the American Association for Accreditation of Laboratory Animal Care.

Intramyocardial injections were performed in female Sprague Dawley rats (225-260 g) as previously described.[49] 75 μL of microparticles (FAST or SLOW, 20 mg/mL in saline) were injected into the LV free wall with a 27 G needle. Rats were divided into three time points (7, 14 or 28 days) and two groups (FAST and

SLOW; n=3 each). Animals were euthanized with an intraperitoneal injection of FatalPlus (Vortech Pharaceuticals; 400 μL) at designated time points to assess histopathology. The heart was resected, rinsed and embedded and fresh frozen in OCT freezing medium. Short axis cross-sections were taken every 350 μm from apex to base throughout each heart and stained with hematoxylin and eosin (H&E). An experienced histopathologist examined the slide for the presence of spindle, small mononuclear, large mononuclear, fibroblast and multinucleate giant cells and provided a score from 0 to 4 (none, minimal, mild, moderate, severe) [16].

3.3 Results

3.3.1 Preparation of Acetalated Dextran with Varying Degradation Rates

AcDex is synthesized by reacting dextran with vinyl ethers and an acid catalyst (Scheme 3.1); specifically, we use methyl vinyl ether and pyridinium *p*-toluenesulfonate as a catalyst.

Scheme 3.1. Synthesis of acetalated dextran (AcDex)

Previously it was demonstrated that the length of reaction time controls the amount of cyclic and acyclic acetals on the dextran backbone with a longer the reaction time yielding a higher amount of cyclic acetals.[102] Acetalation transforms water-soluble dextran into a hydrophobic polymer, and upon exposure to acid the acetals degrade causing the dextran to become water soluble. The cyclic acetals hydrolyze at a slower rate than the acyclic acetals, allowing for tunable solublization of the AcDex polymer based on the ratio of cyclic:acyclic acetals. The acetal content and ratio of cyclic:acyclic were determined by ^{1}H NMR after acid degradation of the purified polymer. The methanol (3.34 ppm) and acetone (2.08 ppm) peaks in D_2O/DCl were used to calculate the cyclic acetal percentage.[102] We used three different procedures to synthesize AcDex. First, we investigated the kinetics of acetalation with 0.062 M catalyst and 1 g of dextran (normal catalyst).[102] This resulted in a rapid increase of cyclic acetals, with 50% of the polymer containing cyclic acetals after 5 minutes and 66% cyclic acetals (the theoretical maximum) after one hour (Figure S3.1). Second, in order to access a wider range of cyclic:acyclic ratios we reduced the amount of catalyst by a third (low catalyst). Here, after 10 minutes only 20% cyclic acetals were present, and after 60 minutes 40% cyclic acetals were present (Figure S3.1). Third, we scaled up the low catalyst procedure to 10 g of dextran to produce a uniform batch for all subsequent studies. We aimed to generate three batches of AcDex with a low, medium and high percent cyclic acetals, respectively. The ^{1}H NMR spectra are shown in Figure S3.2. This allowed us to investigate a range of payload release profiles once

AcDex was formulated into particles. Scaling up the reaction changed the kinetics of acetalation slightly, yielding a narrower range of cyclic acetal percentages. Specifically, the percentage of cyclic acetals from the scale-up was 49%, 54% and 59% at 30 min, 60 min, and 1200 min, respectively, compared to 30%, 40% and 60%, respectively, at the smaller scale (Table 3.1). These three percentages of cyclic acetals represented FAST (49% cyclic acetals), MED (54% cyclic acetals), and SLOW (59% cyclic acetals) degrading AcDex for particle formulation.

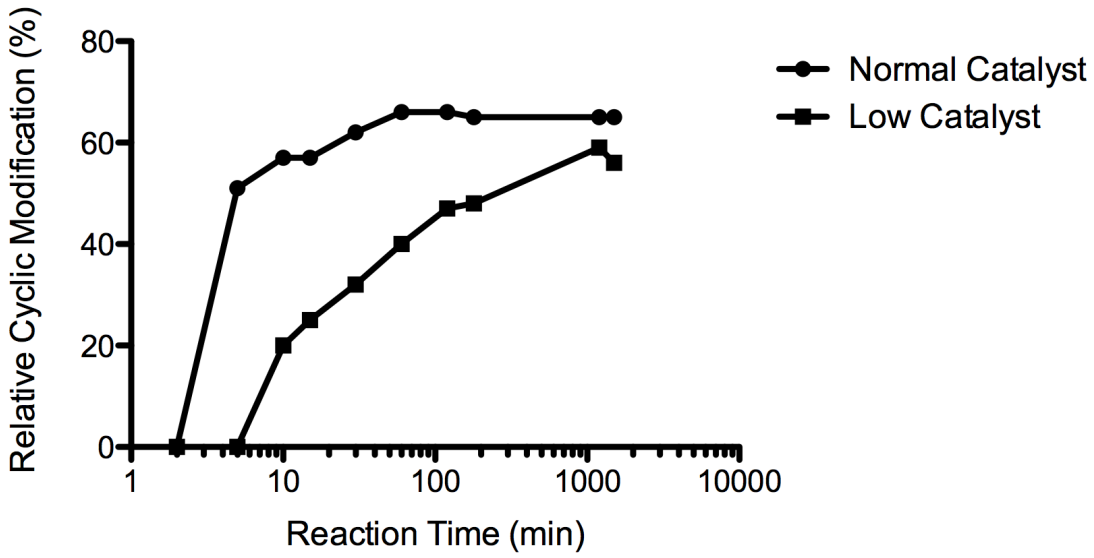

Figure S3.1. Relative cyclic modification present on AcDex over time during kinetic experiments using normal (0.062 M) and low (0.031 M) catalyst conditions. In the normal catalyst conditions the cyclic acetal coverage is greater than 50% after only five minutes. Reducing the amount of catalyst slowed the progression of cyclic acetal formation allowing access to a wider range of cyclic acetal percentages.

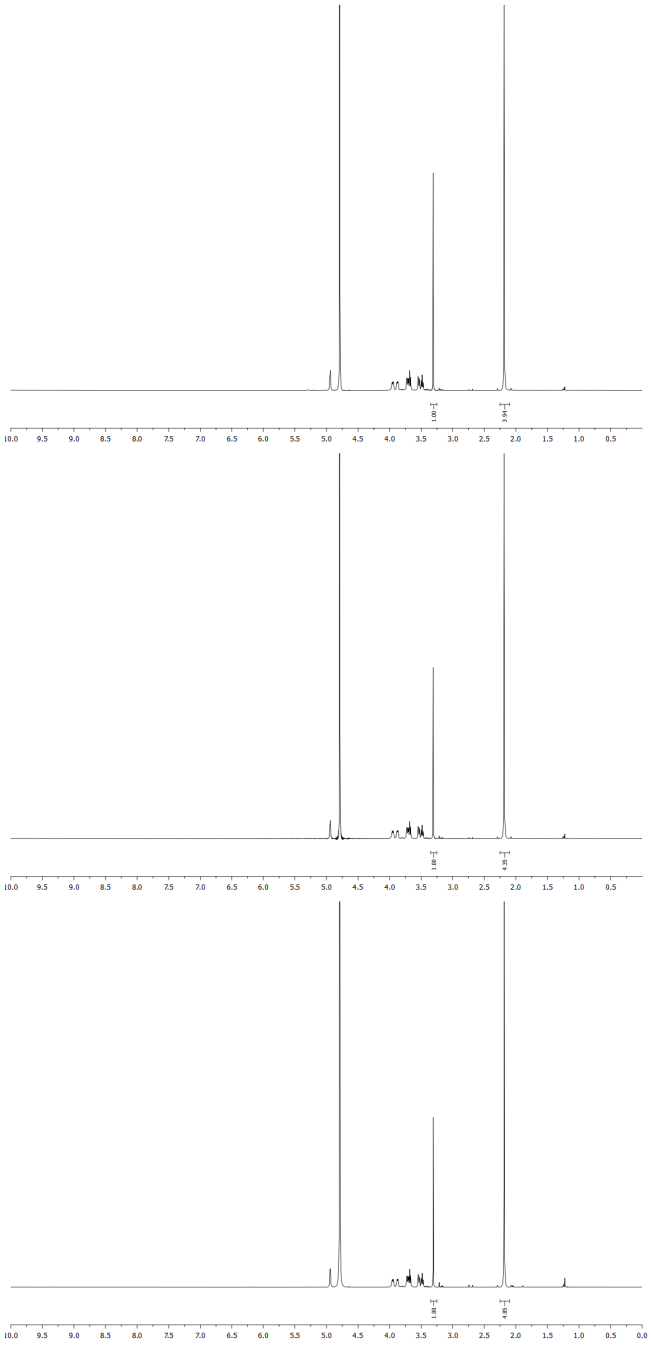

Figure S3.2. ^{1}H NMR of FAST, MED and SLOW (top to bottom) AcDex 10 g batches. As the reaction time increased (bottom to top), the cyclic acetal percentage increased, as indicated by the increase in the area under the acetone peak (2.08 ppm) relative to the methanol peak (3.34ppm).

Table 3.1. Characterization of FAST, MED and SLOW AcDex (10 g batches) used in subsequent studies. Predicted cyclic acetal coverage is based on prior kinetics studies with a 1 g batch.

Name	Quenching Time (min)	Predicted Cyclic %	Actual Cyclic %	Mw	PDI
FAST	30	30	49	7757	1.83
MED	60	40	54	7966	1.79
SLOW	1200	60	59	8199	1.82

3.3.2 Model Protein Release Studies

Previous work with AcDex fabricated nano- and microparticles with diameters of 100 nm to 10 μm for cellular uptake, whereas for delivery of many therapeutic agents post-MI the particles should be larger (20-100 μm)[106] to remain in the extracellular space. AcDex microparticles containing FITC-labeled myoglobin (FITC-myo) were prepared using a w/o/w double emulsion. The average particle size for the FAST, MED and SLOW particles was 46 ± 14 μm, 58 ± 19 μm and 63 ± 27 μm, respectively. Encapsulation efficiency of myoglobin in the FAST, MED and SLOW microparticles was ~100%, 70% and 47%, respectively. An SEM image of the FAST, MED and SLOW particles before the release experiment reveals that the particles are spherical with a smooth surface (Figure 1A).

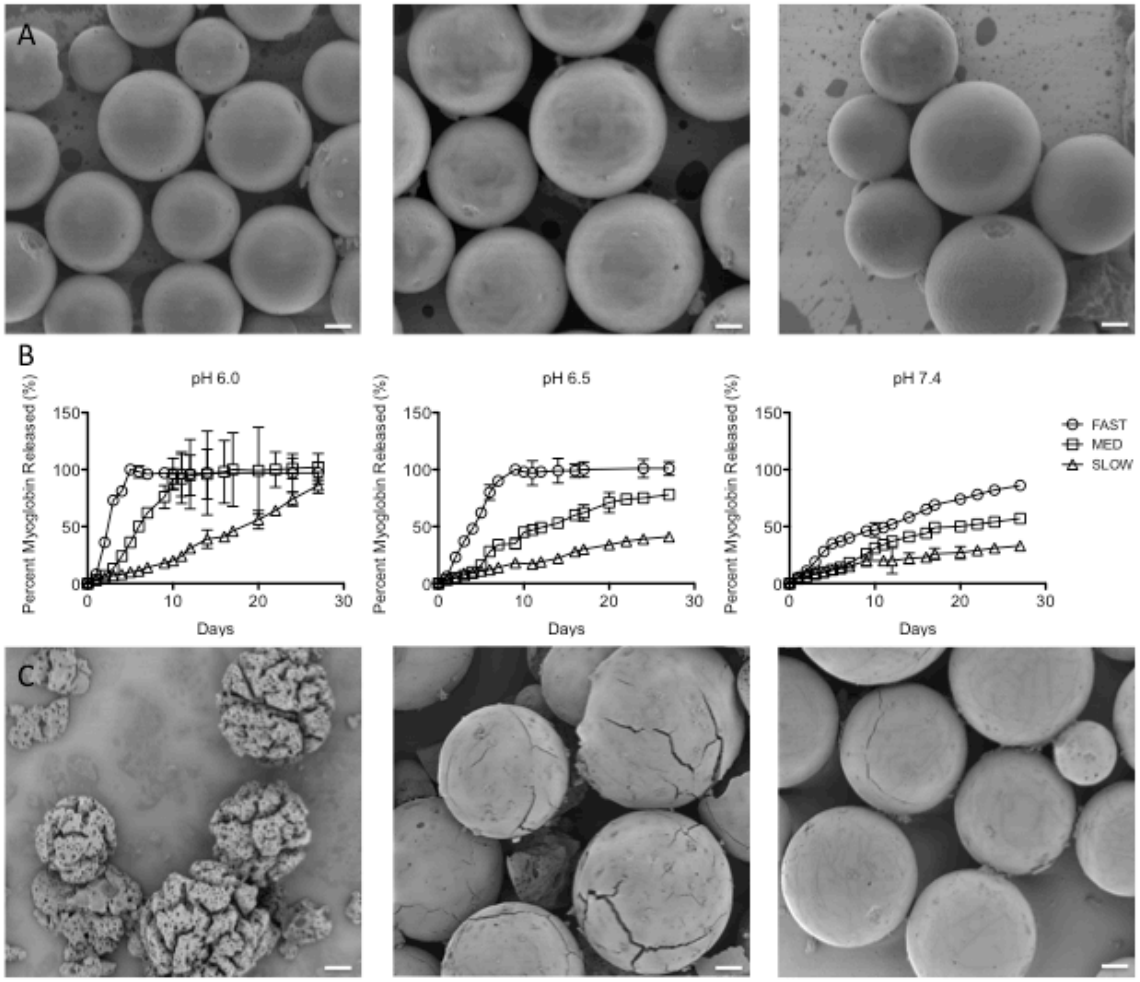

Figure 3.1. Tunable release of a model protein from AcDex microparticles. A. Intact FAST, MED and SLOW (left to right) particles containing FITC-myoglobin before model protein release studies. Particles are spherical with a smooth surface. B. Myoglobin release from FAST, MED and FAST particles at pH 6.0, 6.5 and 7.4. At pH 6.0 complete release of myoglobin was seen at 5, 10 and 60 days for the FAST, MED and SLOW particles, respectively. The same trend was seen at pH 6.5, and at pH 7.4, with progressively slower release; in the latter condition only 50% of encapsulated myoglobin was released after 11, 17 and 63 days, respectively. C. SEM images of the MED particles on day 7 at pH 6.0, 6.5 and 7.4 (left to right). Particle morphology correlates with the observed myoglobin release at this time point. Scale bar: 10μm.

We examined the release of FITC-myo from the microparticles in mildly acidic conditions, representative of the ischemic infarct (pH 6.0 and pH 6.5) and healthy tissue (pH 7.4). At pH 6.0 complete release of myoglobin was seen at 5,

10 and 60 days for the FAST, MED and SLOW particles, respectively. The same trend was seen at pH 6.5, and at pH 7.4, with progressively slower release; in the latter condition only 50% of encapsulated myoglobin was released after 11, 17 and 63 days, respectively (Figure 1B). To corroborate these results, particle degradation was visualized using SEM. The morphology of the MED particles at day 7 is shown in Figure 3.1C at pH 6.0, 6.5 and 7.4. At pH 6.0 the porous interior of the MED particles is clearly visible and deep cracks have formed throughout the particles. At pH 6.5 some surface cracks appear, but the smooth external surface of the particles is still intact. At pH 7.4 only lines on the surface are visible that suggest where cracks will eventually form. The images correlate well with the observed myoglobin release at this time point: 62%, 34% and 18% for pH 6.0, pH 6.5 and pH 7.4, respectively.

3.3.3. Growth Factor Release Studies

To examine whether this system is applicable to growth factor delivery, we encapsulated bFGF. AcDex microparticles containing Alexa594-labeled bFGF were prepared using a w/o/w double emulsion. The average particle size for the FAST and SLOW particles was 60 ± 18 μm and 67 ± 22 μm, respectively. Encapsulation efficiency for bFGF in the FAST microparticles was ~100%. The SLOW microparticles were not fully degraded in this study and thus no encapsulation efficiency was calculated, but it is expected to be similar to that seen with myoglobin, since the FAST values were equivalent. Again, these particles are spherical with smooth surfaces as shown by SEM (Figure 3.2A).

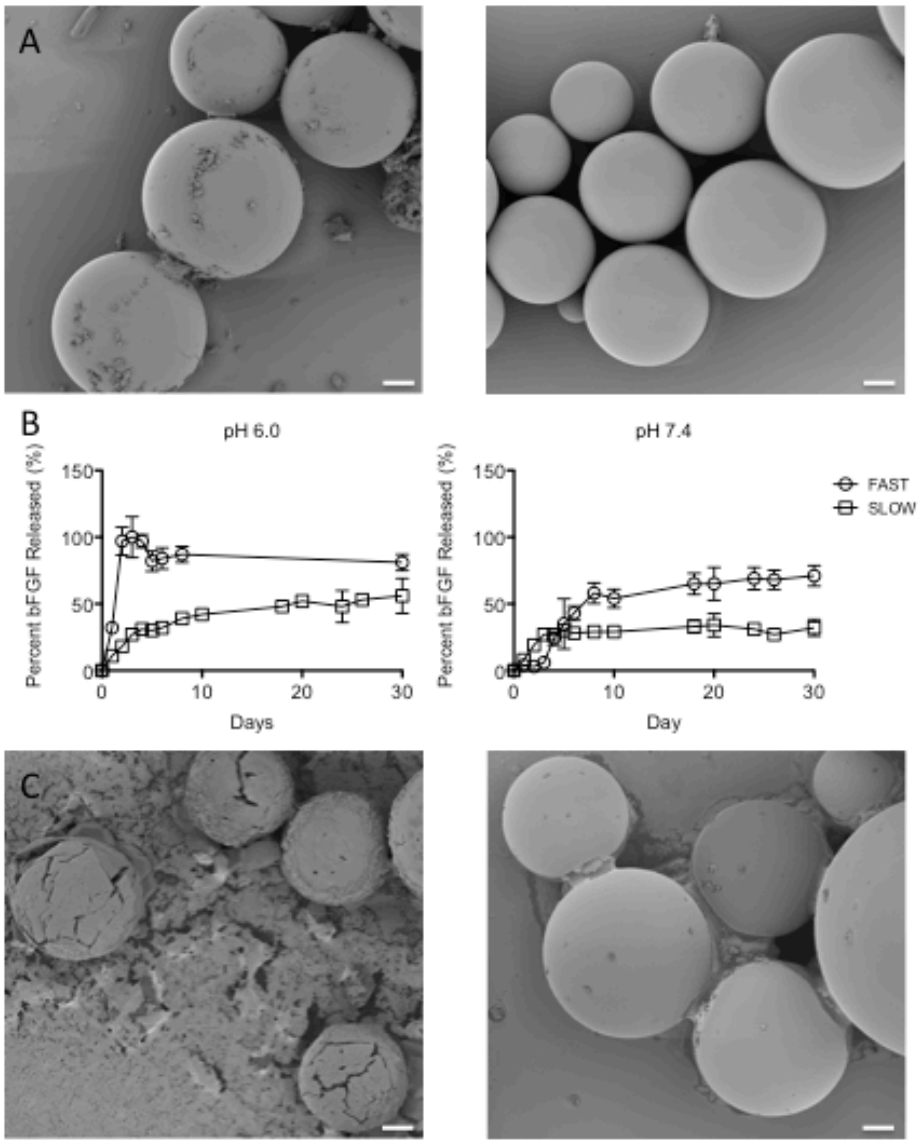

Figure 3.2. Tunable release of a growth factor from AcDex microparticles. A. Intact FAST and SLOW (left to right) particles containing Alexa594-bFGF before bFGF release studies. Particles are spherical with a smooth surface. B. bFGF release from FAST and SLOW particles at pH 6.0 and 7.4. At pH 6.0 complete release was seen after three days from the FAST particles, while only 50% release was seen after 10 days for the SLOW particles. A similar trend was seen at pH 7.4 as 50% of the bFGF was released after one week from the FAST particles, while after one month, only 37% had been released from the SLOW particles. C. SEM images of the FAST particles on day 2 at pH 6.0 and 7.4 (left to right). Particle morphology correlates with the observed bFGF release at this time point. Scale bar: 10 μm.

Release experiments were repeated in the same manner as with the model protein, using the FAST and SLOW AcDex at pH 6.0 and 7.4. At pH 6.0 complete release was seen after three days from the FAST particles, while only 50% release was seen after 10 days for the SLOW particles. A similar trend was seen at pH 7.4 as 50% of the bFGF was released after one week from the FAST particles, while after one month, only 37% had been released from the SLOW particles (Figure 3.2B). As seen by SEM (Figure 3.2C), on day 2 at pH 6.0 the particles were mostly degraded, but the remaining intact particles show visible holes and cracks across the surface. The particles at pH 7.4 at the corresponding time point still maintained a smooth surface.

3.3.4 Growth Factor Activity Assay

To demonstrate that the encapsulated bFGF was still biologically active, we used a cell-based assay that measures the ability of bFGF to stimulate proliferation of fibroblast cells. FAST AcDex microparticles with and without bFGF were prepared as described above. The average particle size for the bFGF-encapsulating and empty particles was 68 ± 22 μm and 58 ± 20 μm, respectively. Both types of microparticles were suspended in PBS pH 6.0 for two days at 37°C. Each day supernatant was removed and added to cells in low serum media (Released bFGF; Empty Supernatant). As a positive control, bFGF that had not been processed in any way (Fresh bFGF) was added to cells at the same concentration as the released bFGF as determined by the release experiment described in the Methods section. An additional negative control was used

consisting of low serum media with no bFGF (No bFGF). After 24 hours, the Fresh bFGF and Released bFGF groups both had significantly more cells per well than either the No bFGF or Empty Supernatant groups. In addition, the Fresh bFGF and Released bFGF groups were not statistically different from one another (Figure 3.3).

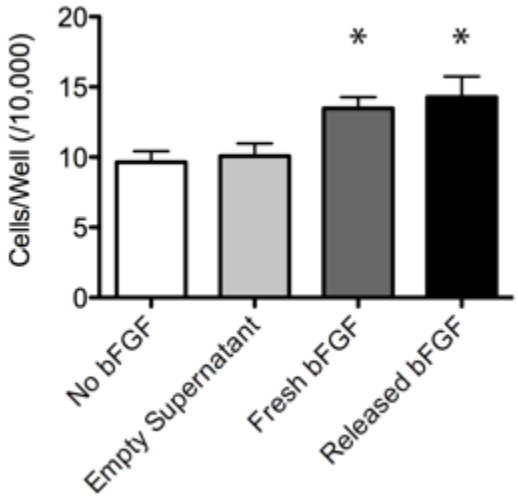

Figure 3.3. bFGF activity after release from AcDex microparticles. Cell number after 24 hours of growth in growth factor activity assay (mean ± SD; *p < 0.05). The LS + fresh bFGF and LS + released bFGF groups both had significantly more cells per well than either control group (LS alone or LS + empty). In addition, the LS + Fresh bFGF and LS + Released bFGF groups were not statistically different from one another. *p<0.05 to both negative control groups.

In this experiment, particles containing labeled bFGF, heparin and BSA (Figure S3.3) displayed slower release of bFGF than observed in the bFGF release study, which omitted BSA (Figure 3.2B). This slowed release rate was more similar to that seen with myoglobin (Figure 3.1B).

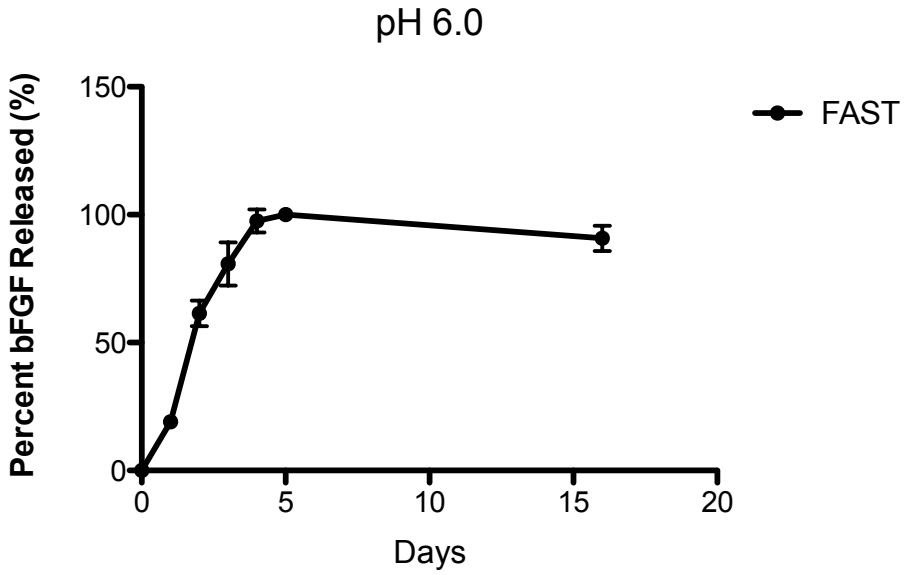

Figure S3.3. bFGF release experiment completed prior to the activity studies. This release profile was used to determine the amount of released bFGF to add to the cells in the bFGF activity assay. AcDex microparticles contained labeled bFGF as well as heparin and BSA as stabilizing agents. The release profile is slower than the release of bFGF without BSA (Figure 3.2B), and is more similar to that of myoglobin (Figure 3.1B).

3.3.5 Biocompatibility

While AcDex has been predicted to have mild degradation products, it has not been tested in an *in vivo* system. Therefore, to examine the biocompatibility of AcDex, empty FAST (69 ± 24 μm) and SLOW (74 ± 20 μm) particles were injected into the hearts of healthy rats. At 7, 14 and 28 days following injection, animals were euthanized and the hearts excised and processed for histological analysis. Spherical voids created by the particles were visible for both the FAST and SLOW groups at all three time points in H&E stained slides (Figure 3.4).

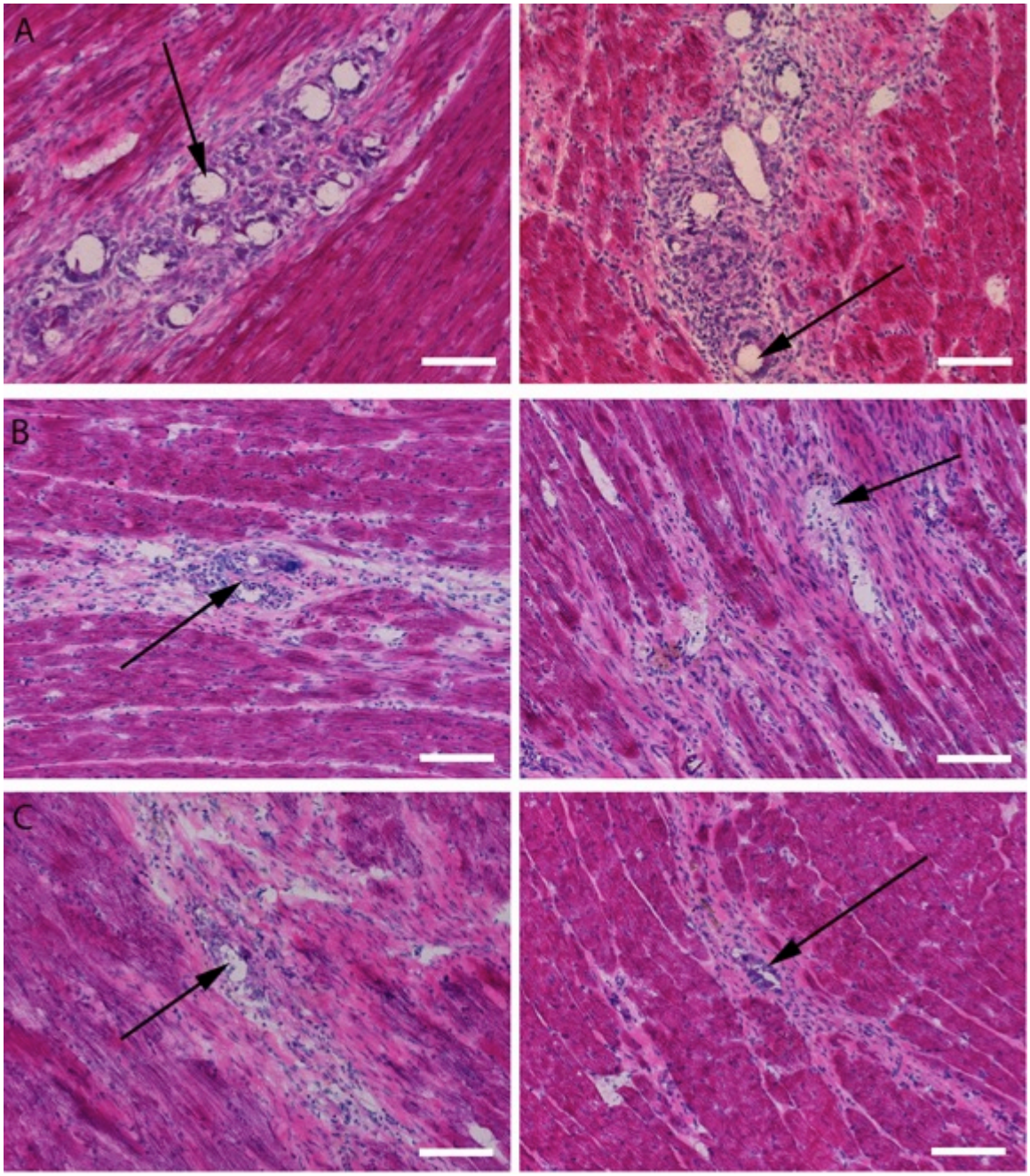

Figure 3.4. Images showing AcDex biocompatibility in healthy rat hearts. H&E images from day 7 (A), 14 (B) and 28 (C) of the biocompatibility study. Spherical voids created by the particles (black arrows) are visible for both the FAST (left) and SLOW (right) groups. As particles degrade, the voids, representative of particle morphology, becomes less spherical. Scale bar: 100 μm.

An experienced histopathologist examined the cellular response to the microparticles using semi-quantitative scoring (1 or minimal = only rare cells of that type are present (<1% of the population); 2 or mild = small numbers of the cells are present, generally not in contact with each other or scattered (<10%); 3 or moderate = moderate numbers of cells are present, which are sometimes in contact with each other (10 - <50%); 4 or marked = cells of the specific type are the primary cell present (> 50%)). On day 7 the cell population around the particles consisted of spindle (immature fibroblast) cells as well as small and large mononuclear cells (all mild to moderate). No mature fibroblasts or multinucleate giant cells were present at this time point (Figure 3.5). On day 14 the cell population shifted to include fewer spindle (immature fibroblast) and mononuclear cells (minimal to mild), with the addition of mature fibroblasts (mild) and a few multinucleate giant cells (none to minimal) (Figure 3.5). On day 28 the cell population consisted primarily of mature fibroblasts with some remaining mononuclear cells (minimal) and a few multinucleate giant cells (none to minimal) (Figure 3.5). Overall the response was described as progressing normally from acute inflammation towards a fibrotic resolution. While not fully resolved at day 28, due to the presence of some mononuclear cells, there was no indication of a severe or abnormal response that would suggest incompatibility of the material.

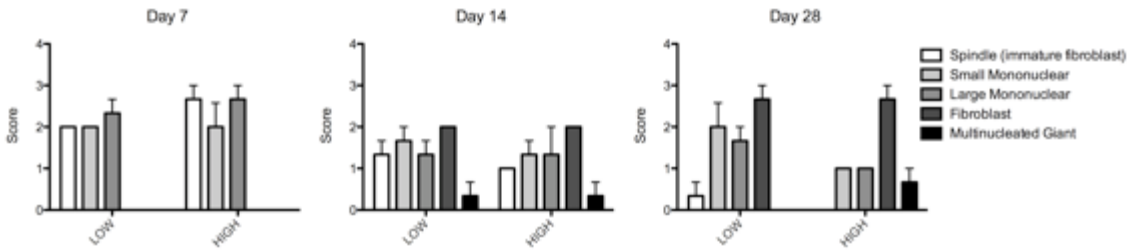

Figure 3.5. Cell type scores from AcDex biocompatibility study. On day 7 the cell population around the particles consisted of spindle (immature fibroblast) cells as well as small and large mononuclear cells. No mature fibroblasts or multinucleate giant cells were present at this time point. On day 14 the cell population shifted to include fewer spindle and mononuclear cells, with the addition of fibroblasts and a few multinucleate giant cells. On day 28 the cell population consisted primarily of mature fibroblasts with some remaining mononuclear cells and a few multinucleate giant cells. Score: none (0), minimal (1), mild (2), moderate (3) and severe (4).

3.4 Discussion

We aimed to design microparticles that could be used to deliver a payload at a variety of relevant time scales. To demonstrate tunable release over the time-scale relevant to healing post-MI, several days or weeks, we encapsulated a fluorescently labeled model protein and measured its release into the surrounding media over time. Myoglobin was chosen as a model protein because its size (17.7 kDa) matches that of growth factors such as bFGF (18 kDa), which are relevant to post-MI healing. As intended, release of the model myoglobin was dependent on environmental pH (faster at lower pH) and cyclic acetal percentage (faster for particles with lower percentage). The difference in loading efficiency between groups was likely due to the increase in hydrophobicity of the polymer as the cyclic acetal coverage increased. Furthermore, SEM images (Figure 3.1) suggest that the payload only diffused out

when the particles degraded, as opposed to passive diffusion through the intact particles.

Growth factors are more susceptible to loss of activity upon sonication or exposure to organic solvents than myoglobin, so showing that bFGF can remain active after encapsulation and release from AcDex microparticles would suggest the system's compatibility with any fragile payloads. bFGF has also been employed in post-MI therapies to stimulate new blood vessel formation [21, 28-30, 109]. Our results demonstrate that the bFGF maintained its activity after encapsulation in and release from the microparticles and suggest that any number of formulation-sensitive growth factors could be delivered using this particle system, if encapsulated with an appropriate stabilizing agent.

For simplicity, in this study the experiment groups were reduced to only the FAST and SLOW microparticles and pH 6.0 and 7.4. Furthermore, while particles in the model protein studies were prepared using Sunsoft as a stabilizing agent, we eliminated the detergent from bFGF-containing formulations to maximize growth factor stability. While the bFGF was also released at a rate dependent on the cyclic acetal percentage and the environmental pH, release was slightly faster than was seen with the myoglobin. This difference was potentially due to the presence of BSA in the myoglobin-loaded particles. The bFGF release studies were performed without BSA for simplicity, but it was later found that the BSA was needed for optimal bFGF activity, in addition to heparin. The hypothesis that BSA changed the release rate was supported by the release experiment completed prior to the activity studies (Figure S3.3).

The tunable release of myoglobin and bFGF suggests that this system could be used to release a variety of payloads. Myoglobin and bFGF were likely in different charge states inside the particles, yet released at comparable rates. At the pHs in these studies, myoglobin (isoelectric point of 7 to 7.5) was likely slightly positively charged, while bFGF (isoelectric point of 9.6) was likely negatively charged. This suggests that electrostatic interactions did not play a role in keeping either protein inside the particles. In addition, AcDex is hydrophobic and both payloads are hydrophilic, so hydrophobic interactions were also not likely playing a role. As a result, the small 17 kDa proteins were likely kept inside the particles simply by physical entrapment until the particles broke down. Therefore, it is expected that the release of a larger protein would be easily controlled as well. All of these considerations suggest that AcDex provides a more versatile delivery vehicle than previously developed systems because compatible payloads are not limited by affinity, size, or charge Finally, AcDex particles are responsive to mildly acidic conditions making them specifically responsive to the infarct environment [61, 62].

Chapter 3, in part, is a reprint of the material as it appears in Biomacromolecules 2014. Suarez S, Grover GN, Braden RL, Christman KL, Almutairi A. Tunable Protein Release from Acetalated Dextran Microparticles: A Platform for Delivery of Protein Therapeutics to the Heart Post-MI. Biomacromolecules. 2014. The dissertation author was the primary investigator and author of this paper.

CHAPTER FOUR:

HGF Cardioprotective Efficacy Post-MI is Maximized When Released From Quickly Degrading Acetalated Dextran Microparticles

4.1 Introduction

Heart failure (HF) post-myocardial infarction (MI) is a leading cause of death in the Western world [110]. The current gold standard treatment for patients with HF is heart transplantation, but a lack of donor hearts is a significant limitation. Many patients waiting for donor hearts are fitted with left ventricular assist devices (LVADs), a mechanical pump inserted into the patient, to replace the function of the failing heart. Both heart transplantation and LVAD implantation require invasive open chest procedures and involve serious risks including infection and stroke, respectively. Furthermore, neither treatment restores native heart function. Thus new therapies for preventing and treating HF post-MI are needed. Injectable biomaterial therapies, in the form of hydrogels [6, 111] and nano- or microparticles [7], hold promise for healing and restoring function of the damaged heart tissue through potentially minimally invasive delivery. A useful property of injectable biomaterials is their ability to protect and sustain release of therapeutic cargo including growth factors, enzymes and small molecule drugs [5, 7].

Hepatocyte growth factor (HGF) is one growth factor of interest for cardiac repair. Following MI, serum levels of HGF are elevated during both acute (hours to one week) and chronic (3 months up to a year) stages [112-115]. This indication of HGF's role in tissue repair following MI has been supported by the efficacy of delivering exogenous HGF or upregulating endogenous HGF expression in animal models. In these models HGF was shown to be cardioprotective by increasing angiogenesis [23, 116-122], reducing apoptosis

[23, 117-121, 123], reducing fibrosis [23, 116, 117, 119, 121-123] and in some cases improving cardiac function [116, 120-122, 124]. In the studies delivering HGF from a biomaterial, HGF was released *in vitro* between 25 and 100% over one week, while release kinetics *in vivo* were not studied [23, 116].

In general, the optimal time frame for delivering HGF, as well as other therapies, is not yet fully understood. One reason is that fixed degradation kinetics of most biomaterials limits a systematic investigation of optimal delivery time frames. Additionally, use of recombinant HGF is limited by poor stability and high cost. A more cost effective and practical alternative is to deliver an engineered HGF fragment (HGF-f), which has shown enhanced stability and expression yield, comparable c-met activation compared to recombinant HGF [125], and efficacy post-MI when delivered in a biomaterial [126]. In this study, we used acetalated dextran (AcDex) microparticles as carriers for HGF-f as these were recently shown to have easily tunable degradation and protein release kinetics in mildy acidic environments [41, 62, 127], as found in the infarcted heart. We aimed to investigate how three different rates of delivery (2-5 days, 1-2 weeks and 3-4 weeks) of HGF-f to the heart post-MI impacted healing. HGF-f was delivered over these time frames in FAST, MEDIUM (MED), and SLOW degrading AcDex particles, respectively. One month after injection we assessed the impact of the delivered HGF-f on angiogenesis, fibrosis and apoptosis to determine the optimal delivery time frame.

4.2 METHODS

All experiments were completed in accordance with the Institutional Animal Care and Use Committee at the University of California, San Diego and the American Association for Accreditation of Laboratory Animal Care.

4.2.1 Synthesis of FAST, MED and SLOW Degrading AcDex

Acetalated dextran (AcDex) was prepared as previously described [41]. Three batches (10 g) were created with the reaction quenched after 20, 45 or 90 minutes to yield FAST, MED and SLOW polymer degradation, respectively. The cyclic to acyclic acetal ratios were determined using ^{1}H NMR as previously described [41].

4.2.2 Particle Degradation and Protein Release Studies Post-MI

4.2.2.1 Fluorescent Labeling of FAST, MED and SLOW Degrading AcDex

FAST, MED or SLOW degrading AcDex (500 mg) was dissolved in dichloromethane (DCM; 12 mL; Sigma Aldrich, St. Louis, MO). Alexa Fluor 647 or 568 carboxylic acid succinimdyl ester (1 mg; Life Technologies, Carlsbad, CA) was dissolved in dimethylsulfoxide (DMSO; 1 mL; Sigma Aldrich, St. Louis, MO) and added to the AcDex/DMSO mixture along with triethylamine (250 μL; Sigma Aldrich, St. Louis, MO). The dye-polymer solution was stirred for 48 hours at room temperature protected from light. Then DCM was removed with rotary evaporation and the remaining product was dissolved in tetrahydrofuran (10 mL; Sigma Aldrich, St. Louis, MO). The dissolved product was precipitated into cold basic water and vacuum filtered. Residual water was removed through

lyophilization. ^{1}H NMR analysis of the labeled AcDex (FAST-647, MED-568 and SLOW-647) confirmed that labeling did not alter the acetal composition.

4.2.2.2 Encapsulation of AF488 Ovalbumin in FAST-647, MED-568 and SLOW-647 Degrading AcDex

Alexa Fluor 488 Ovalbumin (Ova488; Life Technologies, Carlsbad, CA) was encapsulated in AcDex microparticles as previously described [41]. Briefly, a w/o/w double emulsion was used to encapsulate Ova488 (1 mg) and heparin (1 mg; from porcine intestinal mucosa, Sigma Aldrich, St. Louis, MO) in FAST-647, MED-568 or SLOW-647 AcDex polymer (100 mg).

4.2.2.3 Intramyocardial Injections for Particle Degradation

All experiments were completed in accordance with the Institutional Animal Care and Use Committee at the University of California, San Diego and the American Association for Accreditation of Laboratory Animal Care.

MI was induced via a 25-minute ischemia-reperfusion in female Sprague-Dawley rats as described previously (n = 4 per group per time point) [128]. One week following injury rats received a 75 μL injection of FAST-647, MED-568 or SLOW-647 degrading AcDex particles containing Ova488 (5 mg/mL in saline). Injections were made in the LV-free wall using a 27-gauge needle as described previously [128]. At designated time points animals were euthanized with an intraperitoneal injection of FatalPlus (Vortech Pharaceuticals; 300 μL) and hearts were harvested for histological detection of the particles.

4.2.2.4 Histological Assessment for Particle Degradation

Hearts were fresh frozen in Tissue Tek OCT freezing medium and sectioned (10 μm thickness) along the short-axis every 350 μm. One slice at each location was imaged unstained to avoid washing the particles out of the tissue. Images were taken with a Carl Zeiss Observer D.1 (Carl Zeiss, Oberkochen, Germany) using FITC and either DsRed or Cy5 filters to detect co-localization of the encapsulated protein (Ova488) within the labeled-polymer particles (Alexa568 or Alexa647). One slide from each location was stained with hematoxylin and eosin (H&E) to verify the presence of an infarct and determine the location of the particles with respect to the infarcted tissue. Hearts that did not contain an infarct upon histological analysis were excluded from further analysis.

4.2.3 Studies of HGF-f Delivery Rate on Angiogenesis, Apoptosis and Fibrosis Post-MI

4.2.3.1 HGF-f Preparation and Characterization

HGF-f was expressed in Pichia pastoris using growth and induction media conditions and protein purification methods previously described in detail [125, 126]. Protein purity was analyzed using 4–12% Bis-Tris gel (Invitrogen) and quantified using a Nanodrop 2000 (Thermo Scientific) with the extinction coefficient 51324 M^{-1} cm^{-1} for the HGF-f. Protein was flash-frozen in 0.1% Tween-20 in 1x phosphate buffered saline containing an additional 500 mM NaCl (PBS500) and stored at -80 °C. Thawed protein was kept at 4 °C and used within three weeks.

4.2.3.2 Preparation and Characterization of AcDex Particles Containing HGF-f

HGF-f (1.3 mg) was encapsulated with heparin (1.3 mg) in FAST, MED and SLOW degrading AcDex (100 mg) using previously described methods [41]. Using the same procedure, non-loaded MED particles were prepared as a control (Empty). Particle size and morphology were subsequently determined using the Beckman Coulter Multisizer 4 and an Agilent 8500 FE-SEM, respectively. The loading efficiency of HGF-f was determined using a HisDetector Western Blot Kit (24-00-02, KPL, Gaithersburg, MD). HGF-f was encapsulated in and fully released from the particles, then run on an SDS-PAGE gel and detected using Western blot according to manufacturer specifications.

4.2.3.3 Western Blot to Determine Particle-Released HGF-f Activity

HGF-f-loaded particles were suspended (10 mg/mL) in phosphate buffered saline (PBS; pH 6 for FAST and pH 5 for MED and SLOW) containing heparin (1.8 μg/mL) and Tween 80 (0.1 wt%) and incubated at 37° C to release the HGF-f. Following particle degradation the supernatant was collected and saved as the "HGF-f Released from FAST/MED/SLOW" treatment groups. Released HGF-f and unencapsulated HGF-f were diluted to 2 nM concentrations in serum free media (4.5 g/L glucose-Dulbecco's modified Eagle's medium (DMEM), 0.1% bovine serum albumin (BSA), 0.5% pen-strep).

Meanwhile primary rat aortic smooth muscle cells (RASMCs) were cultured to 50% confluence in 6-well plates and serum starved for 24 hours. Then cells were treated with either released HGF-f, unencapsulated HGF-f, or no HGF-f

(serum free media only) for 10 minutes. Following treatment media was removed and cells were washed with 1x PBS. NP-40 lysis buffer (75 μL; 20 mM Tris pH 8.0, 137 mM NaCl, 10% glycerol, and 1% NP40) was added for five minutes to rupture cell membranes. Cellular contents were collected and centrifuged (13400 x g, 20 min) to remove insoluble debris. A BCA protein assay was run to determine protein content in each cell lysate and equal protein concentrations were run on an 8% SDS-PAGE gel. Western blot was performed to probe for Met, phosphorylated-Met (p-Met) and GAPDH. After transfer to a nitrocellulose membrane immunoblotting was completed using a mouse anti-GAPDH monoclonal antibody (ab8245; 1:5000; Abcam, Cambridge, MA), rabbit anti-Met polyclonal antibody (sc-161; 1:500; Santa Cruz Biotechnology, Dallas, TX) and rabbit anti-P-Met monoclonal antibody (#3077; 1:500; Cell Signaling, Danvers, MA) followed by the appropriate horseradish peroxidase-conjugated mouse or rabbit IgG (ab97023 and ab97051, respectively; 1:2000; Abcam, Cambridge, MA).

4.2.3.4 Intramyocardial Injections for HGF-f Delivery

All experiments were completed in accordance with the Institutional Animal Care and Use Committee at the University of California, San Diego and the American Association for Accreditation of Laboratory Animal Care.

MI was induced via a 25-minute ischemia-reperfusion in female Sprague-Dawley rats as described previously (n = 12 per group) [128]. One week following injury rats received a 75 μL injection of FAST, MED or SLOW degrading AcDex

particles containing HGF-f (10 mg/mL in saline), free HGF-f, or empty particles. Injections were made in the LV-free wall using a 27-gauge needle as described previously [128]. Four weeks after injection animals were euthanized with an intraperitoneal injection of FatalPlus (Vortech Pharaceuticals; 300 μL) and hearts were harvested for histological analysis. Some mortality occurred following MI and injection surgeries (MED n = 2; SLOW n = 1; empty n = 3; free n = 2).

4.2.3.5 Histological Analysis Following HGF-f Delivery

At the time of sacrifice, the hearts were excised, arrested in a solution containing 25 mM $NaHCO_3$, 2 mM $CaCl_2$, 5 mM Dextrose, 2.7 mM $MgSO_4$, 22.8 mM KCl, 121.7 mM NaCl, and 20 mM 2,3 butanedione mon- oxime, fresh frozen in Tissue Tek OCT freezing medium and sectioned (10 μm thickness) along the short-axis every 350 μm.

To assess angiogenesis and cardiomyocyte apoptosis, immunohistochemistry was performed on slides from the three locations containing the largest infarct for each heart. For vessel analysis cryosections were fixed with acetone, incubated with anti-smooth muscle actin antibody (Dako, Carpinteria, CA; 1:75 dilution) and von Willenbrand Factor antibody (AbCam, Cambridge, MA; 1:400 dilution) and then stained with Alexa Fluor 568 anti-mouse and Alexa Fluor 488 anti-rabbit antibodies (Life Technologies, Carlsbad, CA; 1:500 dilution). For apoptosis analysis cryosections were fixed with acetone, incubated with cleaved-caspase 3 antibody (Cell Signaling, Danvers, MA; 1:25 dilution) and α-actinin antibody (Sigma Aldrich, St. Louis, MO; 1:800

dilution) and then stained with Alexa Fluor 568 anti-rabbit and Alexa Fluor 488 anti-mouse antibodies (Life Technologies, Carlsbad, CA; 1:500 dilution). Nuclei were visualized with fluorescent Hoescht 33342. Slides were imaged using a Leica DM6000B (Leica Microsystems Inc, Buffalo Grove, IL) immune-fluorescent microscope at 10x magnification. For vessel analysis five 20x images were taken for each slide from within the infarct. Capillary area was quantified by measuring the area stained positive for capillaries per area within the infarct region using a custom macro in ImageJ. Arterioles with lumen diameters in the range of 10-100 μm in the infarct area were quantified as previously described [49]. Caspase positive cardiomyocytes bordering the infarct were manually counted around the entire infarct.

Five slides evenly distributed throughout the infarct were stained with Masson's trichrome and used for fibrosis quantification. Slides were scanned at 20x magnification using an Aperio ScanScope CS2 slide scanner (Leica). The 'Positive Pixel Count V9' algorithm within ImageScope (Aperio) software was used to detect non-nuclear blue staining. Interstitial fibrosis was measured in non-infarcted septal wall regions. Infarct length was calculated as a percentage of the midline circumference that contained infarcted tissue. Hearts with infarct length <10%, which indicated an insufficient infarction procedure, were excluded (FAST: n = 1, MED: n = 2, SLOW: n = 2, empty: n = 2, and free: n = 2). Forty-three animals were included in the study (FAST: n = 11, MED: n = 8, SLOW: n = 9, empty: n = 7 and free: n = 8).

4.2.3.6 Statistical Analysis

A one-way analysis of variance (ANOVA) test with a Dunnet post-hoc test analysis was used to detect differences among groups for blood vessel, apoptosis and fibrosis measurements. All measurements were reported mean ± SEM, unless otherwise specified. Significance was accepted at $p < 0.05$.

4.3. RESULTS

4.3.1 *In vivo* Particle Degradation and Model Protein Release

Three AcDex batches were prepared using 20, 45 and 90 minute reaction times and contained 43, 54, and 57% cyclic acetals, respectively. ^{1}H-NMR of the resulting FAST, MED and SLOW degrading AcDex can be found in Figure S4.1 A, B and C, respectively. In order to evaluate the degradation rates of the particles in the heart post-MI FAST, MED and SLOW degrading AcDex labeled with fluorescent dyes were injected into the heart post-MI. Cyclic to acyclic ratios of the AcDex were maintained following labeling (Figure S4.1 D, E and F, respectively).

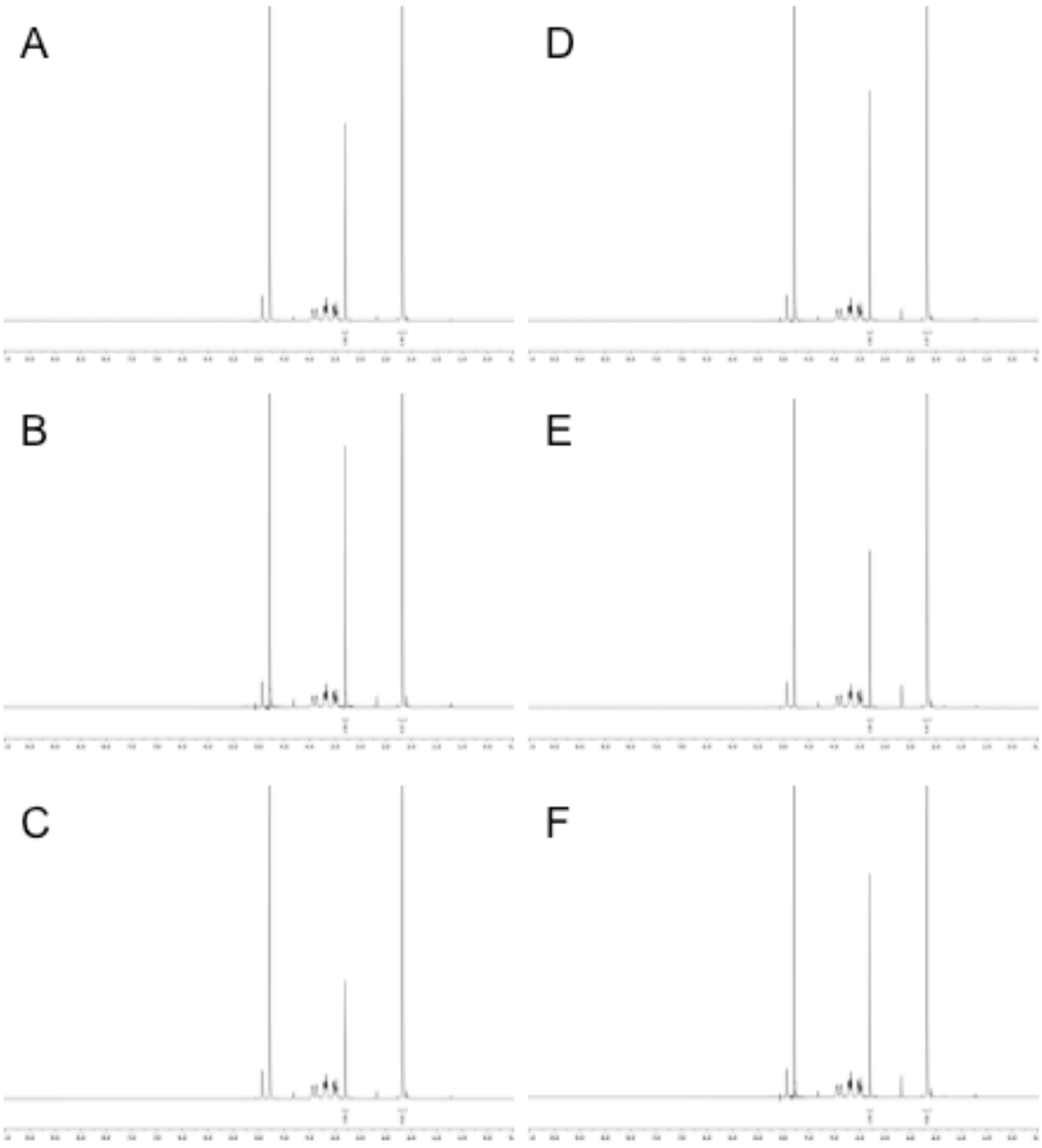

Figure S4.1. ^{1}H-NMR of the (A & D) FAST, (B & E) MED and (C & F) SLOW degrading AcDex before and after fluorescent labeling, respectively. The cyclic acetal percentage increased with increased reaction time (top to bottom). This change is indicated by the increase in the area under the acetone peak (2.08 ppm) relative to the methanol peak (3.34ppm). Fluorescent labeling did not significantly change the cyclic to acyclic acetal ratio as shown by nearly equivalent peak areas before and after labeling.

H&E stained slides were used to confirm that the fluorescent particles were located within the infarcted tissue (Figure 4.1; right column). Hearts injected with FAST particles were harvested after 0, 2 or 3 days. At time zero many intact particles were visible and all contained the encapsulated model protein, Ovalbumin (Figure 4.1; n = 2). At day 2 the visible particles displayed a partially degraded morphology, but still contained the protein (Figure 4.1; n = 3); however, no particles were visible at day 3 (n = 3). Hearts injected with MED particles were harvested at 5, 7 or 14 days post-injection. At day 5 many intact particles were visible throughout the heart, all containing encapsulated protein (Figure 4.1; n = 2). The number of visible particles was greatly reduced on day 7, but remaining particles still contained protein (Figure 4.1; n = 2). No MED particles were visible 14 days after injection (n = 2). Hearts receiving injection of SLOW degrading particles were harvested 14 or 21 days after injection. Protein-containing particles were visible at day 14, with similar density to the MED particles at day 7 (Figure 1; n = 3). Only two SLOW particles were visible in a whole heart at day 21 (n = 2).

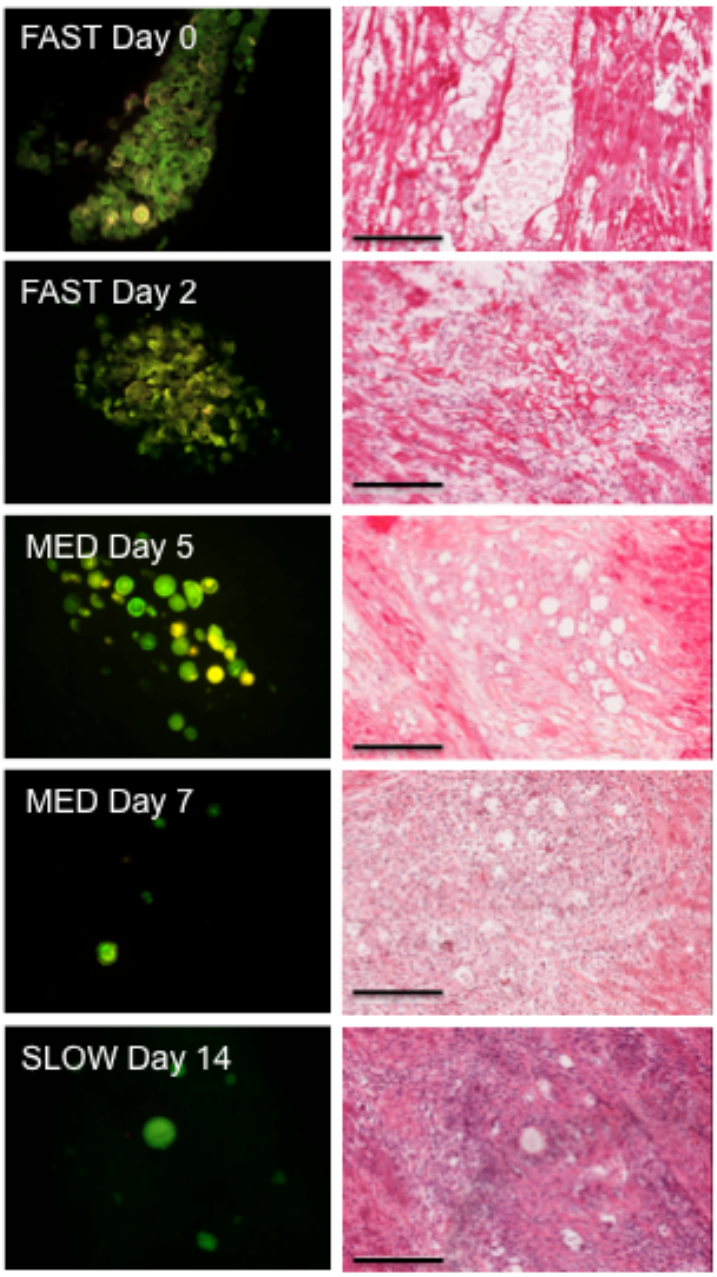

Figure 4.1. Particle degradation and protein release in infarcted hearts. Images of (A) FAST-647 (pink) particles 0 and 2 days post-injection show intact and partially degraded particles, respectively. (B) MED-568 (orange) degrading particles 5 and 7 days after injection show reduced numbers of particles over time and particle retention through one week. (C) SLOW-647 (pink) particles were still visible in the infarct 14 days after injection. In all images in which particles were visible within the infarct, the encapsulated protein, Ova488 (green), was still present as visualized by the colocalization of green and pink or orange. H&E images from each respective location show particles residing within the infarcted myocardium. Scale bar: 200 μm

4.3.2 Characterization of HGF-f-containing AcDex Particles

FAST, MED and SLOW degrading particles contained 12 ± 1.2, 11 ± 1.2 and 11 ± 1.0 μg HGF-f per mg particle, respectively. To assess activity of HGF-f encapsulated in and released from AcDex microparticles, its ability to activate the c-met receptor on rat aortic smooth muscle cells was determined using Western blot. HGF-f was released from FAST, MED and SLOW degrading particles under mildy acidic conditions *in vitro* and added to cells. As expected all cells contained the c-Met receptor (Figure 4.2). Only lanes containing unencapsulated or released HGF-f showed appreciable bands for the phosphorylated c-Met receptor indicating that the released HGF-f maintained its activity (Figure 4.2).

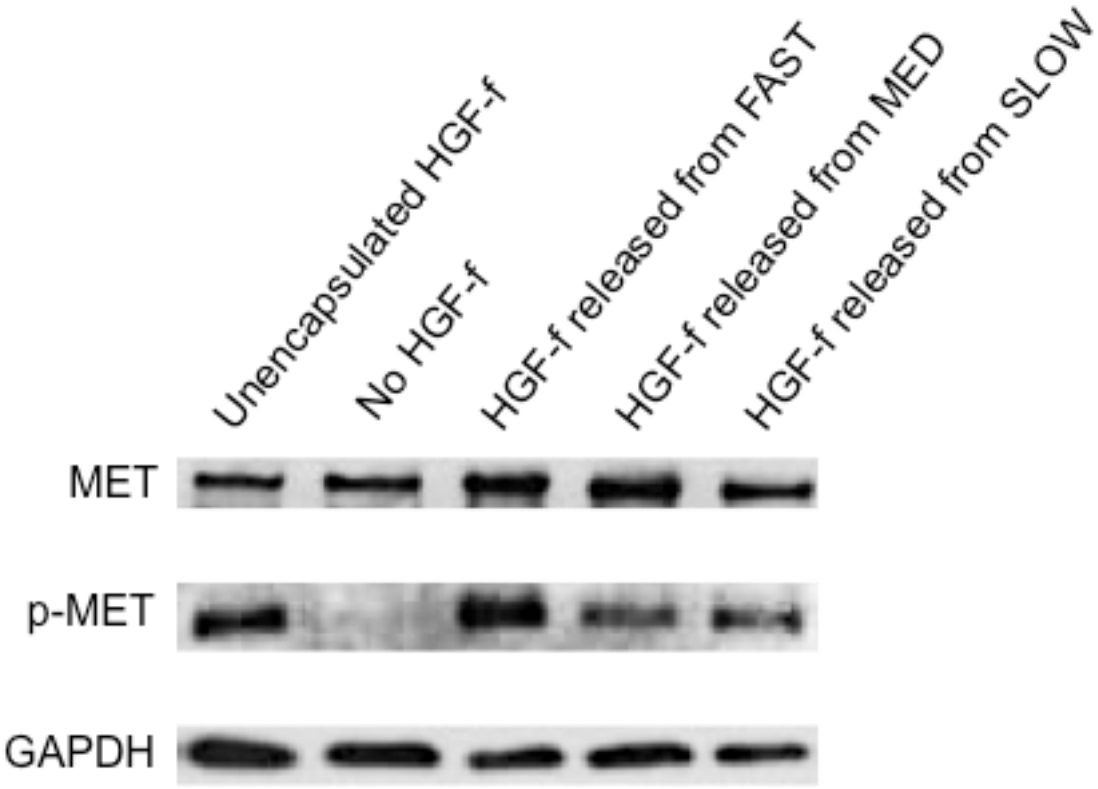

Figure 4.2. Activity of HGF-f released from particles. HGF-f, like native HGF, is an agonist for the c-met receptor. RASMCs were treated with HGF-f released from FAST, MED and SLOW particles as well as unencapsulated HGF-f and no HGF-f as positive and negative controls, respectively. Cellular lysates were analyzed with Western blot to probe for total c-met and phosphorylated c-met receptor content. All cells expressed the c-met receptor on their surface. Only cells treated with HGF-f, whether encapsulated or not, expressed the phosphorylated c-met receptor, indicating that the released HGF-f maintained activity after encapsulation in and release from the particles. GAPDH was used as a control for total cellular protein.

Particles were visualized with SEM and appeared spherical and non-porous (Figure 4.3). Particle diameter of FAST, MED and SLOW particles according to Multisizer analysis was 27.64 ± 1.52, 28.34 ± 1.52, and 32.18 ± 1.41 μm, respectively. Non-loaded MED (Empty) control particles were 28.88 ± 1.66 μm.

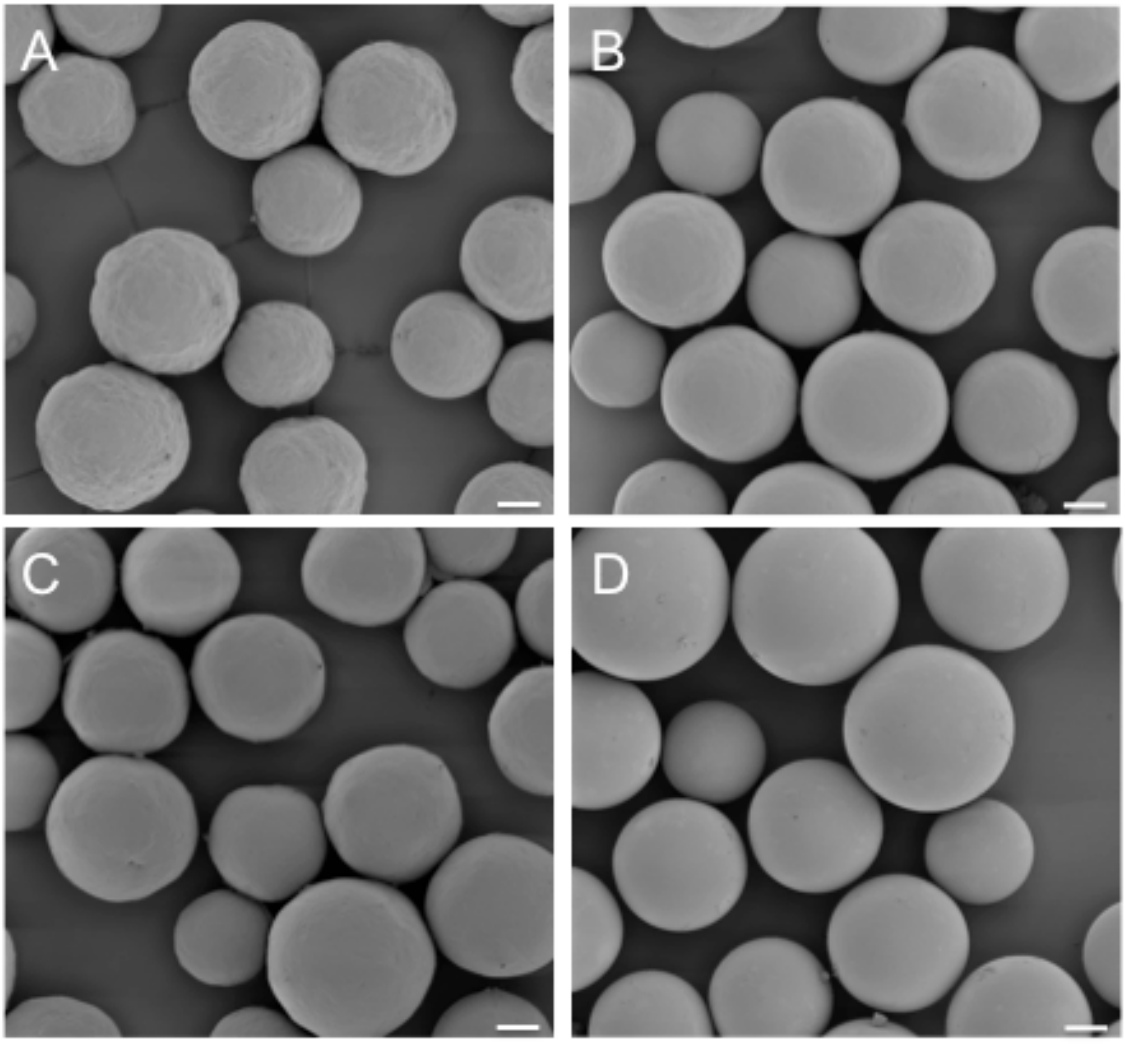

Figure 4.3. AcDex particles for HGF-f delivery post-MI visualized with SEM. Particle size of (A) FAST, (B) MED, (C) SLOW and (D) Empty particles was 27.64 ± 1.52, 28.34 ± 1.52, 32.18 ± 1.41 and 28.88 ± 1.66 μm, respectively. All particles appeared spherical and non-porous. Scale bar: 10 μm.

4.3.3 Effect of HGF-f Delivery Rate on Angiogenesis, Apoptosis and Fibrosis Post-MI

Four weeks after injection of FAST, MED or SLOW particles containing HGF-f into the infarct there was no statistical difference in capillary density or arteriole density between groups (Figure 4.4A, $p = 0.95$ and B, $p = 0.05$, respectively).

However, the HGF-f delivered in the FAST degrading particles yielded the largest arterioles with a significantly greater average arteriole diameter compared to the empty control ($p < 0.04$; Figure 4.4C). Sample images from the FAST and empty treated hearts are shown in Figure 4.4D and E, respectively.

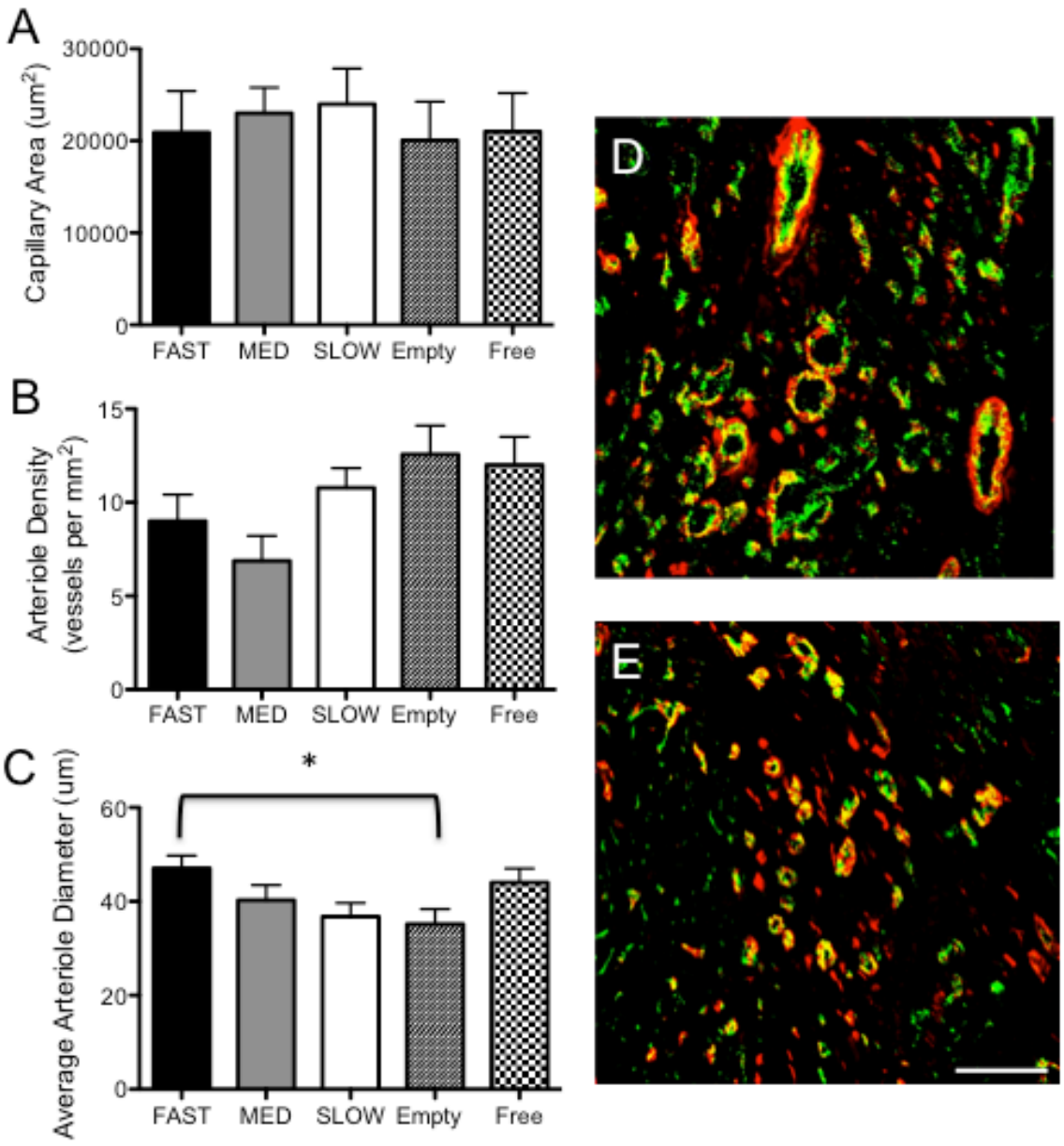

Figure 4.4. Vessel quantification. No differences were observed in (A) capillary area or (B) arteriole density within the infarct between groups. (C) Arterioles within the infarct of hearts treated with HGF-f delivered in FAST degrading AcDex particles had the largest average diameter (*$p < 0.04$). Sample images from (D) FAST and (E) empty treated hearts display the difference in average arteriole diameter. Alpha-SMA (red) and vWF (green) stain smooth muscle and endothelial cells, respectively. Scale bar: 100 μm.

We also assessed the number of apoptotic cardiomyocytes in the borderzone. Significantly fewer apoptotic cardiomyocytes, as identified by co-staining with anti-cleaved caspase and anti-a-actinin were found in hearts treated with HGF-f in FAST and MED degrading AcDex particles compared to empty particle treated hearts ($p < 0.005$; Figure 5A). Example images are shown of infarcts from FAST and empty particle treated hearts in Figure 5 B & C, respectively.

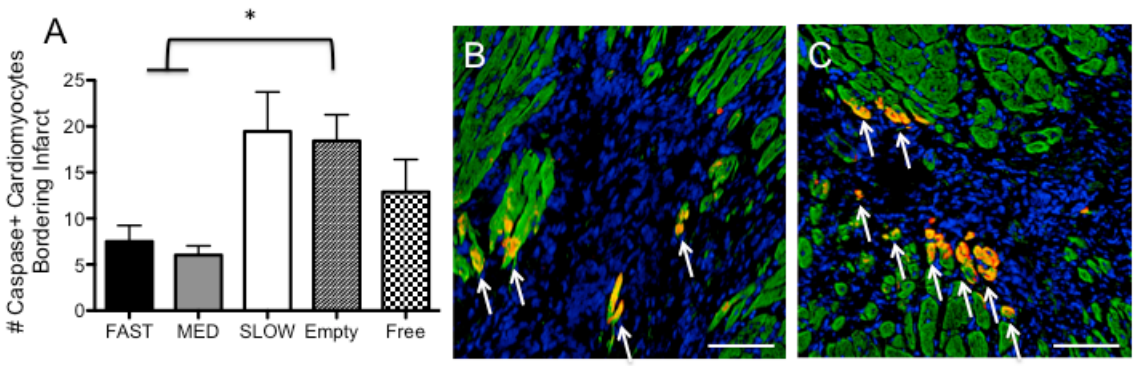

Figure 4.5. Apoptosis quantification. (A) The number of caspase positive cardiomyocytes bordering the infarct was significantly lower when HGF-f was delivered in FAST and MED degrading particles compared to SLOW and empty particles (*$p < 0.005$). Sample images of (B) FAST and (C) empty particle treated hearts are shown. Cleaved-caspase 3 (red) and alpha-actinin (green) visualize apoptotic cardiomyocytes (denoted with white arrows). Scale bar: 100 μm.

Lastly, to evaluate the effects of modulating HGF-f delivery timing on negative LV remodeling, we assessed infarct size and interstitial fibrosis in the remote myocardium. Infarct size, as measured by infarct length, was significantly reduced in hearts treated with HGF-f in FAST degrading AcDex particles when compared to empty particle treatment ($p < 0.02$; Figure 4.6A). HGF-f delivered in MED and SLOW degrading particles also reduced infarct size compared to empty particle treatment, though not significantly. A trend toward reduced

interstitial fibrosis in FAST particle treated hearts was observed, though differences were not significant ($p = 0.1$; Figure 4.6B). Representative infarcts are shown from FAST and empty particle treated hearts in Figure 4.6 C & D, respectively.

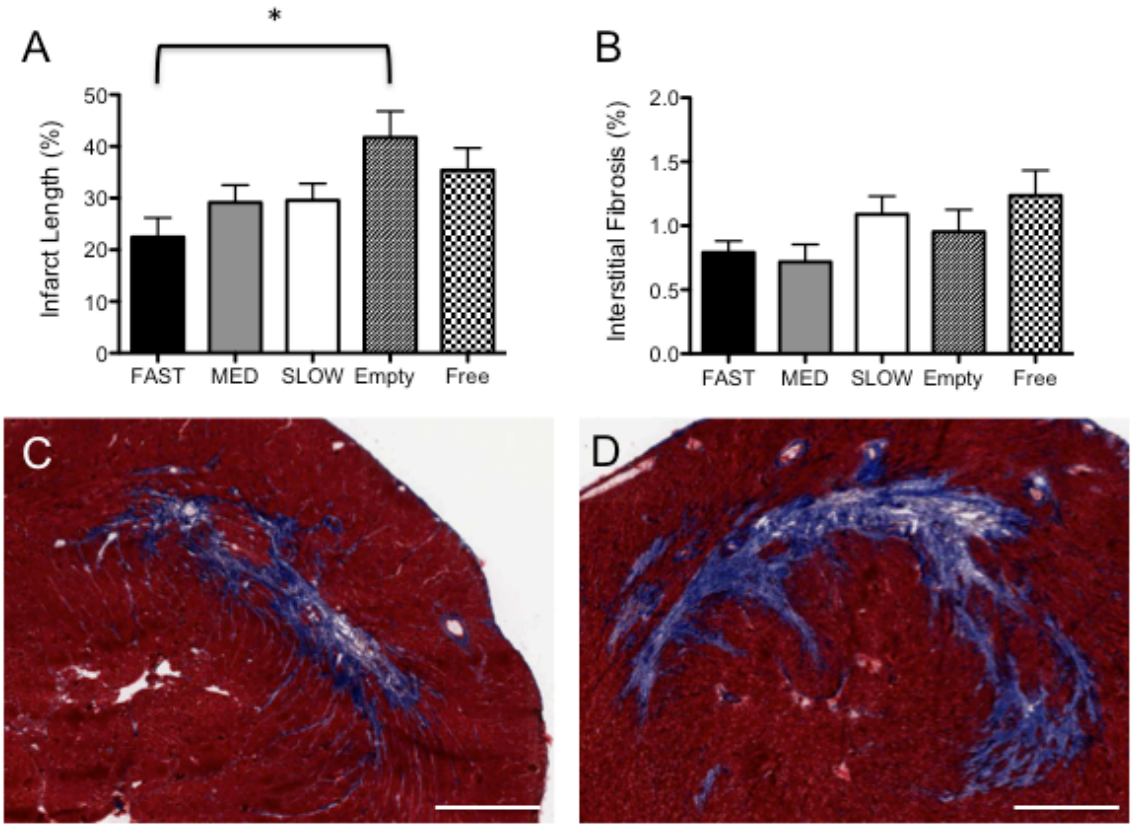

Figure 4.6. Fibrosis quantification. (A) Infarct length was significantly shorter in hearts treated with HGF-f in FAST degrading particles compare to those treated with empty particles ($p < 0.02$). (B) Similar trends for lower interstitial fibrosis in FAST particle treated hearts were observed, though the difference was not significant ($p = 0.1$). Representative infarcts from (FAST) and (empty) particle treated hearts are shown. Fibrotic tissue is stained blue and healthy myocardium is stained red. Scale bar: 1 mm.

4.4 DISCUSSION

Injectable biomaterials are a promising avenue for preventing or treating HF post-MI [6, 7, 111]. One useful property of biomaterials is protecting and

sustaining release of bioactive payloads. However, most biomaterials have a defined degradation profile, thus limiting payload release to one time frame. Herein we designed microparticles with three distinct degradation and consequent protein release profiles without changing any other material properties, enabling a first time look at how changing delivery rate impacted the efficacy of a growth factor known to have cardioprotective properties.

Here we confirm previous reports that the degradation rate of acetalated dextran (AcDex) can be easily tuned by changing the acetalation reaction time, thus enabling tunable release of protein payloads [41, 129]. Changing the acetalation reaction time changes the ratio of cyclic to acyclic acetals along the polymer backbone, thereby affecting degradation properties and the stability of the microparticles. Cyclic acetals both form and degrade more slowly than acyclic acetals, thus increasing the reaction time makes the AcDex more stable. In this study we wanted to create particles with three distinct degradation rates in infarcted hearts. Previously we showed that running the acetalation reaction for increasing duration yielded AcDex batches that could release a protein payload from microparticles between a few days and one month *in vitro* under pH 6 conditions [41], simulating the infarct [62, 127]. For this study we made a FAST degrading AcDex by reacting for a slightly shorter time than the fastest degrading batch in the previous study. We predicted that particles made from FAST AcDex (43% cyclic) would degrade in less than 5 days in the infarct given that 49% cyclic degraded in 5 days *in vitro* at pH 6 [41]. We then created a MED degrading AcDex (54% cyclic) by reacting for similar reaction duration as in the

previous study (54% cyclic), which we predicted would degrade in the infarct after approximately 10 days. Finally we created a SLOW degrading AcDex by reacting for longer than the MED AcDex but shorter than the slowest degrading batch in the former study (59% cyclic). Due to the slightly lower cyclic acetal content we hypothesized that the SLOW degrading AcDex (57% cyclic) would degrade in the infarct in about three weeks. Our results showed that degradation of the particles in the infarcted heart closely matched that of the particles in mildly acidic (pH 6.0) *in vitro* conditions. The predicted degradation rates for the FAST, MED and SLOW degrading AcDex (<5 days, 10 days and ~3 weeks) correlated with the *in vivo* results showing degradation in 3 days, ~1.5 weeks and ~2.5 weeks, respectively. To investigate whether or not a protein payload would be retained in the particles as they degraded, we also encapsulated fluorescently tagged ovalbumin. Ovalbumin was selected as a model protein because its molecular weight (45 kDa) is similar to that of the HGF-f (38 kDa). The encapsulated protein remained inside the particles at all the time points the particles were present within the tissue, confirming that protein release occurred at the same rate as particle degradation. Furthermore, as we showed previously with bFGF AcDex microparticles are able to encapsulate and release active growth factors [41]. Here, heparin was co-encapsulated with the HGF-f to help stabilize the growth factor structure. HGF-f released from FAST, MED and SLOW degrading particles maintained c-met agonist activity (Figure2).

Tunable degradation of AcDex and predictable *in vivo* protein release enabled a never before achieved analysis of the optimal time frame for

delivering a single therapeutic to the heart post-MI. We were able to investigate how delivery rate impacted the efficacy of a known cardioprotective growth factor, HGF. In all measured outcomes, angiogenesis, apoptosis and fibrosis, it was shown that delivering HGF-f over a three-day time frame was optimal. Delivery of HGF-f in the FAST degrading particles resulted in the largest arterioles, the lowest number of apoptotic cardiomyocytes neighboring the infarct and the smallest infarcts compared to empty particle delivery. HGF-f delivered over 1.5 weeks in the MED degrading particles also reduced apoptotic cell number significantly compared to the empty particle treatment and showed a modest but non-significant reduction in infarct size. Delivery of HGF-f over 2.5 weeks in the SLOW degrading particles resulted in only a modest (not significant) reduction in infarct size with no appreciable impact on angiogenesis or apoptosis. These results suggest that especially for vessel formation and cardiomyocyte salvage HGF-f must be delivered quickly. This was further supported by the free HGF-f performing better than the SLOW released HGF-f in both the arteriole diameter and apoptotic cell analyses. The rapid clearance of the free HGF-f, however, likely prevented it from having a significant effect. It has been shown previously that free HGF is ~90% cleared in 5 hours and almost completely cleared in one day after injection into infarcted hearts [130]. The combination of low apoptotic cell number and small infarct size suggests that infarcts were relatively stable in the FAST group, which indicates a long-term benefit of HGF-f delivery even when it is delivered over a short period of time. In

comparison the infarcts were larger in the empty particle group, as indicated by high apoptotic cell number in the borderzone.

We loaded an equivalent amount of HGF-f in all three batches of AcDex particles allowing isolation of time frame of release as the only variable between groups. The total loaded HGF-f was 11-12 μg per mg particle, resulting in 85-90% encapsulation efficiency. For a 75 μL injection of 10 mg/mL of particles this resulted in 8-9 μg of HGF-f per injection. Since the HGF-f has a potency of about 1/10 that of recombinant HGF [125] this equated to about a 1 μg dose of HGF per injection. This dose was selected due to its prior use in studies delivering HGF to the heart post-MI in biomaterials [116, 126]. While it is unknown what the minimum dose of HGF needs to be to observe physiologic changes, another study delivered an order of magnitude less (170 ng per injection) and still observed changes in angiogenesis, apoptosis, and fibrosis [23]. Here the FAST degrading particles yielded the highest dose/day over the shortest number of days. The MED and SLOW degrading particles consequently delivered progressively lower dose/day for a progressively higher number of days. We observed that HGF-f delivery in MED degrading particles reduced apoptotic cardiomyocyte number significantly even though the dose per day was lower than with FAST degrading particles. Furthermore HGF-f released from the MED and SLOW degrading particles slightly reduced infarct size, suggesting that a lower dose/day sustained over a longer time still impacted the fibrosis pathway.

While we did not perform studies to elucidate a mechanism of action of the FAST released HGF-f, we hypothesize that the enlargement of the arterioles within

the infarct may be due to an interaction of HGF-f and angiopoietin-1 (Ang-1). When overexpressed, Ang-1 has been shown to increase the diameter of blood vessels without increasing vessel density [131]. Furthermore, HGF has been shown to be a mediator of Ang-1-induced smooth muscle cell recruitment and vascular maturation *in vivo* [132]. Regarding apoptosis, elevated cleaved-caspase-3 expression has been shown to be elevated in rats models through 7-10 days post-MI compared to 4 weeks post-MI [133]. Perhaps the sustained presence of the HGF-f during the end of this time frame via either FAST or MED degrading particles helped to reduce this early phase of apoptosis. In contrast the majority of the HGF-f from the SLOW particles was delivered after this peak apoptotic window. And finally, collagen deposition begins as early as 3 days post-MI in rats and continues through one month [134, 135]. While the effect was not significant, the SLOW degrading particles were more effective in reducing fibrosis compared to reducing apoptosis or increasing angiogenesis, perhaps due to this longer window of fibrosis development.

A tunable delivery system has the potential to mimic natural tissue repair processes by controlling the temporal presentation of bioactive molecules. The versatility of AcDex particles in encapsulating payloads of different sizes and charges [41] suggests that they could be used to study optimal timeframes of delivery of other cardioprotective proteins, growth factors, or enzymes, which could then be combined with HGF in a dual delivery system. Here we learned that HGF-f was most effective when delivered over a short time frame, thus it would be interesting to next investigate whether addition of a second growth

factor in slower releasing particles would further enhance HGF-induced healing post-MI. Two growth factors have already been delivered with HGF to the heart post-MI: insulin growth factor (IGF) and vascular endothelial growth factor (VEGF) [23, 116]. In both cases the combination of HGF with the second growth factor enhanced post-MI healing beyond that of either factor alone, but these results could be further improved by delivering the factors at their optimal rates. IGF was predicted to release before the HGF when they were both loaded in alginate hydrogels *in vitro* (IGF-1 100% released in 3 days; HGF 25% released in 7 days), yet due to the constraints of the material system the opposite order of delivery was not tested. In the second study, VEGF and HGF were expected to release simultaneously from a PEG hydrogel (50-100% release in 4 days *in vitro*). The positive results observed in this study along with the potential for enhanced efficacy upon pairing with another cardioprotective molecule suggest that HGF-based therapy post-MI is promising. Furthermore, in this study we used a rationally engineered peptide fragment (HGF-f) with c-met agonist activity that mimics the function of full-length recombinant HGF. The *in vivo* efficacy as well as the increased stability and reduced cost of fabricating HGF-f compared to full-length recombinant HGF will aid in the translation of such therapies.

Chapter 4, in part, is in preparation for submission as: Sophia L. Suarez, Adam Muñoz, Aaron Mitchell, Rebecca L. Braden, Colin Luo, Jennifer R. Cochran, Adah Almutairi, Karen L. Christman. HGF cardioprotective efficacy

post-MI is maximized when released from quickly degrading acetalated dextran microparticles.

CHAPTER FIVE:

Summary and Future Work

5.1 Summary and conclusions

Heart failure (HF) post-myocardial infarction (MI) is a leading cause of death in the Western world [110]. Current treatment options for patients with end-stage heart failure include total heart transplantation and implantation of left-ventricular assist devices (LVADs). Unfortunately, donor hearts are in low supply compared to the number of patients waiting. In addition both of these treatment options require invasive surgery that comes with significant risks. Finally, neither treatment acts to restore function of the native heart. Thus new treatment options are needed for patients with end-stage HF.

Injectable biomaterials offer a promising solution as they have the potential for minimally invasive delivery and have properties that facilitate restoration of heart function [5-7]. While much exciting work has been completed to advance injectable biomaterials close to clinical translation, there is still room for understanding and improved design of biomaterial therapies to ensure patient safety and facilitate therapeutic versatility.

In this dissertation we designed a study to investigate the effect of biomaterial injection in the heart on electrophysiology (Chapter 2). Patients eligible for biomaterial therapy may be at increased risk for ventricular arrhythmias [43], thus it is essential to make sure the biomaterial therapy does not increase their risk above baseline. We utilized optical mapping [136] to assess changes in electrophysiology following biomaterial injection. Biomaterials were injected into healthy hearts as well as in the borderzone of infarcted hearts, a common location for biomaterial injections, especially for those containing cells.

After action potential propagation was assessed histological analysis was performed to assess biomaterial interstitial spread, as this parameter varies across different biomaterials. We developed a metric to quantify the amount of interstitial spread of the biomaterial to compare this parameter to electrophysiological outcomes. Specifically, we learned that injection of a highly spread hydrogel in the myocardium does not alter action potential propagation, while injection of a hydrogel with low spread may create a substrate for arrhythmia by causing slowed action potential propagation through reduced gap junction density at the site of injection (Chapter 2). While injection into the infarct may not be a concern given the already slowed or perturbed conduction, our results indicate that delivery of a highly spread hydrogel into viable or border zone myocardium is safe whereas a hydrogel with low spread may have deleterious effects. This work establishes site of delivery and spread of biomaterials in the tissue as important factors in the future use and development of biomaterial therapies for MI treatment, and warrants further investigation in large animal models. Furthermore, the work will help to inform the design of safe biomaterial therapies as a variety of factors can be tailored to alter the degree of interstitial spread of biomaterials following injection.

Typically biomaterial safety is assessed in terms of the degree of immune response induced following injection. While this type of analysis is certainly important, it is not sufficient. The impact of the biomaterial injection on electrophysiology must be understood. This work was a first step towards understanding this relationship. We observed a significant correlation between

biomaterial interstitial spread and action potential propagation. While there is natural variability in the degree of spread of different biomaterials, this parameter has not been a focus of biomaterial design. Yet with the knowledge that high interstitial spread is crucial to biomaterial safety, this should become a priority in biomaterial design. Material concentration, gelation mechanism and injection time are a few ways that interstitial spread can be controlled. Thus while this work suggests a safety risk for some biomaterials (ie. those with low interstitial spread), the risk can be lowered or removed through systematic design. If biomaterial spread cannot be increased, injection location must be carefully considered. Our work shows a risk of arrhythmia induction when biomaterials with low spread are injected into viable myocardium next to an infarct. If the material is contained within the infarct the risk will likely be significantly decreased.

While biomaterials have the ability to protect and sustain release of bioactive payloads, most biomaterials have a defined degradation profile, thus limiting payload release to one time frame. Mimicking a normal healing pathway by delivering exogenous molecules at the proper time could facilitate positive tissue remodeling following ischemic damage post-MI. A tunable delivery system has the potential to mimic natural tissue repair processes by controlling the temporal presentation of bioactive molecules. In order to facilitate this type of work we designed microparticles with never before seen control of payload release ranging from days to months through simple modification of polymer composition. These particles were shown to be promising for delivery of protein therapeutics to the heart post-MI by encapsulating and releasing active growth

factors and by not inducing a negative immune response following injection in healthy hearts [41] (Chapter 3).

Following full characterization, the particles were used for a first of its kind study investigating the optimal time frame for delivery of a known cardioprotective growth factor, hepatocyte growth factor (HGF) (Chapter 4). While HGF is known to impact several important healing pathways necessary for tissue repair post-MI [137-139], and has been shown to protect the heart through delivery of exogenous HGF and induction of increased expression of endogenous HGF [23, 116-124, 126], the optimal time frame for delivery is not known. Using particles with three distinct rates of payload release we determined that HGF-f, a rationally engineered peptide fragment HGF mimic, is optimally delivered over a span of three days (Chapter 4). This delivery time frame resulted in the largest arterioles, the lowest number of apoptotic cardiomyocytes neaighboring the infarct and the smallest infarcts. The use of HGF-f, which is more stable and less expensive than full-length recombinant HGF [125], further improves the translatability of HGF-based therapy into the clinic. This work will help inform the design of future HGF-based therapies and provides a platform for studying additional cardioprotective growth factors to optimize their therapeutic efficacy.

The ability to tune release of therapeutics to the heart post-MI is a crucial step towards developing a comprehensive therapy that can prevent negative remodeling. Of first importance is the ability to study when certain molecules should be delivered to exhibit maximal benefit. This work was a first of its kind to

investigate the relationship between delivery rate and therapeutic outcome. We found that the therapeutic efficacy of HGF-f was significantly different depending on its rate of release from the particles. Thus timing of delivery should become a focus of design considerations when releasing bioactive payloads from biomaterials. Materials properties including concentration, composition and degradation rate can potentially be tuned to change payload release rate. Additionally design of other tunable materials, like AcDex, should be considered.

5.2 Future work

There are several opportunities for future work to expand on the results obtained in this dissertation.

As a next step to gaining a thorough understanding of the impact of biomaterial injection on heart electrophysiology in human patients, a large animal study would be extremely valuable to the field. Moreover, at later time points, degradation of the biomaterial and resulting cell infiltration will both contribute to its level of risk of becoming a substrate for arrhythmia, and therefore, it is also important to continue to study the risk of arrhythmias for each individual biomaterial overtime prior to use in patients. In general, some degree of assessment of electrophysiology following biomaterial injection should be incorporated into future biomaterial studies in order to expand on our understanding of biomaterial safety. And finally, while we hypothesized that biomaterial injection directly into infarcted tissue would not adversely impact

conduction we only studied borderzone injections. A systematic investigation of electrophysiology after infarct injection would also be valuable to the field.

There are several avenues for future work based on the results described in chapter 4. First, since HGF-f was shown to be most effective when delivered over a short time frame (in FAST degrading particles), it would be interesting to next investigate whether addition of a second growth factor in slower degrading particles delivered with HGF would further enhance healing post-MI. This work also provides a platform for the study of the optimal time frame for delivering other growth factors, enzymes and small molecules known to stimulate tissue repair following MI. Once this information has been obtained for a library of cardioprotective molecules, a potent cocktail can be designed that allows distinct and precise delivery of multiple therapies in one injection. It is likely that this type of sophisticated therapy is needed to combat such a complex pathology as seen in the progression to heart failure.

References

[1] Go AS, Mozaffarian D, Roger VL, Benjamin EJ, Berry JD, Blaha MJ, Dai S, Ford ES, Fox CS, Franco S, Fullerton HJ, Gillespie C, Hailpern SM, Heit JA, Howard VJ, Huffman MD, Judd SE, Kissela BM, Kittner SJ, Lackland DT, Lichtman JH, Lisabeth LD, Mackey RH, Magid DJ, Marcus GM, Marelli A, Matchar DB, Mcguire DK, Mohler ER, Moy CS, Mussolino ME, Neumar RW, Nichol G, Pandey DK, Paynter NP, Reeves MJ, Sorlie PD, Stein J, Towfighi A, Turan TN, Virani SS, Wong ND, Woo D, Turner MB. Heart Disease and Stroke Statistics--2014 Update: A Report From the American Heart Association. Circulation. 2014129:e28-e292.

[2] Roger VL, Go AS, Lloyd-Jones DM, Benjamin EJ, Berry JD, Borden WB, Bravata DM, Dai S, Ford ES, Fox CS, Fullerton HJ, Gillespie C, Hailpern SM, Heit JA, Howard VJ, Kissela BM, Kittner SJ, Lackland DT, Lichtman JH, Lisabeth LD, Makuc DM, Marcus GM, Marelli A, Matchar DB, Moy CS, Mozaffarian D, Mussolino ME, Nichol G, Paynter NP, Soliman EZ, Sorlie PD, Sotoodehnia N, Turan TN, Virani SS, Wong ND, Woo D, Turner MB. Heart Disease and Stroke Statistics--2012 Update: A Report From the American Heart Association. Circulation. 2012;125:e2-e220.

[3] Sun Y, Weber KT. Infarct scar: a dynamic tissue. Cardiovascular Research. 200046:250-6.

[4] Christman KL, Lee RJ. Biomaterials for the treatment of myocardial infarction. J Am Coll Cardiol. 2006;48:907-13.

[5] Rane AA, Christman KL. Biomaterials for the Treatment of Myocardial Infarction. J Am Coll Cardiol. 2011;58:2615-29.

[6] Johnson TD, Christman KL. Injectable hydrogel therapies and their delivery strategies for treating myocardial infarction. Expert Opinion on Drug Delivery. 2013;10:59-72.

[7] Suarez S, Almutairi A, Christman KL. Micro- and Nanoparticles for Treating Cardiovascular Disease. Biomaterials Science. 2015;3:564-80.

[8] Dai W, Wold LE, Dow JS, Kloner RA. Thickening of the infarcted wall by collagen injection improves left ventricular function in rats: a novel approach to preserve cardiac function after myocardial infarction. J Am Coll Cardiol. 2005;46:714-9.

[9] Blackburn NJR, Sofrenovic T, Kuraitis D, Ahmadi A, Mcneill B, Deng C, Rayner KJ, Zhong Z, Ruel M, Suuronen EJ. Timing underpins the benefits associated with injectable collagen biomaterial therapy for the treatment of myocardial infarction. Biomaterials. 2015;39:182-92.

[10] Landa N, Miller L, Feinberg MS, Holbova R, Shachar M, Freeman I, Cohen S, Leor J. Effect of injectable alginate implant on cardiac remodeling and function after recent and old infarcts in rat. Circulation. 2008;117:1388-96.

[11] Leor J, Tuvia S, Guetta V, Manczur F, Castel D, Willenz U, Petneházy O, Landa N, Feinberg MS, Konen E, Goitein O, Tsur-Gang O, Shaul M, Klapper L, Cohen S. Intracoronary injection of in situ forming alginate hydrogel reverses left ventricular remodeling after myocardial infarction in Swine. J Am Coll Cardiol. 2009;54:1014-23.

[12] Christman KL, Fok HH, Sievers RE, Fang Q, Lee RJ. Fibrin glue alone and skeletal myoblasts in a fibrin scaffold preserve cardiac function after myocardial infarction. Tissue Eng. 2004;10:403-9.

[13] Lu WN, Lü SH, Wang HB, Li DX, Duan CM, Liu ZQ, Hao T, He WJ, Xu B, Fu Q, Song YC, Xie XH, Wang CY. Functional improvement of infarcted heart by co-injection of embryonic stem cells with temperature-responsive chitosan hydrogel. Tissue Eng Pt A. 2009;15:1437-47.

[14] Okada M, Payne TR, Oshima H, Momoi N, Tobita K, Huard J. Differential efficacy of gels derived from small intestinal submucosa as an injectable biomaterial for myocardial infarct repair. Biomaterials. 2010;31:7678-83.

[15] Singelyn JM, Sundaramurthy P, Johnson TD, Schup-Magoffin PJ, Hu DP, Faulk DM, Wang J, Mayle KM, Bartels K, Salvatore M, Kinsey AM, Demaria AN, Dib N, Christman KL. Catheter-deliverable hydrogel derived from decellularized ventricular extracellular matrix increases endogenous cardiomyocytes and preserves cardiac function post-myocardial infarction. J Am Coll Cardiol. 2012;59:751-63.

[16] Seif-Naraghi SB, Singelyn JM, Salvatore MA, Osborn KG, Wang JJ, Sampat U, Kwan OL, Strachan GM, Wong J, Schup-Magoffin PJ, Braden RL, Bartels K, Dequach JA, Preul M, Kinsey AM, Demaria AN, Dib N, Christman KL. Safety and Efficacy of an Injectable Extracellular Matrix Hydrogel for Treating Myocardial Infarction. Science Translational Medicine. 2013;5:173ra25-ra25.

[17] Jiang XJ, Wang T, Li XY, Wu DQ, Zheng ZB, Zhang JF, Chen JL, Peng B, Jiang H, Huang C, Zhang XZ. Injection of a novel synthetic hydrogel preserves left ventricle function after myocardial infarction. Journal of biomedical materials research Part A. 2009;90:472-7.

[18] Fujimoto KL, Ma Z, Nelson DM, Hashizume R, Guan J, Tobita K, Wagner WR. Synthesis, characterization and therapeutic efficacy of a biodegradable, thermoresponsive hydrogel designed for application in chronic infarcted myocardium. Biomaterials. 2009;30:4357-68.

[19] Wang T, Wu DQ, Jiang XJ, Zhang XZ, Li XY, Zhang JF, Zheng ZB, Zhuo R, Jiang H, Huang C. Novel thermosensitive hydrogel injection inhibits post-infarct ventricle remodelling. Eur J Heart Fail. 2009;11:14-9.

[20] Wang H, Zhang X, Li Y, Ma Y, Zhang Y, Liu Z, Zhou J, Lin Q, Wang Y, Duan C, Wang C. Improved myocardial performance in infarcted rat heart by co-injection of basic fibroblast growth factor with temperature-responsive Chitosan hydrogel. HEALUN. 2015;29:881-7.

[21] Garbern JC, Minami E, Stayton PS, Murry CE. Delivery of basic fibroblast growth factor with a pH-responsive, injectable hydrogel to improve angiogenesis in infarcted myocardium. Biomaterials. 2011;32:2407-16.

[22] Hao X, Silva EA, Månsson-Broberg A, Grinnemo K-H, Siddiqui AJ, Dellgren G, Wärdell E, Brodin LA, Mooney DJ, Sylvén C. Angiogenic effects of sequential release of VEGF-A165 and PDGF-BB with alginate hydrogels after myocardial infarction. Cardiovasc Res. 2007;75:178-85.

[23] Ruvinov E, Leor J, Cohen S. The promotion of myocardial repair by the sequential delivery of IGF-1 and HGF from an injectable alginate biomaterial in a model of acute myocardial infarction. Biomaterials. 2011;32:565-78.

[24] Guo H-D, Wang H-J, Tan Y-Z, Wu J-H. Transplantation of Marrow-Derived Cardiac Stem Cells Carried in Fibrin Improves Cardiac Function After Myocardial Infarction. Tissue Engineering Part A. 2011;17:45-58.

[25] Lin Y-D, Yeh M-L, Yang Y-J, Tsai D-C, Chu T-Y, Shih Y-Y, Chang M-Y, Liu Y-W, Tang ACL, Chen T-Y, Luo C-Y, Chang K-C, Chen J-H, Wu H-L, Hung T-K, Hsieh PCH. Intramyocardial Peptide Nanofiber Injection Improves Postinfarction Ventricular Remodeling and Efficacy of Bone Marrow Cell Therapy in Pigs. Circulation. 2010;122:S132-S41.

[26] Frey N, Linke A, Suselbeck T, Muller-Ehmsen J, Vermeersch P, Schoors D, Rosenberg M, Bea F, Tuvia S, Leor J. Intracoronary Delivery of Injectable Bioabsorbable Scaffold (IK-5001) to Treat Left Ventricular Remodeling After ST-Elevation Myocardial Infarction: A First-in-Man Study. Circulation: Cardiovascular Interventions. 2014;7:806-12.

[27] Bellerophon BCM LLC. NCT01226563: IK-5001 for the Prevention of Remodeling of the Ventricle and Congestive Heart Failure After Acute Myocardial Infarction (PRESERVATION 1). Available at https://clinicaltrials.gov/ct2/show/NCT01226563. Accessed 6 March 2015. 2015.

[28] Iwakura A, Fujita M, Kataoka K, Tambara K, Sakakibara Y, Komeda M, Tabata Y. Intramyocardial sustained delivery of basic fibroblast growth factor

improves angiogenesis and ventricular function in a rat infarct model. Heart Vessels. 2003;18:93-9.

[29] Liu Y, Sun L, Huan Y, Zhao H, Deng J. Effects of basic fibroblast growth factor microspheres on angiogenesis in ischemic myocardium and cardiac function: analysis with dobutamine cardiovascular magnetic resonance tagging. Eur J Cardiothorac Surg. 2006;30:103-7.

[30] Sakakibara Y, Tambara K, Sakaguchi G, Lu F, Yamamoto M, Nishimura K, Tabata Y, Komeda M. Toward surgical angiogenesis using slow-released basic fibroblast growth factor. Eur J Cardiothorac Surg. 2003;24:105-11; discussion 12.

[31] Lin X, Jo H, Ishii TM, Fujita M, Fu M, Tambara K, Yamamoto M, Tabata Y, Komeda M, Matsuoka S. Controlled release of matrix metalloproteinase-1 plasmid DNA prevents left ventricular remodeling in chronic myocardial infarction of rats. Circ J. 2009;73:2315-21.

[32] Wei HJ, Yang HH, Chen CH, Lin WW, Chen SC, Lai PH, Chang Y, Sung HW. Gelatin microspheres encapsulated with a nonpeptide angiogenic agent, ginsenoside Rg1, for intramyocardial injection in a rat model with infarcted myocardium. J Control Release. 2007;120:27-34.

[33] Formiga FR, Pelacho B, Garbayo E, Abizanda G, Gavira JJ, Simon-Yarza T, Mazo M, Tamayo E, Jauquicoa C, Ortiz-De-Solorzano C, Prósper F, Blanco-Prieto MJ. Sustained release of VEGF through PLGA microparticles improves vasculogenesis and tissue remodeling in an acute myocardial ischemia-reperfusion model. J Control Release. 2010;147:30-7.

[34] Simón-Yarza T, Tamayo E, Benavides C, Lana H, Formiga FR, Grama CN, Ortiz-De-Solorzano C, Kumar MNVR, Prosper F, Blanco-Prieto MJ. Functional benefits of PLGA particulates carrying VEGF and CoQ10 in an animal of myocardial ischemia. International Journal of Pharmaceutics. 2013;454:784-90.

[35] Formiga FR, Pelacho B, Garbayo E, Imbuluzqueta I, Díaz-Herráez P, Abizanda G, Gavira JJ, Simón-Yarza T, Albiasu E, Tamayo E, Prósper F, Blanco-Prieto MJ. Controlled delivery of fibroblast growth factor-1 and neuregulin-1 from biodegradable microparticles promotes cardiac repair in a rat myocardial infarction model through activation of endogenous regeneration. Journal of Controlled Release. 2014;173:132-9.

[36] Chang M-Y, Yang Y-J, Chang C-H, Tang ACL, Liao W-Y, Cheng F-Y, Yeh C-S, Lai JJ, Stayton PS, Hsieh PCH. Functionalized nanoparticles provide early cardioprotection after acute myocardial infarction. Journal of Controlled Release. 2013;170:287-94.

[37] Seshadri G, Sy JC, Brown M, Dikalov S, Yang SC, Murthy N, Davis ME. The delivery of superoxide dismutase encapsulated in polyketal microparticles to rat myocardium and protection from myocardial ischemia-reperfusion injury. Biomaterials. 2010;31:1372-9.

[38] Sy JC, Seshadri G, Yang SC, Brown M, Oh T, Dikalov S, Murthy N, Davis ME. Sustained release of a p38 inhibitor from non-inflammatory microspheres inhibits cardiac dysfunction. Nat Mater. 2008;7:863-8.

[39] Gray WD, Che P, Brown M, Ning X, Murthy N, Davis ME. N-acetylglucosamine Conjugated to Nanoparticles Enhances Myocyte Uptake and Improves Delivery of a Small Molecule p38 Inhibitor for Post-infarct Healing. J of Cardiovasc Trans Res. 2011;4:631-43.

[40] Somasuntharam I, Boopathy AV, Khan RS, Martinez MD, Brown ME, Murthy N, Davis ME. Delivery of Nox2-NADPH oxidase siRNA with polyketal nanoparticles for improving cardiac function following myocardial infarction. Biomaterials. 2013;34:7790-8.

[41] Suarez S, Grover GN, Braden RL, Christman KL, Almutairi A. Tunable Protein Release from Acetalated Dextran Microparticles: A Platform for Delivery of Protein Therapeutics to the Heart Post-MI. Biomacromolecules. 2013;14:3927-35.

[42] Laham RJ. Transendocardial and Transepicardial Intramyocardial Fibroblast Growth Factor-2 Administration: Myocardial and Tissue Distribution. Drug Metabolism and Disposition. 2005;33:1101-7.

[43] Menasche P. Stem Cell Therapy for Heart Failure: Are Arrhythmias a Real Safety Concern? Circulation. 2009;119:2735-40.

[44] Hagège AA, Marolleau JP, Vilquin JT, Alhéritière A, Peyrard S, Duboc D, Abergel E, Messas E, Mousseaux E, Schwartz K, Desnos M, Menasché P. Skeletal myoblast transplantation in ischemic heart failure: long-term follow-up of the first phase I cohort of patients. Circulation. 2006;114:I108-13.

[45] Dib N, Michler RE, Pagani FD, Wright S, Kereiakes DJ, Lengerich R, Binkley P, Buchele D, Anand I, Swingen C, Di Carli MF, Thomas JD, Jaber WA, Opie SR, Campbell A, McCarthy P, Yeager M, Dilsizian V, Griffith BP, Korn R, Kreuger SK, Ghazoul M, MacLellan WR, Fonarow G, Eisen HJ, Dinsmore J, Diethrich E. Safety and feasibility of autologous myoblast transplantation in patients with ischemic cardiomyopathy: four-year follow-up. Circulation. 2005;112:1748-55.

[46] Siminiak T, Kalawski R, Fiszer D, Jerzykowska O, Rzeźniczak J, Rozwadowska N, Kurpisz M. Autologous skeletal myoblast transplantation for the treatment of postinfarction myocardial injury: phase I clinical study with 12 months of follow-up. Am Heart J. 2004;148:531-7.

[47] Rane AA. Understanding mechanisms by which injectable materials preserve cardiac function post-MI: University of California, San Diego; 2012.

[48] Ifkovits JL, Tous E, Minakawa M, Morita M, Robb JD, Koomalsingh KJ, Gorman JH, Gorman RC, Burdick JA. Injectable hydrogel properties influence infarct expansion and extent of postinfarction left ventricular remodeling in an ovine model. Proc Natl Acad Sci USA. 2010;107:11507-12.

[49] Christman KL, Vardanian AJ, Fang Q, Sievers RE, Fok HH, Lee RJ. Injectable fibrin scaffold improves cell transplant survival, reduces infarct expansion, and induces neovasculature formation in ischemic myocardium. J Am Coll Cardiol. 2004;44:654-60.

[50] Davis ME, Hsieh PCH, Takahashi T, Song Q, Zhang SG, Kamm RD, Grodzinsky AJ, Anversa P, Lee RT. Local myocardial insulin-like growth factor 1 (IGF-1) delivery with biotinylated peptide nanofibers improves cell therapy for myocardial infarction. Proc Natl Acad Sci USA. 2006;103:8155-60.

[51] Huang NF, Yu J, Sievers R, Li S, Lee RJ. Injectable biopolymers enhance angiogenesis after myocardial infarction. Tissue Eng. 2005;11:1860-6.

[52] Hsieh PCH. Controlled delivery of PDGF-BB for myocardial protection using injectable self-assembling peptide nanofibers. Journal of Clinical Investigation. 2005;116:237-48.

[53] Freeman I, Cohen S. The influence of the sequential delivery of angiogenic factors from affinity-binding alginate scaffolds on vascularization. Biomaterials. 2009;30:2122-31.

[54] Macdonald ML, Rodriguez NM, Shah NJ, Hammond PT. Characterization of tunable FGF-2 releasing polyelectrolyte multilayers. Biomacromolecules. 2010;11:2053-9.

[55] She Z, Wang C, Li J, Sukhorukov GB, Antipina MN. Encapsulation of basic fibroblast growth factor by polyelectrolyte multilayer microcapsules and its controlled release for enhancing cell proliferation. Biomacromolecules. 2012;13:2174-80.

[56] Itoh Y, Matsusaki M, Kida T, Akashi M. Locally controlled release of basic fibroblast growth factor from multilayered capsules. Biomacromolecules. 2008;9:2202-6.

[57] Sukhorukov GB, Antipov AA, Voigt A, Donath E, hwald HM. pH-Controlled Macromolecule Encapsulation in and Release from Polyelectrolyte Multilayer Nanocapsules. Macromol Rapid Commun. 2001;22:44-6.

[58] De Geest BG, Sanders NN, Sukhorukov GB, Demeester J, De Smedt SC. Release mechanisms for polyelectrolyte capsules. Chem Soc Rev. 2007;36:636.

[59] She Z, Antipina MN, Li J, Sukhorukov GB. Mechanism of protein release from polyelectrolyte multilayer microcapsules. Biomacromolecules. 2010;11:1241-7.

[60] Richardson TP, Peters MC, Ennett AB, Mooney DJ. Polymeric system for dual growth factor delivery. Nat Biotechnol. 2001;19:1029-34.

[61] Khabbaz KR, Zankoul F, Warner KG. Intraoperative metabolic monitoring of the heart: II. Online measurement of myocardial tissue pH. A Ann Thorac Surg. 2001;72:S2227-33; discussion S33-4, S67-70.

[62] Kumbhani DJ, Healey NA, Birjiniuk V, Crittenden MD, Josa M, Treanor PR, Khuri SF. Determinants of regional myocardial acidosis during cardiac surgery. Surgery. 2004;136:190-8.

[63] Tengood JE, Ridenour R, Brodsky R, Russell AJ, Little SR. Sequential Delivery of Basic Fibroblast Growth Factor and Platelet-Derived Growth Factor for Angiogenesis. Tissue Engineering Part A. 2011;17:1181-9.

[64] Tengood JE, Kovach KM, Vescovi PE, Russell AJ, Little SR. Sequential delivery of vascular endothelial growth factor and sphingosine 1-phosphate for angiogenesis. Biomaterials. 2010;31:7805-12.

[65] Phatharajaree W, Phrommintikul A, Chattipakorn N. Matrix metalloproteinases and myocardial infarction. Can J Cardiol. 2007;23:727-33.

[66] Roger VL, Go AS, Lloyd-Jones DM, Benjamin EJ, Berry JD, Borden WB, Bravata DM, Dai S, Ford ES, Fox CS, Fullerton HJ, Gillespie C, Hailpern SM, Heit JA, Howard VJ, Kissela BM, Kittner SJ, Lackland DT, Lichtman JH, Lisabeth LD, Makuc DM, Marcus GM, Marelli A, Matchar DB, Moy CS, Mozaffarian D, Mussolino ME, Nichol G, Paynter NP, Soliman EZ, Sorlie PD, Sotoodehnia N, Turan TN, Virani SS, Wong ND, Woo D, Turner MB, Subcommittee AHASCaSS. Heart disease and stroke statistics--2012 update: a report from the American Heart Association. Circulation. 2012;125:e2-e220.

[67] Efimov IR, Nikolski VP, Salama G. Optical imaging of the heart. Circulation Research. 2004;95:21-33.

[68] Mills WR, Mal N, Forudi F, Popovic ZB, Penn MS, Laurita KR. Optical mapping of late myocardial infarction in rats. Am J Physiol Heart Circ Physiol. 2006;290:H1298-306.

[69] Ding C, Gepstein L, Nguyen DT, Wilson E, Hulley G, Beaser A, Lee RJ, Olgin J. High-resolution optical mapping of ventricular tachycardia in rats with chronic myocardial infarction. Pacing Clin Electrophysiol. 2010;33:687-95.

[70] Gepstein L, Ding C, Rehemedula D, Wilson EE, Yankelson L, Caspi O, Gepstein A, Huber I, Olgin JE. In vivo assessment of the electrophysiological integration and arrhythmogenic risk of myocardial cell transplantation strategies. Stem Cells. 2010;28:2151-61.

[71] Costa AR, Panda NC, Yong S, Mayorga ME, Pawlowski GP, Fan K, Penn MS, Laurita KR. Optical mapping of cryoinjured rat myocardium grafted with mesenchymal stem cells. Am J Physiol Heart Circ Physiol. 2012;302:H270-7.

[72] Fedorov VV, Lozinsky IT, Sosunov EA, Anyukhovsky EP, Rosen MR, Balke CW, Efimov IR. Application of blebbistatin as an excitation-contraction uncoupler for electrophysiologic study of rat and rabbit hearts. Heart Rhythm. 2007;4:619-26.

[73] Sung D, JSJP C, Mills R, McCulloch AD. Phase shifting prior to spatial filtering enhances optical recordings of cardiac action potential propagation. Ann Biomed Eng. 2001;29:854-61.

[74] Robey TE, Murry CE. Absence of regeneration in the MRL/MpJ mouse heart following infarction or cryoinjury. Cardiovasc Pathol. 2008;17:6-13.

[75] Sampson KJ, Henriquez CS. Electrotonic influences on action potential duration dispersion in small hearts: a simulation study. Am J Physiol Heart Circ Physiol. 2005;289:H350-60.

[76] Danik SB, Liu F, Zhang J, Suk HJ, Morley GE, Fishman GI, Gutstein DE. Modulation of cardiac gap junction expression and arrhythmic susceptibility. Circulation Research. 2004;95:1035-41.

[77] Saffitz JE, Schuessler RB, Yamada KA. Mechanisms of remodeling of gap junction distributions and the development of anatomic substrates of arrhythmias. Cardiovascular Research.1999;42:309-17.

[78] Van Rijen HVM. Slow Conduction and Enhanced Anisotropy Increase the Propensity for Ventricular Tachyarrhythmias in Adult Mice With Induced Deletion of Connexin43. Circulation. 2004;109:1048-55.

[79] Van Veen TAB. Impaired Impulse Propagation in Scn5a-Knockout Mice: Combined Contribution of Excitability, Connexin Expression, and Tissue Architecture in Relation to Aging. Circulation. 2005;112:1927-35.

[80] Wu TJ, Ong JJ, Hwang C, Lee JJ, Fishbein MC, Czer L, Trento A, Blanche C, Kass RM, Mandel WJ, Karagueuzian HS, Chen PS. Characteristics of wave fronts

during ventricular fibrillation in human hearts with dilated cardiomyopathy: role of increased fibrosis in the generation of reentry. J Am Coll Cardiol. 1998;32:187-96.

[81] Kawara T, Derksen R, de Groot JR, Coronel R, Tasseron S, Linnenbank AC, Hauer RN, Kirkels H, Janse MJ, de Bakker JM. Activation delay after premature stimulation in chronically diseased human myocardium relates to the architecture of interstitial fibrosis. Circulation. 2001;104:3069-75.

[82] Henriquez CS. Simulating the electrical behavior of cardiac tissue using the bidomain model. Crit Rev Biomed Eng. 1993;21:1-77.

[83] Roth BJ. How the anisotropy of the intracellular and extracellular conductivities influences stimulation of cardiac muscle. J Math Biol. 1992;30:633-46.

[84] Rane AA, Chuang JS, Shah A, Hu DP, Dalton ND, Gu Y, Peterson KL, Omens JH, Christman KL. Increased Infarct Wall Thickness by a Bio-Inert Material Is Insufficient to Prevent Negative Left Ventricular Remodeling after Myocardial Infarction. PLoS ONE. 2011;6:e21571.

[85] Lu WN, Lu SH, Wang HB, Li DX, Duan CM, Liu ZQ, Hao T, He WJ, Xu B, Fu Q, Song YC, Xie XH, Wang CY. Functional improvement of infarcted heart by co-injection of embryonic stem cells with temperature-responsive chitosan hydrogel. Tissue Eng Part A. 2009;15:1437-47.

[86] Sabbah HN, Wang M, Gupta RC, Rastogi S, Ilsar I, Sabbah MS, Kohli S, Helgerson S, Lee RJ. Augmentation of Left Ventricular Wall Thickness With Alginate Hydrogel Implants Improves Left Ventricular Function and Prevents Progressive Remodeling in Dogs With Chronic Heart Failure. JACC: Heart Failure. 2013;1:252-8.

[87] Mukherjee R, Zavadzkas JA, Saunders SM, McLean JE, Jeffords LB, Beck C, Stroud RE, Leone AM, Koval CN, Rivers WT, Basu S, Sheehy A, Michal G, Spinale FG. Targeted myocardial microinjections of a biocomposite material reduces infarct expansion in pigs. Ann Thorac Surg. 2008;86:1268-76.

[88] Yang Y, Sun J, Gervai P, Gruwel ML, Jilkina O, Gussakovsky E, Yang X, Kupriyanov V. Characterization of cryoinjury-induced infarction with manganese- and gadolinium-enhanced MRI and optical spectroscopy in pig hearts. Magnetic Resonance Imaging. 2010;28:753-66.

[89] GB H, RB C, DC J, DL R. Comparison of early and late dimensions and arrhythmogenicity of cryolesions in the normothermic canine heart. J Thorac Cardiovasc Surg. 1989;97:313-8.

[90] Yang Y, Gruwel M, Dreessen De Gervai P, Sun J, Jilkina O, Gussakovsky E, Kupriyanov V. MRI study of cryoinjury infarction in pig hearts: i. Effects of intrapericardial delivery of bFGF/VEGF embedded in alginate beads. NMR Biomed. 2011;25:177-88.

[91] Li Z, Guan J. Hydrogels for Cardiac Tissue Engineering. Polymers. 2011;3:740-61.

[92] Tous E, Purcell B, Ifkovits JL, Burdick JA. Injectable Acellular Hydrogels for Cardiac Repair. Journal of cardiovascular translational research. 2011;4:528-42.

[93] Formiga FR, Pelacho B, Garbayo E, Abizanda G, Gavira JJ, Simon-Yarza T, Mazo M, Tamayo E, Jauquicoa C, Ortiz-de-Solorzano C, Prosper F, Blanco-Prieto MJ. Sustained release of VEGF through PLGA microparticles improves vasculogenesis and tissue remodeling in an acute myocardial ischemia-reperfusion model. Journal of Controlled Release. 2010;147:30-7.

[94] Yamamoto T, Suto N, Okubo T, Mikuniya A, Hanada H, Yagihashi S, Fujita M, Okumura K. Intramyocardial delivery of basic fibroblast growth factor-impregnated gelatin hydrogel microspheres enhances collateral circulation to infarcted canine myocardium. Jpn Circ J. 2001;65:439-44.

[95] Seshadri G, Sy JC, Brown M, Dikalov S, Yang SC, Murthy N, Davis ME. The delivery of superoxide dismutase encapsulated in polyketal microparticles to rat myocardium and protection from myocardial ischemia-reperfusion injury. Biomaterials. 2010;31:1372-9.

[96] Bachelder EM, Beaudette TT, Broaders KE, Dashe J, Fréchet JMJ. Acetal-derivatized dextran: an acid-responsive biodegradable material for therapeutic applications. J Am Chem Soc. 2008;130:10494-5.

[97] Bachelder EM, Beaudette TT, Broaders KE, Fréchet JMJ, Albrecht MT, Mateczun AJ, Ainslie KM, Pesce JT, Keane-Myers AM. In vitro analysis of acetalated dextran microparticles as a potent delivery platform for vaccine adjuvants. Mol Pharm. 20107:826-35.

[98] Cohen JA, Beaudette TT, Cohen JL, Broaders KE, Bachelder EM, Fréchet JMJ. Acetal-Modified Dextran Microparticles with Controlled Degradation Kinetics and Surface Functionality for Gene Delivery in Phagocytic and Non-Phagocytic Cells. Adv Mater. 2010;22:3593-7.

[99] Cohen JL, Schubert S, Wich PR, Cui L, Cohen JA, Mynar JL, Fréchet JMJ. Acid-Degradable Cationic Dextran Particles for the Delivery of siRNA Therapeutics. Bioconjugate Chem. 2011;22:1056-1065

[100] Kauffman KJ, Kanthamneni N, Meenach SA, Pierson BC, Bachelder EM, Ainslie KM. Optimization of rapamycin-loaded acetalated dextran microparticles for immunosuppression. Int J Pharm. 2013;422:356-63.

[101] Meenach SA, Kim YJ, Kauffman KJ, Kanthamneni N, Bachelder EM, Ainslie KM. Synthesis, optimization, and characterization of camptothecin-loaded acetalated dextran porous microparticles for pulmonary delivery. Mol Pharm. 2012;9:290-8.

[102] Broaders KE, Cohen JA, Beaudette TT, Bachelder EM, Fréchet JMJ. Acetalated dextran is a chemically and biologically tunable material for particulate immunotherapy. Proc Natl Acad Sci USA. 2009106:5497-502.

[103] Kanthamneni N, Sharma S, Meenach SA, Billet B, Zhao J-C, Bachelder EM, Ainslie KM. Enhanced stability of horseradish peroxidase encapsulated in acetalated dextran microparticles stored outside cold chain conditions. Int J Pharm. 2012;15:1-10.

[104] Holy CE, Dang SM, Davies JE, Shoichet MS. In vitro degradation of a novel poly(lactide-co-glycolide) 75/25 foam. Biomaterials. 1999;20:1177-85.

[105] Zolnik BS, Burgess DJ. Effect of acidic pH on PLGA microsphere degradation and release. Journal of Controlled Release. 2007;122:338-44.

[106] Esposito E, Cortesi R, Nastruzzi C. Gelatin microspheres: influence of preparation parameters and thermal treatment on chemico-physical and biopharmaceutical properties. Biomaterials. 1996;17:1-12.

[107] Frechet JMJ, Broaders KE, Cohen JA, Beaudette TT, Bachelder EM. Acetalated dextran is a chemically and biologically tunable material for particulate immunotherapy. P Natl Acad Sci USA. 2009;106:5497-502.

[108] Bachelder EM, Beaudette TT, Broaders KE, Dashe J, Frechet JM. Acetal-derivatized dextran: an acid-responsive biodegradable material for therapeutic applications. J Am Chem Soc. 2008;130:10494-5.

[109] Seif-Naraghi SB, Horn D, Schup-Magoffin PJ, Christman KL. Injectable extracellular matrix derived hydrogel provides a platform for enhanced retention and delivery of a heparin-binding growth factor. Acta Biomaterialia. 2012;8:3695-703.

[110] Mozaffarian D, Benjamin EJ, Go AS, Arnett DK, Blaha MJ, Cushman M, de Ferranti S, Després J-P, Fullerton HJ, Howard VJ, Huffman MD, Judd SE, Kissela BM, Lackland DT, Lichtman JH, Lisabeth LD, Liu S, Mackey RH, Matchar DB, McGuire DK, Mohler ER, Moy CS, Muntner P, Mussolino ME, Nasir K, Neumar RW, Nichol G, Palaniappan L, Pandey DK, Reeves MJ, Rodriguez CJ, Sorlie PD, Stein J, Towfighi

A, Turan TN, Virani SS, Willey JZ, Woo D, Yeh RW, Turner MB, Subcommittee AHASCaSS. Heart disease and stroke statistics--2015 update: a report from the American Heart Association. Circulation. 2015;131:e29-322.

[111] Ungerleider JL, Christman KL. Concise Review: Injectable Biomaterials for the Treatment of Myocardial Infarction and Peripheral Artery Disease: Translational Challenges and Progress. Stem Cells Translational Medicine. 2014;3:1090-9.

[112] Ono K, Matsumori A, Shioi T, Furukawa Y, Sasayama S. Enhanced Expression of Hepatocyte Growth Factor/c-Met by Myocardial Ischemia and Reperfusion in a Rat Model. Ciculation. 1997;95:2552-8.

[113] Matsumori A, Furukawa Y, Hashimoto T, Ono K, Shioi T, Okada M, Iwasaki A, Nishio R, Sasayama S. Increased circulating hepatocyte growth factor in the early stage of acute myocardial infarction. Biochem Biophys Res Commun. 1996;221:391-5.

[114] Soeki T, Tamura Y, Shinohara H, Tanaka H, Bando K, Fukuda N. Serial changes in serum VEGF and HGF in patients with acute myocardial infarction. Cardiology. 2000;93:168-74.

[115] Lamblin N, Bauters A, Fertin M, De Groote P, Pinet F, Bauters C. Circulating levels of hepatocyte growth factor and left ventricular remodelling after acute myocardial infarction (from the REVE-2 study). European Journal of Heart Failure. 2014;13:1314-22.

[116] Salimath AS, Phelps EA, Boopathy AV, Che P-L, Brown M, García AJ, Davis ME. Dual Delivery of Hepatocyte and Vascular Endothelial Growth Factors via a Protease-Degradable Hydrogel Improves Cardiac Function in Rats. PLoS ONE. 2012;7:e50980.

[117] Wang Y, Ahmad N, Wani MA, Ashraf M. Hepatocyte growth factor prevents ventricular remodeling and dysfunction in mice via Akt pathway and angiogenesis. J Mol Cell Cardiol. 2004;37:1041-52.

[118] Jayasankar V, Woo YJ, Pirolli TJ, Bish LT, Berry MF, Burdick J, Gardner TJ, Sweeney HL. Induction of angiogenesis and inhibition of apoptosis by hepatocyte growth factor effectively treats postischemic heart failure. J Card Surg. 2005;20: 93-101.

[119] Jayasankar V. Gene Transfer of Hepatocyte Growth Factor Attenuates Postinfarction Heart Failure. Circulation. 2003;108:230II--6.

[120] Rastogi S, Guerrero M, Wang M, Ilsar I, Sabbah MS, Gupta RC, Sabbah HN. Myocardial transfection with naked DNA plasmid encoding hepatocyte growth

factor prevents the progression of heart failure in dogs. AJP: Heart and Circulatory Physiology. 2011;300:H1501-H9.

[121] Li Y. Postinfarction Treatment With an Adenoviral Vector Expressing Hepatocyte Growth Factor Relieves Chronic Left Ventricular Remodeling and Dysfunction in Mice. Circulation. 2003;107:2499-506.

[122] Cho KR, Choi J-S, Hahn W, Kim DS, Park JS, Lee DS, Kim K-B. Therapeutic angiogenesis using naked DNA expressing two isoforms of the hepatocyte growth factor in a porcine acute myocardial infarction model. Eur J Cardiothorac Surg. 2008;34:857-63.

[123] Nakamura T, Mizuno S, Matsumoto K, Sawa Y, Matsuda H, Nakamura T. Myocardial protection from ischemia/reperfusion injury by endogenous and exogenous HGF. J Journal of Clinical Investigation. 2000;106:1511-9.

[124] Jin H. Early Treatment with Hepatocyte Growth Factor Improves Cardiac Function in Experimental Heart Failure Induced by Myocardial Infarction. Journal of Pharmacology and Experimental Therapeutics. 2003;304:654-60.

[125] Jones DS, Tsai P-C, Cochran JR. Engineering hepatocyte growth factor fragments with high stability and activity as Met receptor agonists and antagonists. Proceedings of the National Academy of Sciences. 2011;108:13035-40.

[126] Sonnenberg SB, Rane AA, Liu CJ, Rao N, Agmon G, Suarez S, Wang R, Munoz A, Bajaj V, Zhang S, Braden R, Schup-Magoffin PJ, Kwan OL, Demaria AN, Cochran JR, Christman KL. Delivery of an engineered HGF fragment in an extracellular matrix-derived hydrogel prevents negative LV remodeling post-myocardial infarction. Biomaterials. 2015;45:56-63.

[127] Khabbaz KR, Zankoul F, Warner KG. Intraoperative metabolic monitoring of the heart: II. Online measurement of myocardial tissue pH. Ann Thorac Surg. 2001;72:S2227-33.

[128] Singelyn JM, Sundaramurthy P, Johnson TD, Schup-Magoffin PJ, Hu DP, Faulk DM, Wang J, Mayle KM, Bartels K, Salvatore M, Kinsey AM, Demaria AN, Dib N, Christman KL. Catheter-Deliverable Hydrogel Derived From Decellularized Ventricular Extracellular Matrix Increases Endogenous Cardiomyocytes and Preserves Cardiac Function Post-Myocardial Infarction. J Am Coll Cardiol. 2012;59:751-63.

[129] Broaders KE, Cohen JA, Beaudette TT, Bachelder EM, Frechet JM. Acetalated dextran is a chemically and biologically tunable material for particulate immunotherapy. Proc Natl Acad Sci U S A. 2009;106:5497-502.

[130] Ruvinov E, Leor J, Cohen S. The effects of controlled HGF delivery from an affinity-binding alginate biomaterial on angiogenesis and blood perfusion in a hindlimb ischemia model. Biomaterials. 2010;4573-82.

[131] Thurston G. Complementary actions of VEGF and angiopoietin-1 on blood vessel growth and leakage. J Anat. 2002;200:575-80.

[132] Kobayashi H, DeBusk L, Babichev Y, DJ D, PC L. Hepatocyte growth factor mediates angiopoietin-induced smooth muscle cell recruitment. Blood. 2006;108:1260-6.

[133] Rafatian N, Westcott KV, White RA, Leenen FHH. Cardiac macrophages and apoptosis after myocardial infarction: effects of central MR blockade. AJP: Regulatory, Integrative and Comparative Physiology. 2014;307:R879-R87.

[134] Yang F, Liu Y-H, Yang X-P, Xu J, Kapke A, Carretero OA. Myocardial infarction and cardiac remodelling in mice. Exp Physiol. 2002;87:547-55.

[135] Dean RG. Connective Tissue Growth Factor and Cardiac Fibrosis after Myocardial Infarction. Journal of Histochemistry and Cytochemistry. 2005;53:1245-56.

[136] Efimov IR. Optical Imaging of the Heart. Circulation Research. 2004;95:21-33.

[137] Nakamura T, Sakai K, Nakamura T, Matsumoto K. Hepatocyte growth factor twenty years on: Much more than a growth factor. ournal of Gastroenterology and Hepatology. 2011;26:188-202.

[138] Grant DS, Kleinman HK, Goldberg ID, Bhargava MM, Nickoloff BJ, Kinsella JL, Polverini P, Rosen EM. Scatter factor induces blood vessel formation in vivo. Proc Natl Acad Sci USA.1993;901937-41.

[139] Bussolino F, Di Renzo MF, Ziche M, Bocchietto E, Olivero M, Naldini L, Gaudino G, Tamagnone L, Coffer A, Comoglio PM. Hepatocyte growth factor is a potent angiogenic factor which stimulates endothelial cell motility and growth. J Cell Biol.1992;119:629-41.